Bachelor's thesis

NTNU
Norwegian University of Science and Technology
Faculty of Information Technology and Electrical Engineering
Department of Engineering Cybernetics

Halvor Tøfte Johnsen, Jørgen Andreas Mo, Eivind Stellef Rønningen and Sigurd Belland Hovet

Modelling and Assessment of Overhead Crane for Automatic Control

A Feasibility Study of Automatic Pit Stripping

Bachelor's thesis in Electrical Engineering
Automation and Robotics
Supervisor: Kåre Bjørvik
Co-supervisor: Simen Vatslid Øystese
May 2023

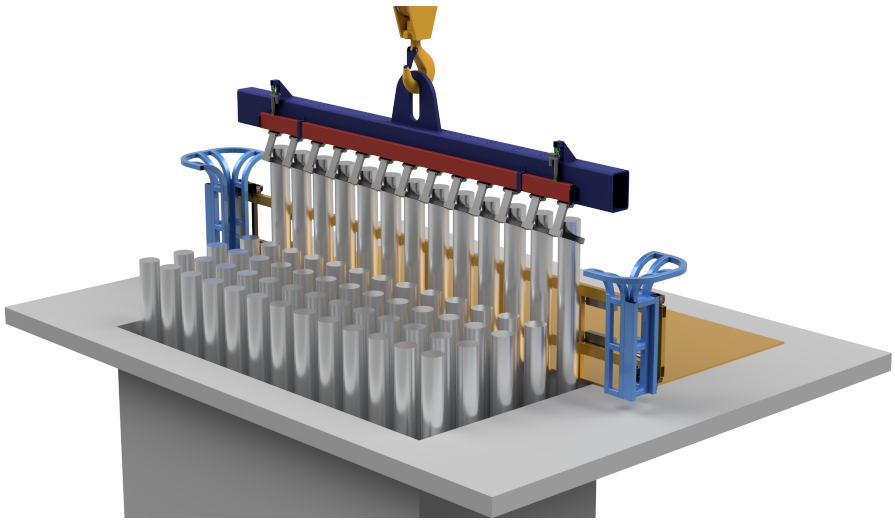

NTNU
Norwegian University of Science and Technology

Hydro

Halvor Tøfte Johnsen, Jørgen Andreas Mo, Eivind Stellef Rønningen and Sigurd Belland Hovet

Modeling and Assessment of Overhead Crane for Automatic Control

A Feasibility Study of Automatic Pit Stripping

Bachelor's thesis in Electrical Engineering - Automation and Robotics
Supervisor: Kåre Bjørvik
Co-supervisor: Simen Vatslid Øystese
May 2023

Norwegian University of Science and Technology
Faculty of Information Technology and Electrical Engineering
Department of Engineering Cybernetics

NTNU
Kunnskap for en bedre verden

Hydro

Project title: Modeling and Assessment of Overhead Crane for Automatic Control	
Authors: Jørgen Andreas Mo Sigurd Belland Hovet Halvor Tøfte Johnsen Eivind Stellef Rønningen	**Project number:** E2301 **Due date:** 22.05.2023 **Grade:** [X] Open [ ] Closed
Study program: Bachelor in Electrical Engeneering	
Field of study: Automation and Robotics	
Internal superviser: Kåre Bjørvik **Department:** Department of Engeneering Cybernetics	
Client: Norsk Hydro ASA **Contact:** Simen Vatslid Øystese	

Abstract:

This bachelor thesis documents the assessment of the existing installations in casting center no. 9 at Casthouse Sunndal, and its viability for automatic pit stripping. The overhead crane was modelled in, and a control system was developed in Simulink.

Sammendrag:

Denne bacheloroppgaven dokumenterer vurderingen av eksisterene infrastruktur på støpesenter 9 i Hydro sitt støperi i Sunndal, og muligheten for å automatisere uttak av pressbolt. Traverskranen ble modelert, og et kontrollsystem ble utviklet for å styre den i Simulink.

Keywords:	**Stikkord:**
Overhead crane, pit stripping, modelling, simulation	Traverskran, utheising av pressbolt, modelering, simulering

Acknowledgements

This thesis concludes our bachelor's degree in Electrical Engineering with a specialisation in automation and robotics at the Norwegian University of Science and Technology (NTNU), under the Department of Engineering Cybernetics. The thesis has been carried out in collaboration with Norsk Hydro.

Foremost, we would like to acknowledge and express our sincere gratitude to our supervisor assistant professor Kåre Bjørvik for his support during our project. Without his guidance and advice, this project would not have been possible. Associate professor Christian Fredrik Sætre at the Department of Engineering Cybernetics has also provided guidance and excellent answers to our many questions during our thesis, and we would like to acknowledge his time and effort.

We would also express our deepest appreciation to co-supervisor Simen Øystese from Norsk Hydro. This endeavour would not have been possible without his facilitation and knowledge. We would also like to thank the TOS department at Norsk Hydro for financing our trip to Casthouse Sunndal, and Remi Amundø from Hycast AS for the help during the trip.

Last, but not least we would be remiss in not mentioning our family and friends. Their belief and support have kept our spirit and motivation during this thesis.

Norwegian University of Science and Technology

Trondheim, May 2023

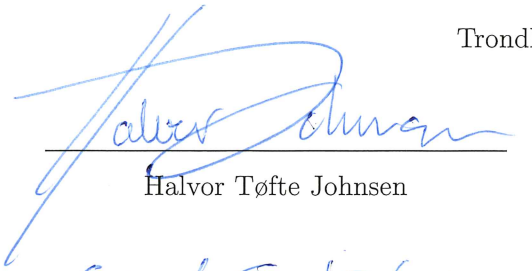

Halvor Tøfte Johnsen

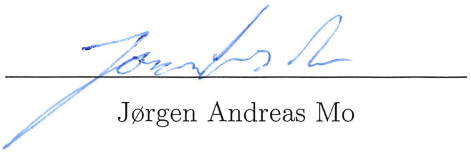

Jørgen Andreas Mo

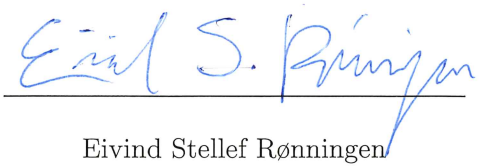

Eivind Stellef Rønningen

Sigurd Belland Hovet

Abstract

This bachelor's thesis explores the possibility of automating the pit stripping process at Hydro's extrusion ingot cast houses. To avoid downtime in production and significant investments, this is proposed solved through moderate modifications to the existing installation. Hydro has 11 casthouses, but this analysis is based on the SU-M4-MUN-M60 overhead crane at casting center 9 in Hydro's Casthouse at Sunndalsøra. The crane is currently controlled manually by an operator and the task consists of extracting ingots from the casting pit and transporting them to the laydown station. The crane is equipped with a lifting yoke, where billet rings utilise friction to clamp the ingots. The process involves driving the crane directly above the ingots, and lowering the lifting yoke down to the ingots. The operator then manually threads the billet rings onto the ingots, and dislodges them from their starting blocks. When the yoke is lifted, the rings clamp onto the ingots and lift them out of the pit. The ingots are finally transported to the laydown station.

Solving this problem, solely through control engineering, is considered challenging due to the crane's proportions and the precision required. Furthermore, the current lifting yoke is constructed for simple manual handling but is not suitable for automatic operation. These challenges have led to the suggested development of various mechanical solutions that could be combined with an automatic control system. These mechanical modifications reduce the accuracy requirements of the crane's control system and ensure increased robustness. A significant modification involves the redesign of the billet rings, where the chain connecting the ring to the girder is replaced by a rigid stem and a single revolute joint. To ensure the precise positioning of the lifting yoke, a retractable cradle system has been developed. This system effectively guides the lifting yoke into the desired position.

In addition to the mechanical solutions, comprehensive instrumentation is crucial in order to achieve desired control system performance. In terms of instrumentation, the requirements finally depend on the level of control system sophistication. The instrumentation package presented in this thesis aims to suffice for complex control strategies. The complexity of the instrumentation can however be limited once the final needs of the control system are known.

To perform tests, a mathematical model of the crane was developed in MATLAB's Simulink. This model, although somewhat simplified, simulates the dynamics of the crane and allowed for testing of various control strategies. By comparing the developed model with available documentation of the crane and videos taken at the Casthouse, the model was verified.

A control system was developed for the model of the crane's dynamics. This control system includes path planning, as well as position- and sway control, and is constructed using PID controllers, feedforward control and an input shaper. The PID- and feedforward controllers are responsible for position control, while the input shaper reduces sway. Despite its simple implementation, these control strategies have proven to work satisfactorily in collaboration with the proposed mechanical alterations.

This bachelor's thesis results in a set of proposed mechanical alterations to the crane system, as well as proposals for control strategies. From this thesis' research and development, it appears that automatic pit stripping is achievable through modest modifications to the existing installations. The weaknesses in the proposed mechanical solutions are addressed and further improvements are proposed. After the design process is finalised, the functionality and safety aspects of the mechanical solutions will need to be validated through prototyping. In terms of control engineering, it is proposed to first test the suggested control system on a physical system. If the performance is deemed inadequate, further development is needed. The recommendation for further control engineering consists of developing a more advanced and accurate model of the system. In case the system performance still is inadequate after adapting the suggested control system to the more advanced model, more complex control strategies will have to be utilised.

Sammendrag

Denne bacheloroppgaven ser på muligheten for å automatisere prosessen ved utheising og nedlegging av produktet pressbolt ved Hydros pressboltstøperier. Analysen har tatt utgangspunkt i traverskranen SU-M4-MUN-M60 ved støpesenter 9 på Hydro Sunndals pressboltstøperi. For å unngå nedetid i produksjon og store investeringer på grunn av omfattende ombygninger, er dette forsøkt løst gjennom begrensede inngrep i eksisterende installasjoner. På nåværende tidspunkt utføres denne oppgaven av en operatør ved hjelp av en traverskran utstyrt med et spesialbygd løfteåk. Løfteåket består av en bom, der en rekke løfteringer er koblet til gjennom stållenker. Utheisingsprosessen innebærer å kjøre løfteåket over en pressboltrekke, hvor operatøren manuelt trer løfteringene ned over pressboltene. Når løfteåket heises opp, låses ringene til pressboltene gjennom friksjon. Boltene heises så ut av støpegropen og transporteres til en nedleggingsstasjon for klargjøring til homogenisering.

Å løse denne oppgaven som et rent reguleringsteknisk problem ansees som svært krevende på grunn av kranens størrelse i kombinasjon med presisjonen som kreves. Gjennom modifikasjon av systemets mekaniske løsninger, har presisjonskravene til posisjoneringssystemet blitt redusert betydelig. En vesentlig endring involverer omstrukturering av løfteringenes oppheng på løfteåket. Ifra å henge i stål-lenker, er det foreslått en ny type ring som bare kan pendle rundt ett rotasjonsledd. For å sikre presis posisjonering av løfteåket blir det videre foreslått en mekanisk krybbe. Den monteres slik at løfteåket guides til ønsket posisjon over en boltrekke i støpegropen. Totalt sett vil disse mekaniske løsningene kompensere for mindre svingninger og usikkerhet i kranens posisjoneringssystem, samt sikre forutsigbarhet og robusthet under drift.

I tillegg til de mekaniske løsningene, er en tilstrekkelig dekkende instrumenteringspakke avgjørende for å oppnå ønsket ytelse fra reguleringssystemet. Instrumenteringskravet avhenger av hvor sofistikert reguleringssystem som til slutt kreves for å oppnå ønsket systemytelse. Denne bacheloroppgaven har likevel hatt som mål å foreslå en instrumenteringspakke som er tilstrekkelig for komplekse reguleringsstrategier, men som kan begrenses dersom behovet for avanserte styringssystemer ikke er til stede. Konkrete forslag til sensorer og instrumenteringsstrategier blir presenterte.

For å ha en plattform for testing av kranens reguleringssystem, er det utviklet en modell av kranens dynamikk i simuleringsverktøyet Simulink. Ved å sammenligne resultater fra simuleringer med videodokumentasjon fra støperiet, har modellen blitt verifisert. Selv om modellen er en forenkling av det faktiske systemet, tilrettelegger den for testing av ulike reguleringstrategier.

Et forslag til posisjoneringssystem for traverskranen har videre blitt utarbeidet. Dette styringssystemet dekker baneplanlegging i rommet, samt banefølging og begrensing av pendelutslag. Reguleringssystemet er i stor grad bygd opp ved hjelp av klassiske reguleringsstrategier og nyttegjør PID-regulatorer, foroverkoblinger og en input shaper. PID-regulatoren og foroverkoblingen brukes til posisjonsregulering, og input shaperen bidrar til å dempe svingninger i løfteåkets posisjon.

Gjennom simuleringer av automatisk uttak av pressbolt har denne reguleringstekniske løsningen, til tross for sin relativt enkle utforming, vist seg å fungere tilfredsstillende i kombinasjon med de foreslåtte mekaniske endringene.

Oppgaven konkluderes med en rekke forslag til videreutvikling av konseptene presentert, der svakheter i de presenterte løsningene blir adressert. Oppgavens forskning og utvikling peker mot at det er mulig å oppnå automatisk uttak av pressbolt. Av mekaniske løsninger anbefales det å gjøre noen mindre endringer på det foreslåtte løfteåket og løfteringene. Etter designrevisjon bør konseptene videreutvikles til prototyper slik at sikkerhetsaspektene verifiseres i fullskala. På reguleringssiden av oppgaven anbefales det først og fremst å gjennomføre tester på et fysisk system for å verifisere ytelsen til det foreslåtte styringssystemet. Dersom ytelsen til antisving-systemet viser seg å ikke være tilstrekkelig, anbefales det å basere input shaperen på en mer nøyaktig modell av kranens dynamikk. Dersom ytelse og robusthet fortsatt ikke er tilstrekkelig for et fullskala system anbefales det å utvikle et mer sofistikert posisjons-reguleringssystem basert på mer avanserte reguleringsstrategier.

Contents

List of Figures

List of Tables

Chapter 1

Introduction

Hydro Aluminium AS is a subsidiary of Norsk Hydro ASA, which is regarded as one of the top ten largest aluminium producers worldwide [1]. In addition to their aluminium production units, Hydro Aluminium AS also owns Hydro Extruded Solutions AS and Hycast AS, which is a spin-off of Hydro Aluminium's RnD-division. Extruded Solutions make aluminium profiles and tubes, and Hycast provides Hydro Aluminium with casthouse equipment and technology.

Hydro Aluminium provides various casthouse products, ranging from wire rods [2] to remelt ingots [3]. Extrusion ingots [4] are cylindrical billets used in extrusion processes and are produced in various alloys, specified by their customers. Currently, Hydro Aluminium has 11 extrusion ingot casthouses in Europe and US, which collectively have a production capacity of 2 million tons, and is their flagship product.

The process of casting extrusion ingots has a high degree of automation, which is achieved through the HyCast® CMV [5] technology. The process of extracting the finished extrusion ingots from the casting pit is however performed manually by an operator, which represents labour cost and risk of injuries.

As such, Hydro could greatly benefit from automating their extraction processes. Initial studies and proposed solutions have all included large investments in new equipment and major reconstructions of existing casthouses. These suggestions would have caused prolonged shutdowns in production, with significant production loss. However, by using existing infrastructure, these processes can be upgraded with minimal disruption to production. Hydro's 11 casthouses all use overhead cranes to extract the ingots from the casting pit. The main part of this thesis looks at the possibilities of using existing infrastructure such as overhead cranes and laydown stations, but only modifying their control systems and instrumentation. It will also touch upon mechanical difficulties like replacing the existing lifting yoke and its ring design. A critical manual operation is connecting the billets to its lifting device, and this operation has to be solved to have a fully automated pit stripping operation with an overhead crane.

Chapter 2

Background

2.1 Introduction to Casthouse Processes

This thesis is primarily focused towards automating the process of extracting extrusion ingots from a casting pit. It is however important to put this task into context, and through this chapter, the aim is to provide a framework around the operation.

2.1.1 Billet Casting

Billet casting is the process of converting liquid aluminium provided by the electrolysis plant, to solid cylinders. The billets are cast in a range of standard alloys [6], where the composition of aluminium, magnesium, cobber, manganese and other metals determine the alloy's properties to meet the customer's needs. Hydro currently uses two different technologies provided by HyCast AS in their extrusion ingot production lines.

Gas Cushion (GC) billet casting is based on a mould construction where patented dual graphite rings supply gas and oil to the mould wall[7]. Liquid aluminium is led through a network of chutes from the oven to the GC mould, where it is evenly distributed. Casthouse Sunndal utilises this casting technology and will be the reference throughout this thesis.

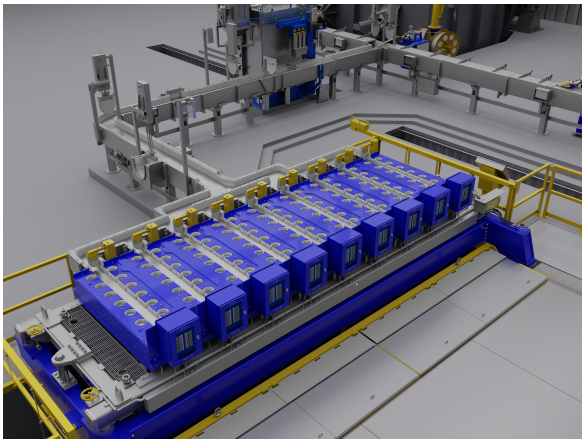

Figure 2.1: HyCast GC Billet Casting [7].

The Low-Pressure Casting System (LPC) [8] is a new patented casting technology for extrusion ingots. LPC is based on proven GC technology and offers a new standard in surface quality and flexibility [9]. In addition to facilitating higher homogenising temperatures, it results in an improved surface appearance and sub-surface microstructure.

Figure 2.2: HyCast LPC Billet Casting [9].

As both technologies are based around the HyCast Casting Machine Vertical (CMV) [5], and the difference in casting technology doesn't affect the properties of the billets in terms of handling, this thesis will not distinguish between the two in further analysis. When casting billets with the HyCast CMV liquid metal is solidifying on top of an array of starter blocks. The blocks are then progressively lowered into the pit throughout the casting process, building the billets vertically.

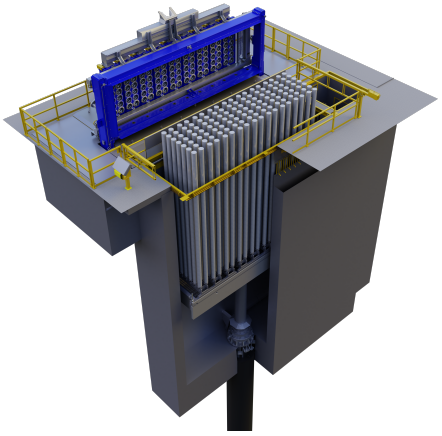

Figure 2.3: HyCast Casting Machine Vertical with GC mould [5].

Once the billets have reached their nominal length of $7240mm$, the supply of liquid aluminium is cut off and the billets are left to cool down, while an operator is cleaning the system and preparing for the next cast. Upon reaching the handling temperature, the top mould is removed from the pit, and the billets are ready for extraction.

The amount of ingots cast simultaneously depends on the mould dimension, and at Casthouse Sunndal's casting center the billet dimensions are $\varnothing 254mm$, $\varnothing 228mm$, $\varnothing 203mm$, $\varnothing 178mm$ and $\varnothing 152mm$, with the number of billets being 54, 70, 96/98, 128 and 152.

2.1.2 Pit Stripping

The process of extracting the aluminium ingots from the casting pit is referred to as pit stripping. This process is done by an operator utilising an overhead crane equipped with a specialised lifting yoke. This lifting yoke is composed of a girder with an attachment point for a crane hook. An array of lifting rings are attached to this girder through chain links. Once the casting process is finished, the ingots remain in place on top of the starter block. The operator places the lifting yoke close to the front ingot row. Then, they thread the rings of the lifting yoke over the billets. Next, the operator moves the yoke towards the safety railing, dislodging the billets from their starter blocks. When hoisting upwards, the rings bite into the billets and create enough friction for the billets to remain attached to the yoke. Once securely attached to the yoke, the billets are lifted out of the pit. This operation is however considered a significant risk, as the operators are unable to maintain the desired safety distance from the hanging load during extraction.

Figure 2.4: Pit stripping. The lifting yoke (yellow) is attached to the hook of a gantry crane. The lifting yokes vary in ring placement- and dimension, depending on the billet dimension.

From the casting pit, the billets are transported to a lay-down station where the billets are put horizontally on a conveyor and fed into an oven for homogenisation.

2.1.3 Homogenisation

In this case, homogenisation refers to the process of making the aluminium billets more uniform. Essentially, the billet is heated close to its melting point and then slowly cooled down. Through this process, the different components in the alloy get more evenly distributed. The process also reduces internal stress and makes the material more suitable for post-processing [10].

2.2 Previous Studies and Development

2.2.1 Motorised Billet Tong

As a step towards making the pit stripping process less labour-intensive and potentially automating the process, a motorised billet tong was acquired from TC Engineering [11]. This tong could handle all billet dimensions and simplified the process of detaching the billets at the lay-down station. The main problem with this tong was, however, its mass, essentially making pit stripping a two-man operation, due to the additional force needed to guide it into place above the billets.

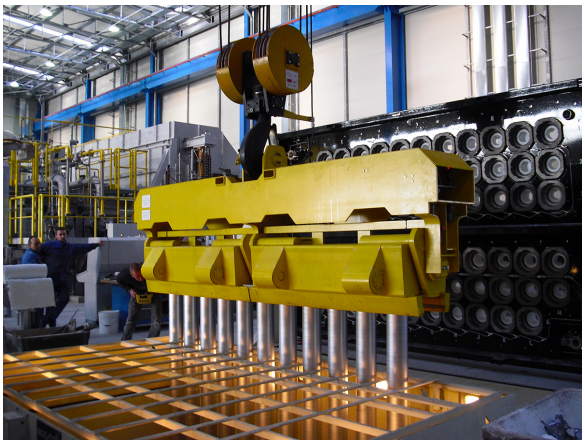

Figure 2.5: Hydraulic billet tong (TC Engineering) [11].

2.2.2 Automatic Pit Stripping

In 2018, a position paper on the engineering of an automatic pit stripping machine for the Lucé EI casthouse was submitted. The background for the paper was the following:

> ***2 Background***
> *Today's stripping solution involves an overhead crane with rings or slings to hoist the logs from the casting pit to the lay-down station. This process is very man intensive with a hanging load representing a significant risk in the casting area and preventing necessary turn-around activities to take place in parallel. A concept exists (patented through Hycast) to atomise the process.*

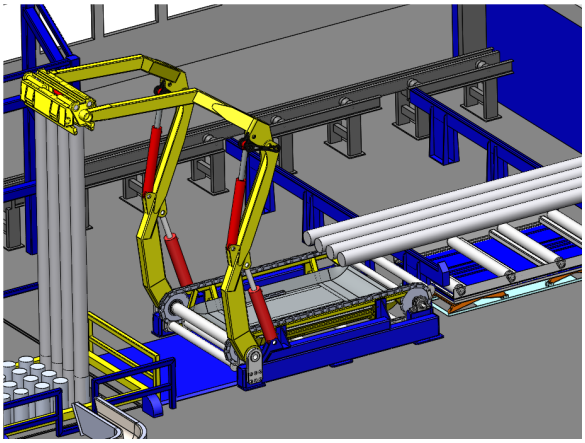

Figure 2.6: HyCast Automatic Pit Stripping Concept [12].

In 2019, a pre-study was conducted on the concept of a fully automated casthouse. This report concluded that even though HyCast had developed a fully automatic pit stripping solution, it would be cheaper to automate the existing cranes in the production lines. The following points are extracted from the report [12]:

> ***6.2.2 Automatic pit stripping machine***
>
> *An automatic pit stripping machine was developed by Hycast for Lucé EI casthouse, but it has not been built. It uses a TC Engineering tong at the end of two manipulator arms to lift the billets from the casting pit to the lay-down station after cast. It is fully automatic and would shorten pit stripping time, which is an advantage where the casting machine is the bottleneck.*
>
> ***6.3.3 Automatic pit stripping using existing crane***
>
> *It is most likely cheaper to automate the existing crane in the casthouse than to install the automatic pit stripping machine described in section 6.2.2. A new tong is needed since it is difficult to automate putting rings on billets, and a company with experience in automating cranes should be used. Tronrud Engineering suggested they are able to do this. Automating the existing crane is not likely to improve cycle time.*

Based on this, the scope of this thesis is analysing the current infrastructure in the casthouses and providing suggestions on actions to take to achieve a reliable automatic system, with limited need for investments and downtime at the plant.

2.2.3 Rockwell Automation Solutions for Automatic Control

Rockwell automation group have developed two systems for automatic control of overhead cranes, although not for billet handling, but for more simple lifting operations. Their systems utilise lasers, encoders and anti-sway technology to automatically move the overhead crane to desired positions, and collect the payload. It also features anti-collision control, safe torque control to avoid slipping risk, and different operation modes - local, remote and autonomous [13].

2.3 Motivating Factors for Increasing the Level of Automation

The current processes at Hydro's casthouses are renowned for their high efficiency. Despite these achievements, there is still a demand for greater efficiency and cost-effectiveness in the ever-evolving global market. Especially in Norway where the labour cost is high compared to other industrial countries. Therefore it is crucial to find ways to increase efficiency with technology to keep up with the competitors in the market.

Automation of the aluminium casting process has been associated with gains in quality because it leads to a more reliable casting process and fewer flaws brought on by human error. Automation reduces the chance of variation in the production process, resulting in more consistency in the finished product, by automating specific jobs, such as those that call for exact measurements or repetitive motions. By eliminating the human element from some jobs, the adoption of automation technology can also lower the likelihood of errors. As a result, the product's total quality is raised, which is crucial for preserving customer happiness and market competitiveness.

Hydro has a philosophy of continuously improving workers' safety and their environment. Therefore, Hydro has identified the most critical risks involving a potential fatality and life-changing injury. One of those is overhead crane operations. Although incidents regarding crane operations are rare, Hydro seeks to automate this process to remove the interaction between crane and operator.

Chapter 3

Assessment of existing installation

In order to fully understand the nature of the pit stripping operation, a visit to Hydro Sunndal was carried out from the 26th to the 27th of January 2023. Casthouse Sunndal has two parallel production lines for extrusion ingots (casting center no. 8 and no. 9), which have similar properties. During this visit, a set of velocity- and acceleration measurements were carried out on the crane at Casting Center no. 9. Additionally, extensive video and photo documentation was collected from both production lines, displaying the differences between them, the crane dynamics and in general how the pit stripping process was carried out.

Figure 3.1: Video documentation of the acceleration test in the horizontal plane was gathered from the mezzanines surrounding the crane.

Furthermore, discussions with skilled operators in charge of the billet casting led to a better understanding of known issues and difficulties throughout the production. This could involve errors in the casting process, the pit stripping process and the transport process, all of which could affect the possibility of automating the process.

The current pit stripping process involves a set of tools used by an operator to extract the aluminium billets from the casting pit and position them for being fed into the homogenisation furnace.

- Overhead crane equipped with a lifting yoke for extrusion ingots
- Motorised safety platform
- Lay-down station (either motorised or static)

3.1 Overhead Crane

The SU-M4-MUN-M60 crane is an overhead crane supplied by the manufacturer Munck, and is classified for loads of 20 metric tonnes at the primary hoist and at 5 metric tonnes at the secondary hoist. Data on the masses of the different crane components were gathered from the crane's documentation, as well as information on maximum velocity, which was verified on-site.

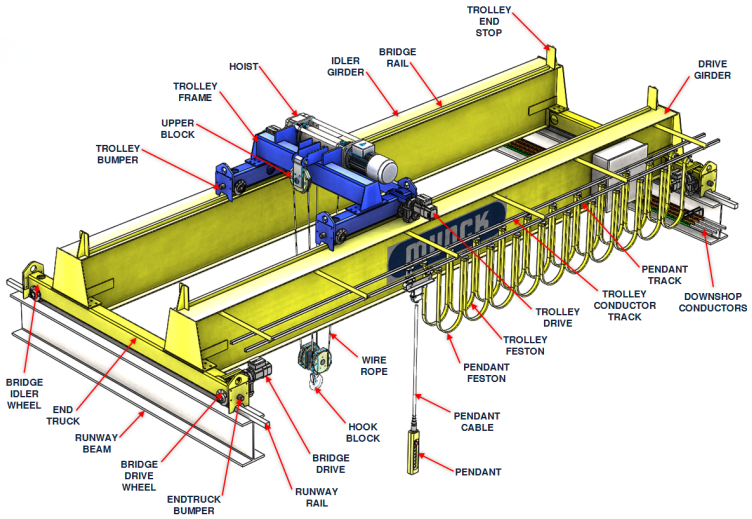

(a) Overhead crane principle and component descriptions [14].

Bridge	m_{BR}	7700 $[kg]$
	$p_{BR_{max}}$	33.0 $[m]$
	$v_{BR_{max}}$	1.0 $\left[\frac{m}{s}\right]$
Trolley	m_{TR}	5600 $[kg]$
	$p_{TR_{max}}$	13.2 $[m]$
	$v_{TR_{max}}$	0.5 $\left[\frac{m}{s}\right]$
Hoist	$p_{HOI_{max}}$	22 $[m]$
	$v_{HOI_{max}}$	0.125 $\left[\frac{m}{s}\right]$

(b) Properties of motion for the SU-M4 crane.

Figure 3.2: Overhead crane components and properties.

3.1.1 Crane Actuators

The SU-M4 crane has a total of six degrees of freedom in its current configuration, where only three are directly controllable. The hoist trolley position is a result of rigid translations in the horizontal plane (xy). As given by the SU-M4-MUN-M60 PLC program (Appendix A10), the motors for hoist trolley travel in the horizontal plane, as well as hoist itself (l), are VFD-controlled (Variable Frequency Drive). The drive motors are connected to gearboxes, which again are connected to drive wheels running along steel girders.

Two of the degrees of freedom that are not directly controllable are the two angles describing the hoist wire orientation in space.

The final degree of freedom is currently uncontrollable and is located in the hook block, where the hook rotates freely around its own axis.

3.1.2 Crane Instrumentation

In the SU-M4 crane's current configuration, its instrumentation package does not monitor the crane's position in space, as it is designed to be controlled by an operator with visual control of the system at any given time. However, to avoid de-railing and damage to the system, all directions of travel are equipped with limit switches that limit motion in case the moving body has reached the end of its defined working area. In the horizontal plane, all directions of travel

are equipped with a double set of limit switches, where the first one limits the maximum jog speed and the final one stops the motion in the given direction of travel.

The hoist is equipped with the same double set of limit switches for upward motion as the trolley and the bridge, but only one stop stitch for downward motion. Additionally, the hoist is equipped with a load sensor, determining the mass of the load with a resolution of $100kg$

Further machine-safety-related instrumentation includes monitoring of fuse states, VFD temperature, hoist brake errors, load cell errors, etc. This kind of instrumentation is not directly related to the problem of automating crane operations and is therefore regarded as beside the scope of this thesis. These will therefore not be further elaborated.

3.1.3 Crane Controls

All instrumentation and actuators are connected to a Siemens S7-315-2 PLC. While most of the signals are linked directly to the IO modules of the PLC, the VFDs are linked to the PLC through Profibus DP.

Operating the crane is normally done through a wireless controller, sending commands to the crane PLC through a radio link. This controller is equipped with continuously variable joysticks, enabling accurate control of the VFDs and determining the speed of travel in the respective directions. Moreover, a secondary tableau is located at the crane bridge, intended for service purposes. This tableau does not provide continuously variable throttle for the VFDs, but offers two preset speeds of travel in each direction, namely 10% and 100%

3.2 Lifting Yoke

The design of Hydro's billet lifting yokes varies across the different casthouses. They are designed and manufactured by Nøsted & AS through their brand FRAM [15]. Although their appearance differs, their function is equal and aims to make the process of threading the lifting rings onto the aluminium billets simple and flexible for an operator. The current lifting yokes are constructed with an array of lifting rings, connected to one common girder through chain links. These lifting rings typically have an inner diameter $\sim 20mm$ larger than the ingot diameter. When the girder is lifted, these sharp steel rings will bite into the sidewall of the aluminium billet and create enough friction to keep the ingots from sliding out. This solution is constructed to reduce the need for yoke positioning accuracy. Though efficient and effective for manual pit stripping operation, the chain link system is too unpredictable for automatic operation [12].

Figure 3.3: Current ⌀178mm billet lifting yoke design (Casthouse Husnes).

Figure 3.3 shows the yoke design implemented in Hydro Casthouse Husnes. The model used in Hydro Casthouse Sunndal is constructed with a rectangular steel pipe as girder but is otherwise very similar. The total length of the lifting yoke in Sunndal is measured at 4920mm.

3.3 Safety Platform

As aluminium billets are extracted from the casting pit, a motorised safety platform is moved over the casting pit to facilitate simple billet attachment and thereby increase the level of safety for the operator.

When the billet rings are threaded onto the ingots, the lifting yoke is moved towards the safety railing to dislodge the ingots from their starter blocks. It is therefore important that the safety platform is not moved too close to the ingot row, as this will prevent the billets from becoming dislodged from their starting blocks. This platform is controlled by an operator through a rotary switch mounted at the end of the platform.

3.4 Lay-down Station and Homogenisation Line

From the casting pit, the billets are transported to the lay-down station, where they are put horizontally on top of a conveyor, queuing for the homogenisation furnace. The lay-down stations are to a certain degree different in the two casting centers at Casthouse Sunndal. While Casting Center no. 8 has a motorised cradle that simplifies the lay-down process for the operator, the cradle in Casting Center no. 9 is static. Though one has a higher degree of automation than the other, their shapes are however very similar. This lay-down station analysis will be based on casting center no. 8, as it has the highest degree of automation.

Figure 3.4: Static lay-down station at casting center no. 9 (Casthouse Sunndal). The lay-down cradle is painted turquoise.

Both casting centers in Sunndal have equal solutions for transporting the billets from the lay-down station to the queue for the homogenisation furnace. After the billets have been placed in a horizontal position, they are stowed together by two hooks. A trolley is then driven underneath the billets and elevated slightly, freeing the billets of the rails they are resting on.

While the billets are being transported to the homogenisation queue by the trolley, the system moves to its initial position, preparing for a new row of ingots

3.4.1 Lay-down Station Actuators and Instrumentation

Within the scope of this thesis, the lay-down station can be regarded as a turn-key product with a high degree of automation. The details surrounding its construction, including its actuators, instrumentation and safety measures, will therefore not be elaborated.

3.4.2 Lay-down Station Controls

Although the lay-down station is a machine where numerous sensors and actuators interplay, the user interface is constructed to be simple and intuitive for an operator to interact with. The lay-down station is controlled from the safety railing across the transport zone from the casting pit. The operator interacts with the station through a tableau and a foot switch, where the foot switch controls the translatory movement of the lay-down cradle, while the tableau controls the trolley, the gathering hooks, and the resetting of the machine in between the transport of ingot rows. In essence, the operator steps on the foot switch to move the billets horizontally away from their lowered position while simultaneously lowering the crane hoist to place the billets onto the conveyor. Once the lifting yoke is detached from the billets, the operator presses the start button on the tableau. The station then automatically feeds the billets forward and resets the cradle for the next row of billets.

3.5 Delicate Aspects and Problem Areas

Through dialogue with the operators on-site, the most common issues were addressed. These will briefly be described in this chapter.

3.5.1 The Domino-effect

One well-known problem in billet casting is the case when one billet in the pit is thrown off balance and falls into the billets standing next to it. This often results in a domino effect, where all billets eventually fall over, demanding single-ingot extraction instead of entire rows. This issue is most common in the smaller billet dimensions as they are more easily affected by small shocks. Worn-out starting blocks have proved to be a triggering factor for this problem, as the ingots aren't as firmly attached as with new starting blocks.

3.5.2 Cast Bleed-out

If the casting process itself fails due to aluminium bleed-out, the billets don't end up being shaped as perfect cylinders. In the best-case scenario, the billets will appear as if lumps or scars are attached to the cylinder wall. On the other hand, in the worst case scenario, the "cylinders" might turn into one large lump of aluminium. Automatic bleed-out detection is an RnD focus area in Hydro, but currently, the casting process relies on manual inspection.

3.5.3 Carillon Tunes

One effect that might occur, especially with inexperienced crane operators is referred to as "carillon tunes". When a row of ingots hangs from the lifting yoke, each ingot represents a pendulum. When applying sudden movements to the yoke, the billets are known to swing into each other and make a "carillon-like" sound. Though usually not problematic, this might reduce the friction between the lifting ring and the billet, and might potentially cause the billets to fall to the ground, representing a potential danger to people in the area.

3.6 Human Safety

Crane operations inherently represent a safety hazard due to the risk of falling loads. Factors such as failing lifting equipment, poorly secured loads and distracted operators all contribute to the total risk, and especially in cases where tall, wide and/or heavy loads are transported, the consequence of a failure might be fatal.

In the extrusion ingot handling process, ~ 7 metre-long metal billets are transported by means of a friction-based lifting yoke, through a transportation zone, a walking path, and above a set of safety railings. Although accidents are rare, the consequences of an incident might be human injuries or even casualties. An upright billet dropped two meters above floor level could bounce off the floor upon impact and move unpredictably. In any case, the safety distance from the billets being transported could be no less than the length of the billet plus the distance they

might bounce upon impact. Although most operators are trained and experienced with lifting operations, repetitive tasks such as pit stripping might result in a reduced focus on continuous risk assessments. The operator then might not detect hazardous situations, as the initially dangerous operation becomes mundane.

Since billet transportation is regarded as the most dangerous part of the pit stripping operation, the other hazards become much smaller in comparison. Even though the operators might keep a safe distance from the billets that are being transported, they are physically in contact with the yoke and the lifting rings when threading the lifting rings onto the billets. While this represents a small risk in comparison, there have been cases of hoist brake failure, which could result in human injuries.

Chapter 4

Prerequisites for automatic operation

The greatest challenge in automating the pit stripping operation, while still utilising the existing infrastructure, is achieving adequate accuracy in the crane's positioning system. This is mainly a problem during the billet attachment process, as using the current lifting yoke would require positioning accuracy of less than $\sim 10mm$. In combination with the proportions of the system, where the lifting yoke is hanging 10-15 meters below the hoist trolley, it is assumed that measurement errors, residual vibrations and sway in the hoist will result in poor system performance. One prerequisite for achieving reliable automatic pit stripping would therefore be increasing the lifting yoke positioning margins.

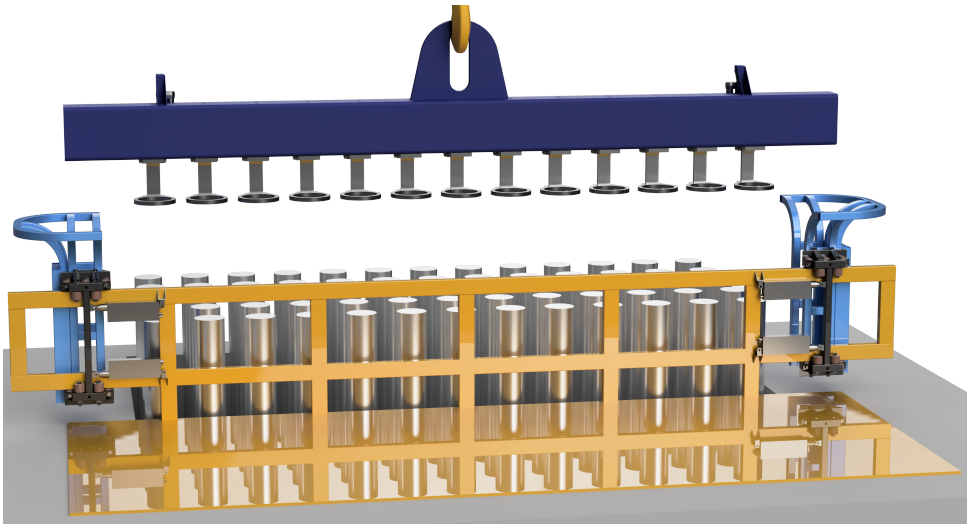

Figure 4.1: Lifting yoke guide cradles attached to the safety platform railing.

Another challenge in the ingot attachment procedure is accounting for minor deviations in ingot placement inside the pit. In sum, these challenges point towards the need for a certain degree of mechanical engineering to complement the crane's positioning system. Re-designing and replacing the current lifting yoke, as well as developing a ground-mounted system for guiding the new lifting equipment into position, is assumed effective in terms of achieving robust and reliable operation.

While mechanical solutions reduce the requirements for the crane's positioning system, the performance still needs to be high. As the overhead cranes in Hydro's casting centres generally have limited instrumentation packages, a sensor upgrade will furthermore be required. The main actuators on the cranes, namely the hoist, bridge and trolley drive are foreseen reused, although with some modifications increasing controllability.

Automating the pit stripping process requires interplay between all the standalone subsystems used in the process. Through this chapter, prerequisites for being able to implement an automatic

control system for the existing installations will be presented. Furthermore, conceptual mechanical solutions, aiming to enable automatic control and increase robustness and predictability, are presented.

4.1 Possible Lifting Equipment Replacements

As briefly mentioned in this thesis' background (chapter 2.2.1), Hydro has previously utilised a hydraulic billet tong provided by TC Engineering during a test period. This solution was however not considered suitable for the application due to its significantly larger mass and momentum, compared to the ring-based lifting yoke.

From a systems theory perspective, a greater mass at the end of a pendulum will result in less dampening, which implies that oscillations decay at a slower rate compared to systems with smaller masses. If a robust and accurate anti-sway control system is successfully implemented, this dampening factor will be of less significance. However, if the anti-sway system does not perform at an acceptable level, the momentum of the heavier lifting equipment will apply higher levels of stress on the ground-based guide system, than lighter lifting equipment would.

Another considerable aspect of such a billet tong is its size and bulkiness. To maximise capacity, the extrusion ingots are cast in close proximity to each other in the pit. As the ingots are balancing on their starter blocks 6 meters below the floor level, only small forces are required to knock the billets over, causing a domino effect. Precise guide equipment will alleviate this problem, but due to the mass of the tong, this guiding equipment will simultaneously need to be constructed more rigidly to withstand substantial forces.

From a safety perspective, a ring-based solution appears preferable compared to a hydraulic tong. As both solutions rely on the friction between the extrusion ingot and the lifting equipment, there is assumed no considerable difference in safety once the lifting equipment is clamped onto the billet. In a faulty situation, the ring-based system would however be preferable. If the hydraulic billet tong loses oil pressure, either due to a blown hose, a malfunctioning valve or similar, the extrusion ingots could be dropped to the floor if no fail-safe mechanisms are in place. Likewise, if a control system error results in a command to open the billet tong at an undesirable point in time, the billets may again be dropped. A ring-based solution will however still clamp onto the billets regardless of failures, as the rings' equilibrium position causes them to bite into the billets they are threaded onto. The only foreseen failure would then be a crane failure, which is a problem regardless of lifting tools.

Although both a hydraulic billet tong and a modified ring-based lifting yoke could work for this application, the different aspects discussed above point towards a modified lifting yoke as the preferred solution. Throughout the following chapter, design suggestions and different considerations to take into account will be elaborated on.

4.2 Revised Lifting Yoke Design

When exploring alternative lifting yoke designs, the lifting yokes at Casthouse Sunndal were used as references. A set of problem areas were particularly focused on during the revision process:

- Increasing control system margins in terms of lifting yoke positioning and being able to extract slightly misplaced extrusion ingots
- Increasing the predictability and repeatability of the ring motion
- Limiting the need for actuators and sensors on the yoke as much as possible [16]

4.2.1 Lifting Yoke Girder

To facilitate for a set of guide cradles that can position the lifting yoke above the extrusion ingots, it is proposed to extend the lifting yoke girder by 500mm on each side to ensure that the billet rings do not collide with the guide cradles during positioning. By increasing the overall length of the lifting yoke from 4920 mm to 5920mm, the lifting yoke will become heavier and less manoeuvrable. Based on the cast floor layout in Hydro Sunndal, this is however not regarded as an issue, as the space suffices, even with the increased equipment size.

Furthermore, to achieve greater predictability, the attachment/coupling point for the crane hook should be shaped in such a way that the hook is not able to rotate relative to the lifting yoke once hooked. The main motivation for this is that rotation in this "joint" is both uncontrollable and hard to monitor, and by limiting its freedom, correct lifting yoke orientation around the hoist wire axis is easier to achieve.

4.2.2 Billet Ring Design

When revising the billet ring design, there are a set of aspects that are essential for safe and predictable operation.

- The lifting ring needs to bite into the billet with sufficient force to keep it from sliding out during transportation
- The ring design cannot be too bulky, causing the ring to touch other billets while the "current" row of billets is being extracted.
- The design needs to provide predictable results every time

The most effective measure for increasing the predictability of the current ring design would be replacing the chain link with a single, snug revolute joint. In the current design, where the ring is linked to the girder through a chain link, the resting position of the ring is at a 90-degree angle, relative to the horizontal plane, as displayed in figure 4.2. The result of this is that the ring bites into the billet with a significant force while being lifted.
Furthermore, the chain link allows for the ring to move freely relative to the lifting yoke, during lifting, which ensures that small pendulum motions in the billet do not result in the billet being wiggled loose from the ring.

Figure 4.2: Existing billet rings

The figures 4.3a to 4.3c display iterations on a single-joint billet ring design, improving on the previously mentioned design considerations at each iteration.

(a) Billet ring V1. (b) Billet ring V2. (c) Billet ring V3.

Figure 4.3: Iterative billet ring revision process.

Figure 4.3a displays the 1st iteration on the single-joint billet ring design. Though this design is similar to the one currently used and provides a sharp bite into the billet during transportation, it represents a greater challenge in being threaded onto the extrusion ingots, as well as detaching them at the lay-down station.

Figure 4.3b displays the 2nd iteration on the billet ring design. In this version, the ring would be resting at a $\sim 23°$ angle relative to the horizontal plane, in its equilibrium position. The idea behind this design is to facilitate easier threading onto the billets, as well as easier detachment at the lay-down station. The stem of the billet ring would be mounted flush to the sidewall of the lifting yoke girder, making it possible to attach an actuated bar to the girder, moving vertically (as shown in red in figure 4.4). Once actuated, this bar would then tilt the billet ring into horizontal position, maximising the area of the threading-hole in the ring while being lowered onto a billet.

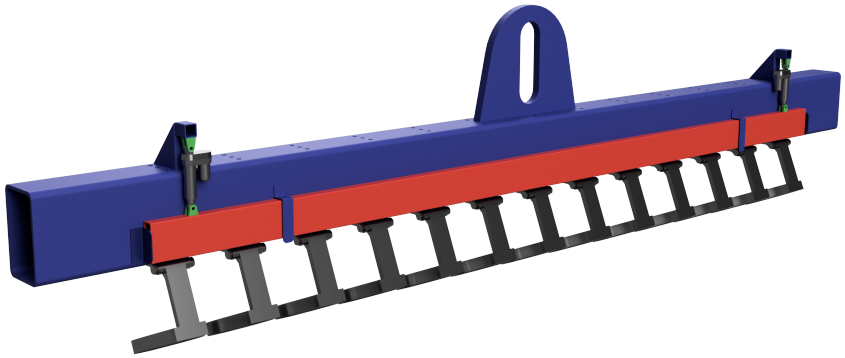

Figure 4.4: Proposed lifting yoke, equipped with billet ring V2 (un-actuated).

The main concern with this design is however if the billet rings bite into the extrusion ingots with a sufficient force to ensure safe lifting. The bite force could be increased by prolonging the distance from the ring stem to the centre of the ring hole, but this would then result in the stem colliding with the "next" row of billets upon attachment.

Alike the lifting rings on the yokes provided by Nøsted & AS, the inner ring diameter is approximately $20mm$ larger than the extrusion ingot diameter. As this does not allow for more than $10mm$ radial misplacement of the billets in the pit, a conical entrance is added to the 2^{nd} revision in the new ring design. This modification will help increase the ingot mispositioning tolerance from $\sim 10mm$ to $\sim 40mm$ off-centre. The thickness of the lifting ring will then be doubled compared to the ones currently in operation, and the additional material will be manufactured conically, aiming to "funnel" the billets into the ring. This increases the inner diameter of the lifting ring upon entering, while the clamping diameter stays the same. The conical ring entrance is currently tapered at a $45°$ angle, to add a certain degree of leverage for moving either the billet or the yoke, while still providing a sharp enough edge to bite into the billets.

Figure 4.3c displays the 3^{rd} iteration on the billet ring design. The design is still based on a ring that can be tilted into a horizontal position by means of one common "pushbar" at the back of the lifting yoke girder. The aim for this revision was however to increase the biting force exerted on the billet while hanging from the ring, by increasing the leverage.

In this design proposal, the rings rest at an angle $\sim 32°$ relative to the horizontal plane. To avoid hitting the "next" billet row when attaching the current, the single stem was replaced by two stems, spaced at the same distance as the inner diameter of the ring. This allows for increasing the distance from the ring centre to the stem axis, in essence minimising the angle between the ring plane and the attachment point on the girder. The conical ring entrance remains for this version of the ring design as well. It is assumed that the solution proposed in the 3^{rd} version of the revised billet ring design could work adequately if applied in the proposed framework.

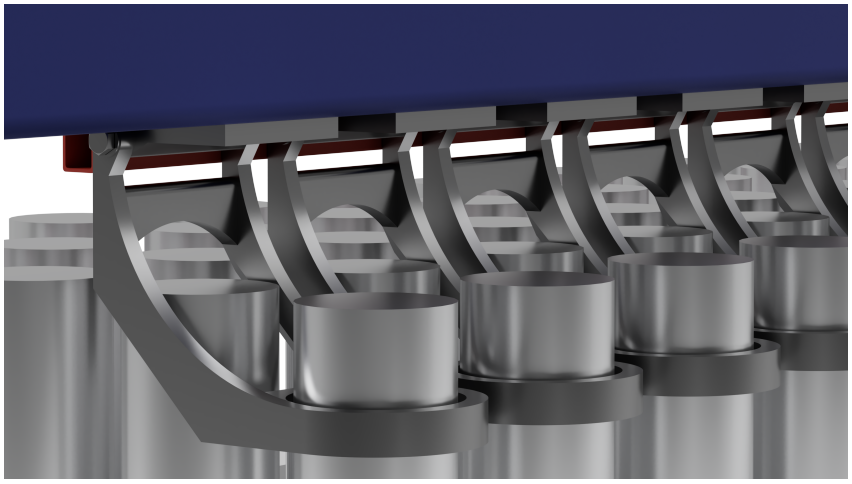

Figure 4.5: The billet ring does not conflict with the billet row behind the one being extracted.

One of the known weaknesses in this version is however that the levelling of the billet ring is done through only one actuator at the rear end. This, in essence, means that the billet ring is still able to rotate freely forwards. If an ingot is misplaced, the ring will be swivelled further, instead of the yoke or billet being moved. In the next iteration of the ring design, the front part of the stem should therefore be straight instead of curved in the top part, to facilitate a locking bar in the front as well. This would leave the billet rings unable to swivel in their revolute joints when being lowered onto the billets.

4.2.3 The Mechanism for Levelling Lifting Rings Upon Attachment

Placing the billet rings in a horizontal position when being threaded onto the extrusion ingots, severely simplifies the path the crane needs to make. If the billet rings are not placed horizontally when being lowered onto the ingots, it will be complicated to utilise a static guide system.

In terms of reliability, a purely mechanical solution to locking the rings into a horizontal position would be preferable. This would, however, be challenging to achieve, as the rings need to be oriented horizontally before being lowered onto the billets, and simultaneously be able to move freely after being lowered far enough onto the billets.

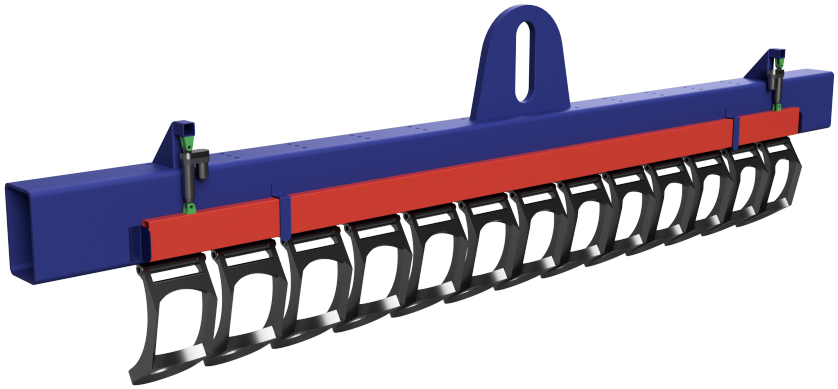

Figure 4.6: Proposed lifting yoke, equipped with billet ring V3 (un-actuated). An enlarged version is added in appendix A2.

With simplicity as a priority in the design process, a suggestion for levelling the billet rings when attaching the extrusion ingots, is simply adding one common linearly actuated beam to the rear side of the lifting yoke girder, as displayed in the figures 4.6 and 4.7. By pushing down on the stems of the lifting rings, all billet rings are swivelled into a horizontal position simultaneously. The nature and placement of the actuators are less important than the concept itself, and could also be solved through a bell crank [17] or a rack and pinion drive system [18] to relieve strain on the actuators. Figure 4.8a displays the state where the billet rings are swivelling freely and figure 4.8b displays the state where the actuated beam is lowered and the rings are oriented horizontally.

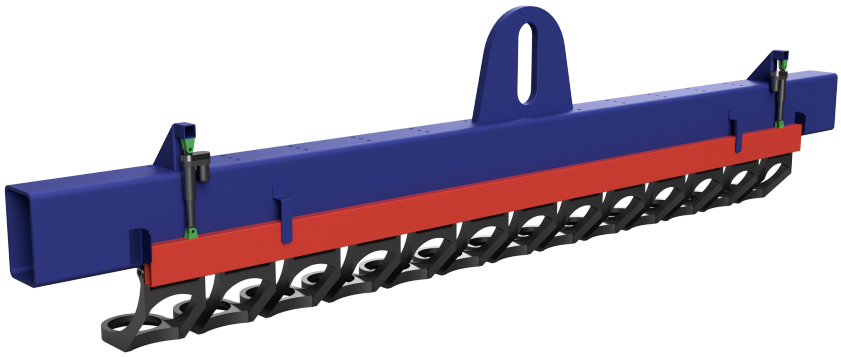

Figure 4.7: Proposed lifting yoke, equipped with billet ring V3 (actuated). An enlarged version is added in appendix A3.

Although this "push-bar" successfully changes the ring's orientation from $\sim 32°$ to $\sim 0°$ relative to the horizontal plane, it does not lock the ring joint for further forward motion. As addressed in chapter 4.2.2, it will therefore be beneficial to implement a similar push-bar to the front part of the ring stem, locking further forward motion as well.

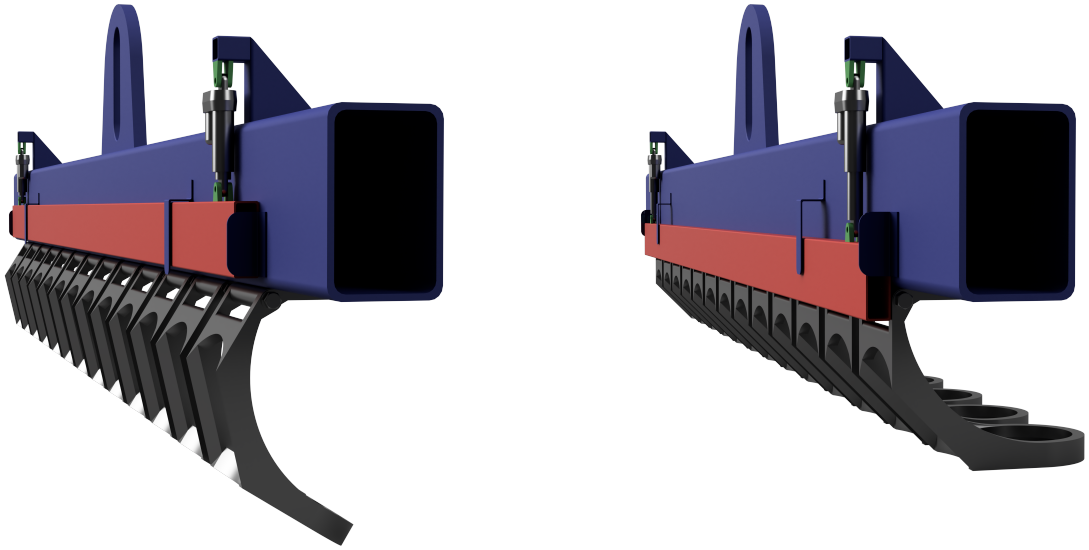

(a) Unactuated pushbar (b) Actuated pushbar

Figure 4.8: Proposed lifting yoke, equipped with billet ring V3. Enlarged versions are added in appendix A4.

Following the need for a push-bar for the front ring stem as well, basing the new yoke design on the one currently in place in Hydro Husnes (displayed in figure 3.3), instead of the one that is modelled, appears beneficial. As the frame of this lifting yoke is significantly thinner, the thickness of the lifting ring stem could be matched to the thickness of the yoke. When installing a push-bar on each side of the lifting yoke, the ring would then be completely locked into position.

4.3 Guide Cradles

As discussed at the beginning of this chapter (4), positioning the lifting yoke with less than $10mm$ precision and no oscillations is assumed to be a challenging task, regardless of instrumentation package and control system sophistication. In order to increase the positioning margins, it is therefore proposed to develop a guiding contraption, leading the lifting yoke into position above the extrusion ingots with high precision. This guide system needs to move in a translatory motion towards the extrusion ingots as they are being extracted, always positioned such that when the lifting yoke is lowered into the cradles, the billet ring will line up with the billets being extracted.

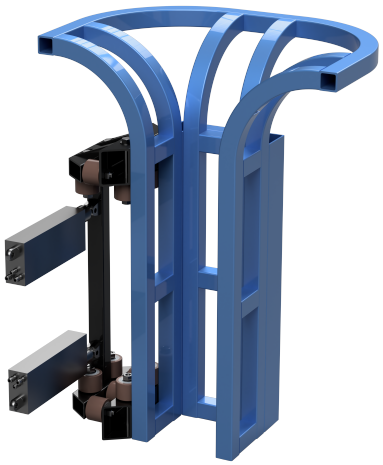

Figure 4.9: Guide cradle assembly. An enlarged version is added in appendix A5

As the casting pit's safety platform is already motorised, the proposed solution is to rebuild the safety railing attached to the safety platform and install a set of movable guide cradles to it. A design proposal for such cradles is displayed in figure 4.9. This design is purely a concept proposal and has not been dimensioned based on the forces that will be exerted on the assembly during guiding.

With a pair of these guide cradles, the positioning accuracy demand is limited to $\sim 20cm$ in the horizontal plane. This will allow for minor oscillations in the lifting yoke position, and still provide predictable results. As it is necessary to dislodge the billets from the starter blocks before extracting them from the pit, the guide cradles need to be retractable. In the proposed concept design, DC-motor linear actuators have been implemented for simplicity, but will probably not provide the best results in operation, in terms of reliability. A better solution could be a more rigid set of hydraulic cylinders or a rack and pinion drive system [18], as these would better withstand the forces from the lifting yoke colliding into the cradles.

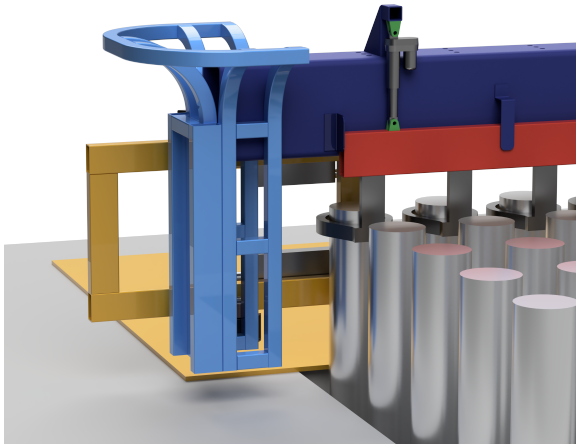

(a) Guide cradles positioned narrow to facilitate guiding of the lifting yoke when being lowered onto the extrusion ingots.

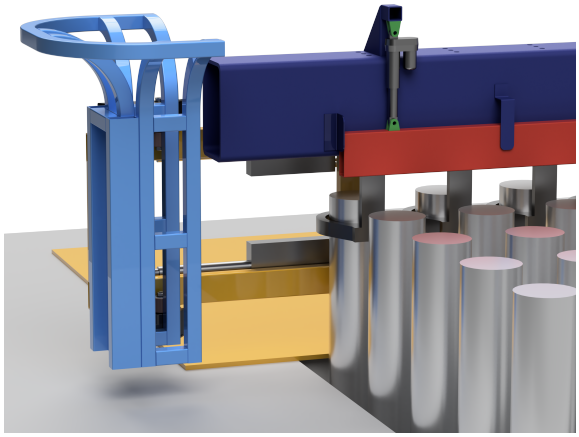

(b) Guide cradles positioned wide, so that the lifting yoke can be moved towards the safety railing for billet dislodgement before extraction.

Figure 4.10: Safety platform with retractable guide cradles.

As a precise model of the casting floor layout was not available during this solution's design process, the proposed design might collide with other safety railings in place. The proposal is however just a concept suggestion and will need further iterations before being implemented. The figures added to this chapter are furthermore based on the lifting yoke with a rectangular girder and the 2nd ring design revision. If the final lifting yoke will be based on the 3rd ring design proposal and the lifting yoke currently implemented in Casthouse Husnes, the cradle design will need to be revised regardless.

Figure 4.11: Overview of guide cradles mounted to safety platform

4.4 Billet Support Mesh

One way to remove the risk of all billets in the pit being knocked over due to the domino effect presented in section 3.5.1, could be implementing a re-bar mesh/wire grid inside the casting pit itself. It is worth mentioning that a comprehensive model of the casting pit has not been available when discussing this, and if it is practically implementable is uncertain based on current information. It has however been implemented successfully at other manufacturer's billet casting stations, and it might be beneficial to investigate if it could be implemented in Hycast's systems as well. An example of where such a grid has been implemented is shown in figure 2.5, where TC engineering's billet tong was discussed.

4.5 Lay-down Station

As the lay-down station has quite large margins in terms of extrusion ingot placement on the station itself, and as the system already has a high degree of automation, it is not foreseen that any significant modifications will need to be performed to this subsystem. It will however be necessary to incorporate the controls for the lay-down station in a higher level controls architecture, ensuring interplay between all the involved subsystems.

4.6 Overhead Crane

In order to facilitate the automatic extraction of extrusion ingots, the overhead cranes installed in Hydro's casthouses must be outfitted with sufficiently comprehensive instrumentation- and actuator packages. In generic robotic applications, the position and orientation of the robot's end-effector need to be determinable and controllable. In the case of automatic pit stripping and billet handling, the overhead crane is regarded as a robot manipulator, where the crane hook (or lifting yoke) represents the robot's end-effector.

Most of the overhead cranes installed in Hydro's casthouses are designed to be controlled by an operator that has a comprehensive visual overview of the situation at any given time. The need for sensors, to monitor the crane's position, has therefore been non-existing in the past. In robotic applications, it is, however, crucial to be able to determine the position and orientation of the different manipulator components, to achieve reliable and accurate operation.

The analysis of the crane installed at Casting Center no. 9 in Sunndal, carried out in section 3.1, is considered representative of most overhead crane installations. This section will provide a list of prerequisites for being able to automate an overhead crane, as well as concrete examples of sensors and actuators.

While automatic crane operation is the goal of this study, the system should not be modified to an extent where manual crane operations are no longer possible. In case of cast replacements, billet bleed-outs etc. the crane still needs to work like a normal manual overhead crane.

4.6.1 Actuators

A fundamental aspect of this study is discussing the feasibility of automatic pit stripping operation with only limited upgrades to the existing installations. To the extent where it is possible, the currently implemented actuators will therefore be used further. In the joints where the existing actuators are not adequate, or in the joints where no actuators are present, there will however be a need for certain upgrades.

4.6.1.1 Translatory Movement in the Horizontal Plane

Being able to control the speed and acceleration of the crane's bridge and trolley is considered a crucial factor in terms of positioning the crane hoist, and subsequently the lifting yoke's position and oscillations correctly. Not being able to control the speed and acceleration of the hoist trolley will in practice represent an on/off-controller that inherently generates oscillations in the lifting yoke's position. Controlling the speed of the drive motors is therefore regarded as a prerequisite for automatic operation.

In large, industrial overhead cranes, three-phase asynchronous AC motors are commonly implemented in the system for translatory movement of the crane bridge and trolley. The motors are in most cases connected to drive wheels through a gearbox that reduces the maximal rotational speed, while simultaneously increasing its momentum.

The speed of asynchronous AC motors is determined by the number of poles in the motor's stator and the frequency of the voltage applied to its windings. As the number of poles is static, the way of controlling the speed of the motor is by controlling the frequency of the voltage applied. This is achieved through a variable-frequency drive (VFD) [19], which is easily retrofitted to any three-phase asynchronous AC motor. If other types of motors are used for the crane bridge and trolley travel, other control units will need to be implemented, to achieve controllable speed and acceleration.

4.6.1.2 Hoist

As for the crane bridge and trolley travel, the acceleration and speed of the hoist itself would need to be controllable. Not being able to control the hoist speed will result in mechanical stress on the crane components because of the "jerks" generated when hoisting.

Crane hoists are often also equipped with three-phase asynchronous motors, that could be controlled by VFDs. The main difference between hoist motors and standard motors is however that hoist motors are equipped with brakes and in some cases also thermistors and other safety-related sensors.

4.6.1.3 Hook Block Rotation

When eliminating the operator from the pit stripping process, it becomes increasingly important to be able to monitor and control the angle of the lifting yoke (around the hoist wire axis) automatically. Although the guide cradles will compensate for some orientation errors, this is

limited to only a few degrees. In chapter 4.2.1, the problem of small rotations in the coupling "joint" between the lifting yoke and the hook was addressed and proposed solved through shaping the attachment point on the lifting yoke to match the shape of the hook. The current crane hooks are furthermore rotating freely around the vertical axis in the hook block. Locking this revolute joint is possible, but would not be a solution in the casthouses where the billet row needs to be rotated 90 degrees when put down at the lay-down station.

A motorised hook block would be the most flexible solution to this issue. With the crane in casting center no. 9 in Casthouse Sunndal as a reference, the hoist is constructed as an 8-wire system, providing a higher degree of torsional rigidity than a system with fewer wires. A lifting yoke, or especially a hydraulic billet tong, would however have a high moment of inertia, and controlling the lifting yoke's orientation would have to be done using a non-aggressive controller to avoid twisting the hoist wires. Relevant instrumentation and control strategies will be discussed in chapter 4.6.2.3.

Figure 4.12: Motorised hook block [20].

4.6.2 Instrumentation

In the introduction to this chapter, it was noted that overhead cranes designed for operator control often lack advanced instrumentation. A broader range of instrumentation is however essential for automatic operation, and for an overhead crane this in essence means being able to determine the crane hook's position and orientation in space, as well as monitoring the various joints on the crane to optimise movement. The following table and figure provide an overview of the most important variables to monitor.

Var.	Explanation	Comment
x_h	Bridge position	Referenced to hoist centre
y_h	Trolley position	Referenced to hoist centre
l	Wire length	Referenced to Hook Centre
α	Wire rope angle	Between the hoist wire projection onto the xz-plane and the hoist wire
β	Wire rope angle	Between the z-axis and the hoist wire projected onto the xz-plane
γ	Hook orientation	Relative to the inertial frame measured around the z-axis
m	Load mass	Total mass of load, including hook block, for predicting dampening of oscillations etc.

Table 4.1: Instrumentation prerequisites for automatic control.

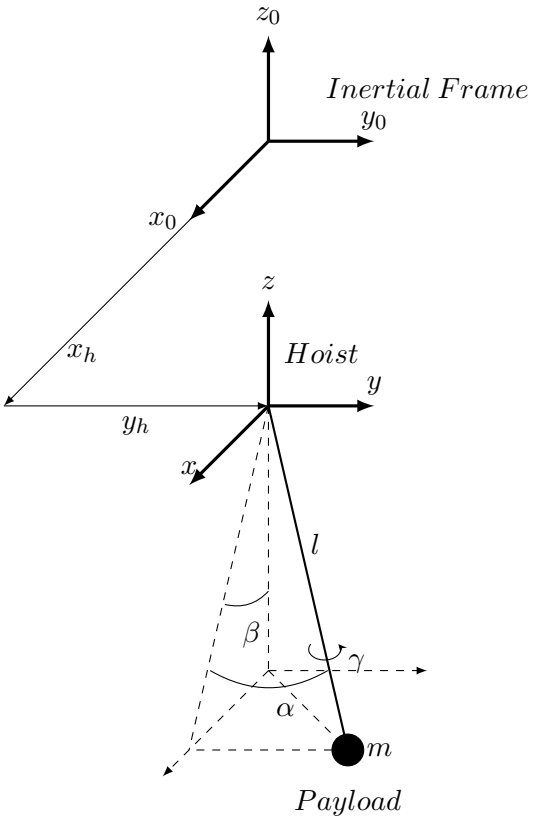

Figure 4.13: Variable placement illustration of overhead crane for automatic control.

From the variables provided in the table above, the crane hook's position and orientation can be derived using basic trigonometry.

4.6.2.1 Trolley Positioning in the Horizontal Plane ($\mathbf{x_h}$ & $\mathbf{y_h}$)

As the hook block position is subject to time delay and oscillations due to the hoist wire's inherent pendulum dynamics, monitoring the hoist's position in the horizontal plane gives a better basis for controlling the hook block's position. Monitoring the hoist's position in the

horizontal plane could be achieved through a broad range of measurement strategies, but should be performed in a way providing robustness and accuracy.

One broadly implemented solution for measuring movement, both in general robotic applications and in overhead cranes, is the implementation of rotary encoders. Both incremental and absolute rotary encoders would provide accurate results but would rely on calibration at given intervals to avoid errors. The rotary encoder would then either be mounted to the drive wheels running along the rails, or to a separate positioning wheel. A linear encoder is a different solution and exists both as magnetic encoders [21] and vision-based encoders. However, these particular encoders lack tolerance for sudden movements, such as jerks or sliding between the rails and the trolley, resulting in inaccurate positioning. This needs to be considered when choosing the type of instrumentation.

Another approach to accurately positioning the crane bridge and trolley is through industrial range lasers. This type of solution is implemented by manufacturers such as Rockwell Automation and is reported as highly reliable. The accuracy given by these types of sensors is also very high, often with a resolution of 1 mm and an accuracy of $\pm 3mm$ [22]. A laser solution is also relatively easy to duplicate to ensure redundancy. To measure the position in the x direction, a laser can be placed on the bridge girder and positioned towards a fixed object. The same principle can be applied to the trolley to measure the position in the y direction.

If range lasers are to be used in industrial environments, it would be beneficial to install a dust cap above, reducing the probability of inaccurate readings due to dust.

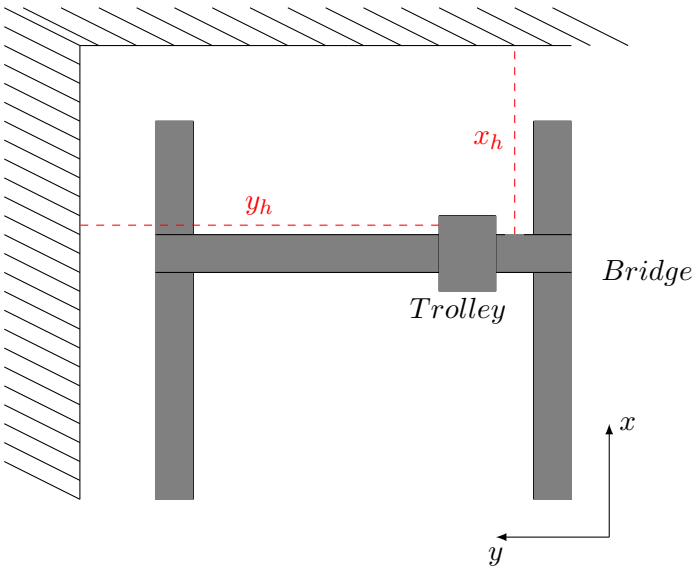

Figure 4.14: Bridge and trolley positioning through laser distance sensors.

4.6.2.2 Hoist Wire Angle (α & β)

Determining the angles of the hoist wire, denoted by α and β in the explanatory figure next to table 4.1 is considered challenging for a number of reasons.

Although a highly accurate gyroscope (Angle Measurement Unit) could have been mounted to the static end of the hoist wires, the hoist length and the relatively small pendulum motions in this system could lead to the measurement errors being greater than the value being monitored, and could again lead to inaccurate and unpredictable results.

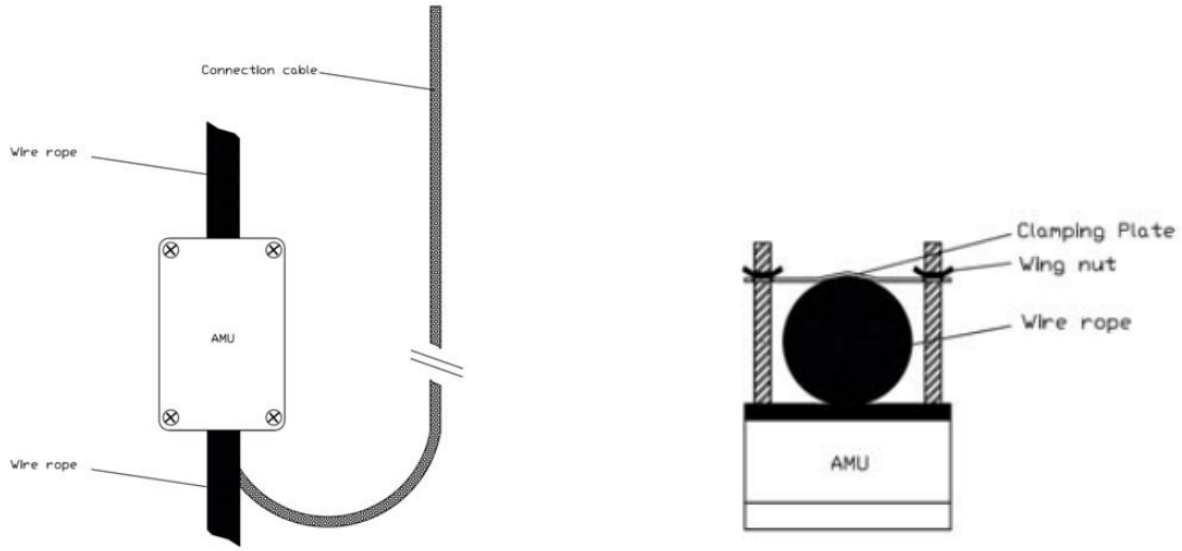

(a) AMU mount front view.

(b) AMU mount top view.

Figure 4.15: AMU - Angle Measurement Unit [23].

One challenge with using a gyroscope to determine the payload angle is the hoist construction. As the hoist's anchoring points on the crane trolley are positioned wider than the pulley diameter in the hook block, the hoist wire angle will always differ from 0° in an equilibrium position and change based on the length of the hoist wire. This problem could be solved by monitoring the angle of the moving hoist wires as well as the static ones and subtracting the difference between the two measurements. Achieving reliability could however be an issue as the gyroscope monitoring the angle of the moving wires could not be attached to the wires themselves.

Furthermore, the hoist wire cannot be regarded as a rigid body and might have a greater angular deviation close to the hook block than in close proximity to the hoist.

In the two casting centers in Casthouse Sunndal, the crane trolley is located approximately 15 meters above ground level. With a 15m pendulum, a lifting yoke misplacement of, for instance, 10 cm would result in an angular offset of:

$$\begin{aligned} \theta &= asin\left(\frac{0.1m}{15m}\right) \\ &= 0.38^\circ \end{aligned} \tag{4.1}$$

Even small deviations in the measured hoist wire angle could then result in poor system performance.

Vision-based control has been used in industrial robot applications for decades. In assembly lines, where robots need to use vision-based controls, the environment surrounding the objects is normally constructed to create a large contrast between the object and the background. By constructing a noise-free environment around the object, the task of classifying the object can be performed by a simple algorithm. However, in visually noisy environments, like those in Hydros casthouses, complex machine learning algorithms would be required to distinguish the different crane components from the background and determine their orientation and position in space.

One way of increasing the reliability of vision-based control in such applications is to utilise a motion capture system based on infrared cameras and reflective markers, optimised for reflecting a certain wavelength in the infrared spectre. Although this technology was previously mostly used in the movie industry, it has become increasingly common to implement in robotic applications and UAVs manoeuvring in spaces without GPS signals.

In 2016, a paper on using a motion capture system to control a UAV in a space without GPS reception was published in conjunction with the 2016 5th International Conference on Electronic Devices, Systems and Applications (ICEDSA) [24]. In this case, motion capture markers were mounted to a UGV. The position and orientation were then detected by a Vicon motion capture camera system and used to set a position reference for the UAV, also equipped with markers, to hover over.

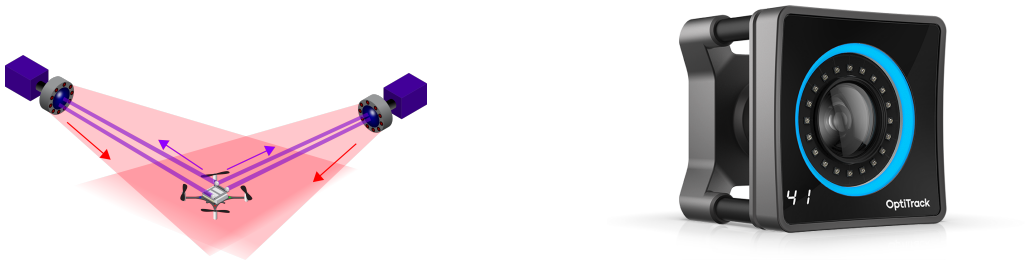

(a) Motion capturing principle [25]. (b) *OptiTrack* $PRIME^X$ 41 [26].

Figure 4.16: Motion capture camera systems.

Another example of use in robotics is from 2022 where Shane Wighton constructed a moving basketball hoop that ensured that wherever a basketball was thrown within a certain space, the hoop would move in order to interpolate the trajectory of the ball. [27]. In this project, eight IR cameras from OptiTrack were mounted to the walls of a small warehouse and tracked the movement of an array of IR markers integrated in a basketball.

Although costly, the system is an easily expandable platform that can be used to monitor a range of variables, by simply adding IR markers to the relevant bodies and arranging them in groups in the software. In an overhead crane, the camera system could first and foremost provide data on the crane's hoist wire angles, but could furthermore be expanded to monitoring, for instance, the orientation of the lifting yoke around the vertical axis (yaw), relative to the ingot row. This would easily be achieved by installing a row of IR markers on top of the lifting yoke, as well as on the sides and top of the hook block and right below the centre of the hoist wire attachment

points. Using the manufacturer OptiTrack as an example, given a $9m \times 9m$ space, their most advanced camera system is able to determine an IR marker's position in space with an accuracy of $\pm 0.10mm$ [26]. Although the casting centers in Hydro's casthouses are larger than this, such a high degree of precision is not required.

In the case of complex control strategies, this system will also be capable of precisely monitoring the roll and pitch of the lifting yoke, the orientation of the different lifting rings, the twist in the hook block and hoist pulley system etc.

As the hoist position is already known, the camera system could be mounted to either the crane bridge, giving information on the marker's position in space relative to the bridge, rather than their absolute position in space. This would reduce the size of the camera system needed.

It is worth mentioning that this kind of instrumentation will mainly be required for advanced positioning and anti-sway control.

4.6.2.3 Lifting Yoke Orientation (γ)

Under the assumption that there is no rotation in the coupling between the crane hook and the lifting yoke attachment point, the angle of the lifting yoke relative to the hook will equal zero. With a motorised hook joint, the angle of the lifting yoke relative to the hook block is determined by the orientation of the hook in the hook block. Monitoring the angle of the crane hook relative to the hook block could be solved easily by mounting an absolute encoder to the hook and hook block.

This measurement will however only represent the hook's (and thereby also the lifting yoke's) angle relative to the hook block. The absolute orientation of the lifting yoke (relative to the crane trolley) is however unknown due to a certain degree of twist in the 8-wire hoist pulley system.

If a motion capture camera system is installed on the crane to determine the wire rope angle and the hook block's absolute position, IR markers could furthermore be installed on the extremities of the lifting yoke. This would facilitate the reading of the lifting yoke's orientation in space.

If both the lifting yoke's absolute orientation in space is known, as well as its orientation relative to the hook block, a control system should be able to efficiently control the lifting yoke orientation without torsional oscillations.

4.6.2.4 Hoist Wire Length (l)

Measuring the length of the hoist wire is important for several reasons. First and foremost, knowing the hoist wire length is crucial in positioning the crane hook and subsequently the lifting yoke correctly in three-dimensional space. It is furthermore important to know the length of the hoist wire to be able to predict the pendulum frequency of the payload.

For measuring the hoist travel, and in essence, the position of the hook block and lifting yoke, a rotary encoder mounted to the hoist drum is proposed. This will then be redundant to any readings provided by a potential motion capture camera system.

4.6.2.5 Payload Mass (m)

Being able to determine the mass of the load attached to the hoist is first and foremost a safety feature, ensuring that the crane is not loaded beyond its capacity. Secondly, knowing the mass of the load will heuristically provide information on the moment of inertia in the system, given that the general shape of the load is known. This would again be beneficial for a yoke orientation control system. Finally, knowing the mass of the load will give some information on how much time residual oscillations will need to die out, as the dampening coefficient is reduced when the mass increases.

Being able to determine the mass of the load might furthermore assist in error detection in the billet attachment process. Given that the billet rings are locked into position and cannot swivel freely, some of the lifting yoke mass will then rest on any extrusion ingot that does not enter the billet ring correctly.

The cranes in the casthouse in Sunndal are equipped with load cells. For cranes not equipped with load cells, these could be mounted between the hoist construction and the trolley construction of a crane.

4.6.2.6 Redundancy and Detection of Faulty Measurements

In all disciplines of engineering, the "fail to safe" principle is considered fundamental in the development of equipment that has the potential to harm either individuals or the environment it operates in. Essentially, this principle prioritises safety above all other aspects and designs that fulfil the "fail to safe" principle will not represent a danger, even when the system fails.

An automatic overhead crane potentially represents a risk to both individuals and its environment in case of a system failure, in case such failures are not detected and handled in a safe manner. In case of failing instrumentation, the crane is no longer able to correctly orient itself in space and might behave unpredictably.

Redundant instrumentation through duplicated sensors is a relatively cost-effective way of detecting failures and discrepancies in the system's sensory data. An example of critical parts of this system's instrumentation is the range lasers providing information on the crane hoist's position in the horizontal plane. If two range lasers are installed for each of the two measurements, the difference in the two measured signals provides information on the state of the sensors. If the measurements from the two sensors are identical, it is reasonable to assume that both sensors are intact. However, if one of the sensors at some point stops updating its values during travel, the system is still able to read its position from the sensor providing updated readings. Simultaneously, the control system can rise a flag requiring a service inspection before further operation to avoid catastrophic failures.

Applying redundant instrumentation in all critical measurements, where it is reasonably implementable, is, therefore, an approach that is considered to minimise the risk of catastrophic failures at a low cost.

4.7 Control System

The different subsystems playing a role in the pit stripping process, are all standalone systems that do not interact with the others. Automating the pit stripping process, therefore involves incorporating all these subsystems in a higher-level control framework. Centralising the control logic for the different sub-systems would furthermore make more data available to the top-level control system and make software upgrades simpler, as most of the software would be gathered in one common unit.

As Hydro casts extrusion ingots in a range of dimensions, the amount of ingots, as well as their placement in the casting pit varies. The system behaviour, therefore, needs to be defined for all casting dimensions, including guide cradle placement, crane trajectories etc.

4.7.1 Manual Control

Although the goal for this upgrade is achieving automatic pit stripping operation, the different subsystems still need to be manually controllable after the upgrade. This is both to be able to handle faulty situations in operation, but also because some of the sub-systems are used for more than just the pit stripping process itself.

When changing between extrusion ingot dimensions, the crane is for instance used to replace both the starter blocks and the cast itself, and as this operation is initially not foreseen automated, the crane needs to remain possible to run in manual mode. Furthermore, in case of billets falling over in the pit, each extrusion ingot will need to be extracted individually.

A commonly implemented solution for ensuring that a system is not suddenly starting automatically during manual operation is a single lockable switch changing between local and remote operations.

4.7.2 Automation Hardware

The control hardware architecture for such a large system could be solved through a number of different strategies. In the past, a common strategy has been designing centralised control systems, where all automation hardware has been located in one large control cabinet. This would require a significant amount of control cables running to the different sub-systems and could result in a signal loss in the case of long cables. In the case of automatic pit stripping, such a solution would require large control system modifications. A different solution that has become increasingly common with bus-based communication is the implementation of decentralised/deported IO-units, connected to a central processing unit (CPU) through for example Industrial Ethernet, PROFIBUS or PROFINET. Using this approach, the only additional control hardware installation required would be running bus cables from a small centralised control cabinet containing the CPU, to the existing control cabinets for the different subsystems. Bus-based IO modules would furthermore need to be integrated into the existing control cabinets.

Siemens provides decentralised IO solutions, and Python libraries for communication between

a computer and a Siemens CPU already exist [28]. Through discussions with automation technicians in Vik Ørsta AS, Beckhoff's TwinCat system has also come up as a potential solution for controlling PLC-based IO systems from a centralised computer, enabling both Matlab, Simulink and C++ control [29].

4.7.3 Automation Software

Although it might be possible to construct such a control system using only classical PLC programming, it is regarded as an inflexible solution and might be labour-intensive to develop. It is therefore assumed beneficial to develop the top-level control system in a robotics framework like ROS or at least with a high-level programming language, like for example Python, C++, or even Matlab. In the case of complex control strategies, demanding a high degree of processing power, it would especially be beneficial to have more computational power available than what is available in a PLC.

4.8 Proposed Pit Stripping Sequence

Once the billet casting process has finished, the extrusion ingots will be cooled down while operators are preparing equipment for the next cast. The following sequence displays the proposed billet attachment operation. Note that the figures in this sequence are based on the 2nd billet ring iteration instead of the 3rd, as the guide cradles have not been adapted to fit the 3rd billet ring version. This sequence is however only aiming to display the operational principle and would be similar regardless of yoke, ring and cradle design.

When extracting a new row of billets, the lifting yoke is first put into position above the guide cradles mounted to the safety platform. The platform is positioned such that when the lifting yoke is lowered into the cradles, the billet rings will be threaded onto the extrusion ingots. The cradles are positioned in the narrow position

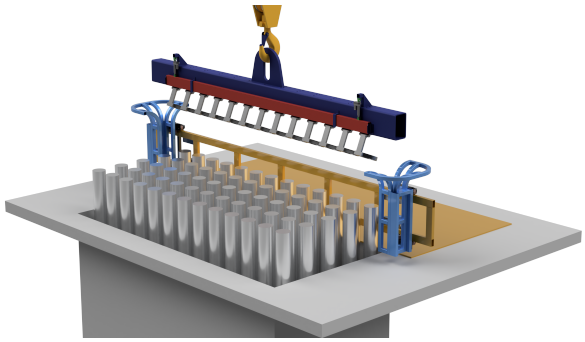

Figure 4.17: Yoke positioning above cradles.

Before the lifting yoke is lowered into the guide cradles, the linear actuators at the back of the lifting yoke are fully extended, resulting in the red push-bar being pushed down and swivelling the lifting rings into horizontal position. This enables simple threading of the extrusion ingots.

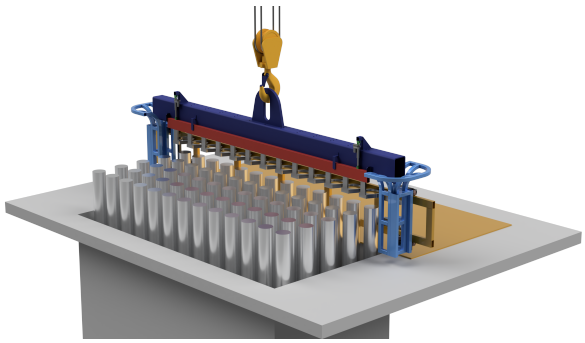

Figure 4.18: Accurate positioning with guide cradles.

When the oscillations in the position of the lifting yoke have reached an adequate level, the lifting yoke is lowered into the cradles. Given that all billets are positioned within the defined limits, the rings will be threaded onto the extrusion ingots

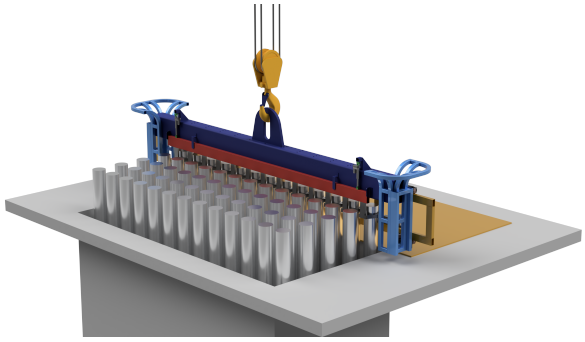

Figure 4.19: Threading billet rings onto the extrusion ingots.

Once the billet rings are threaded far enough down the extrusion ingots, the guide cradles are driven to the widest position and the push-bar on the back of the lifting yoke is retracted, allowing the billet rings to swivel freely. The crane is then pulling the lifting yoke towards the safety platform, dislodging the extrusion ingots from their starter blocks.

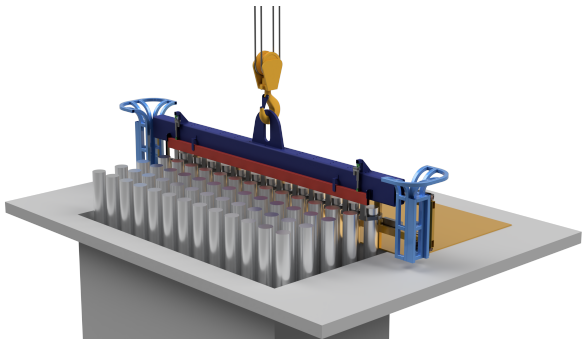

Figure 4.20: Cradle removal and ingot dislodgement.

Once dislodged from the starter blocks, the crane will hoist the extrusion ingots to a height, sufficient to clear all objects in its trajectory. The billets will furthermore be transported to the lay-down station and be prepared for homogenisation.

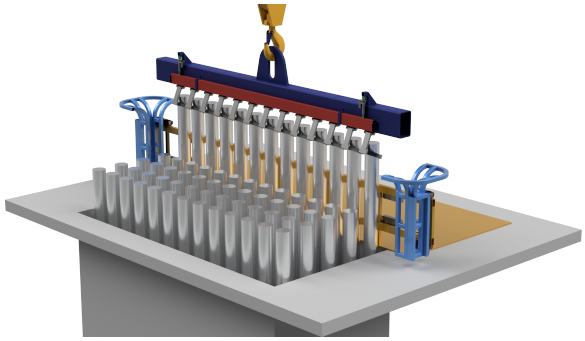

Figure 4.21: Extrusion ingot extraction from pit.

4.9 Safety Measures in Automatic and Robotic Application

Although the human safety aspect of automating such a system is generally disregarded in this thesis, due to its complexity, it is worth mentioning that automatic crane operation will demand strict safety measures. On par with other industrial, non-collaborative robots, the area in which the robot (crane) is operating, would need to be blocked from human access. Using Casthouse Sunndal as an example, the extrusion ingot transportation is done through a transport zone, a walking zone and in areas where people might be present. This entire area would probably need to be fenced off when the crane is operating to avoid potentially hazardous situations and ensure a safe working environment.

Flexibility could however be increased by dividing the crane's operation area into smaller zones,

for instance, one zone for the lay-down station, one zone for the casting pit and one zone for the transport area in between. The crane would then not be allowed to enter a zone where people or objects are detected, or where the entrances to that zone are not closed off. An automatic gate could for instance be added to each side of the cell containing the transportation zone.

The gates could normally be open but would close when automatic crane operations were being performed. A system for requesting passage through the cell during lifting operations could furthermore be implemented, where a button could be pushed, requesting the cell to open once the crane is operating in a different zone. If, for instance, the crane is working on attaching a new row of billets, there is no reason why the transportation zone should not be possible to open. If the transportation zone is opened during the attachment of billets, the crane could be programmed to not lift the billets out of the pit before the transportation zone once again was closed and no people or objects are detected within the zone.

Chapter 5

Theoretical Framework

This chapter will present the theoretical framework necessary to understand the work in this thesis. It will only be presented abstractly and will be utilised in the different chapters of this thesis.

5.1 Robot Manipulators

A robot manipulator is a kinematic chain and consists of joints, links, actuators, and end effectors. Joints are where the links of the robot meet, and are what allow for movement in the robotic manipulator. Common robotics joints are prismatic joints, allowing for linear motion, or revolute joints allowing for rotational motion. The manipulator links are the rigid bodies that are connected through joints, and might vary in shape and size depending on the properties of the robot. Actuators are components that apply the necessary forces to move the robotic joints. Some common kinds of actuators are electric, pneumatic, or hydraulic actuators. What kind of actuator is chosen for a robot depends on the precision and force required for its task. The end effector is the tool at the end of the robot that enables it to carry out its task. End effectors can vary from robotic fingers to welding torches and even leaf blowers.

5.2 Kinematics

"Kinematics is the study of the motion of mechanical points, bodies and systems without consideration of their associated physical properties and the forces acting on them" [30]. In robotics, kinematics can be used to describe how a robotic manipulator is positioned and oriented in space through relationships between coordinate frames.

5.2.1 Forward Kinematics

Forward kinematics considers the problem of determining the position and orientation of a manipulator end effector, based on knowledge about its links and joint configurations. By attaching coordinate frames to each of the manipulator's links, the relationships between the links can be expressed as homogeneous transformations between these frames. A homogeneous transformation matrix can be written as

$$H = \begin{bmatrix} R_n^0 & o_n^0 \\ 0 & 1 \end{bmatrix} \tag{5.1}$$

where R_n^0 is the rotation of coordinate frame n with respect to the inertial frame and o_n^0 is the distance from the origin of the inertial frame, o_0, to the origin of the n^{th} frame o_n. H, in sum, describes the end effector's position and orientation with respect of the inertial frame. A standard

practice in robot modelling is to use the Denavit-Hartenberg convention when attaching these coordinate frames to a manipulator links.

5.2.1.1 Denavit Hartenberg Convention (DH)

The Denavit Hartenberg convention provides a systematic procedure for computing forward kinematic equations [31]. Kinematic analysis can be complex, and DH gives rise to a universal language between engineers. First, each homogeneous transformation A_i can be represented by four successive basic transformations

$$A_i = Rot_{z,\theta_i} Trans_{z,d_i} Trans_{x,a_i} Rot_{x,\alpha_i} \tag{5.2}$$

where

$$\begin{aligned} Rot_{z,\theta_i} &= \begin{bmatrix} \cos\theta_i & -\sin\theta_i & 0 & 0 \\ \sin\theta_i & \cos\theta_i & 0 & 0 \\ 0 & 0 & 1 & 0 \\ 0 & 0 & 0 & 1 \end{bmatrix}, Trans_{z,d_i} = \begin{bmatrix} 1 & 0 & 0 & 0 \\ 0 & 1 & 0 & 0 \\ 0 & 0 & 1 & d_i \\ 0 & 0 & 0 & 1 \end{bmatrix} \\ Rot_{x,\alpha_i} &= \begin{bmatrix} 1 & 0 & 0 & 0 \\ 0 & \cos(\alpha_i) & -\sin(\alpha_i) & 0 \\ 0 & -\sin(\alpha_i) & \cos(\alpha_i) & 0 \\ 0 & 0 & 0 & 1 \end{bmatrix}, Trans_{x,a_i} = \begin{bmatrix} 1 & 0 & 0 & a_i \\ 0 & 1 & 0 & 0 \\ 0 & 0 & 1 & 0 \\ 0 & 0 & 0 & 1 \end{bmatrix} \end{aligned} \tag{5.3}$$

With matrix multiplication, the following homogeneous transformation matrix can be computed

$$A_i = \begin{bmatrix} \cos(\theta_i) & -\sin(\theta_i)\cos(\theta_i) & \sin(\theta_i)\sin(\alpha_i) & a_i\cos(\theta_i) \\ \sin(\theta_i) & \cos(\theta_i)\cos(\alpha_i) & -\cos(\theta_i)\sin(\alpha_i) & a_i\sin(\theta_i) \\ 0 & \sin(\alpha_i) & \cos(\alpha_i) & d_i \\ 0 & 0 & 0 & 1 \end{bmatrix} \tag{5.4}$$

θ_i, a_i, d_i and α_i are parameters associated with the link i, and defines the link length, link twist, link offset and joint angle, respectively. These parameters are defined using the following conventions.

a_i = Distance of link, distance along x_i from the intersection of x_i and z_{i-1}.
d_i = Distance of link, distance along z_i from o_{i-1} to the intersection of the x_i and z_i axes.
α_i = Angle of rotation, angle from z_i to z_{i-1} measured about x_i.
θ_i = Angle of rotation, angle form x_i to x_i measured about z_i.

The DH convention table can then be constructed

Link	$\mathbf{a_i}$	$\alpha_\mathbf{i}$	$\mathbf{d_i}$	$\theta_\mathbf{i}$
1	a_1	α_1	d_1	θ_1
2	a_2	α_2	d_2	θ_2
3	a_3	α_3	d_3	θ_3
...	...	...	...	...
n	a_n	α_n	d_n	θ_n

Table 5.1: DH parameters for a given kinematic chain.

When analysing a manipulator following the DH convention, two additional constraints needs to be met, in order to express the transformation in the form of equation (5.4).

$DH1 =$ The axis x_n is perpendicular to the axis z_{n-1}
$DH2 =$ The axis x_n intersects z_{n-1}

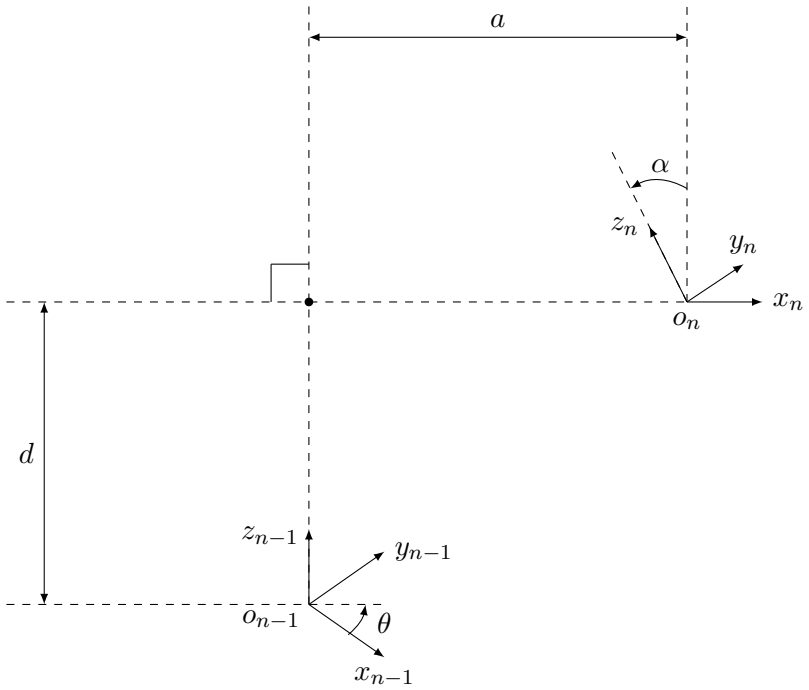

Figure 5.1: DH1 and DH2 satisfied coordinate frames.

Furthermore, the position and orientation can be given by the product

$$H = T_n^0 = A_1(q_1) \dots A_n(q_n) \tag{5.5}$$

5.2.2 Inverse Kinematics

Inverse kinematics aims to solve the opposite problem of forward kinematics, namely where the position and orientation of a manipulator's end effector is known, but the manipulators joint configuration is unknown. In robotics engineering, solving this problem is essential for trajectory planning, and provides joint configurations resulting in a requested end effector position and

orientation. Inverse kinematics are notoriously complex to compute, as the calculations result in a large number of unknown variables.

To explain inverse kinematics, a general problem can be considered. Given a 4×4 homogeneous transformation matrix

$$H = \begin{bmatrix} R & o \\ 0 & 1 \end{bmatrix} \in SE(3) \tag{5.6}$$

the joint configurations can be calculated through solving the equations

$$T_n^0(q_1, \ldots, q_n) = H \tag{5.7}$$

where

$$T_n^0(q_1, \ldots, q_n) = A_1(q_1) \ldots A_n(q_n) \tag{5.8}$$

The joint configurations are then given as the variables $q_1, \ldots, q_n$ which gives the specified transformation matrix H.

5.3 Trajectory Planning

Trajectory planning considers the problem of finding a time series of successive joint configurations that moves a manipulator's end effector from an initial position towards a goal position. To be able to do this, the robot must be given some constraints. Joint angles, velocities, and accelerations should be within specified limits, the robot should avoid objects and the robot should not be outside its physical configurations area. When the time series is computed the robot should also consider other aspects, like time execution and energy consumption, and optimise such objectives.

5.3.1 Trajectories for Point-to-Point Motion

Point-to-point motion path planning generates a curve that can be used as a reference signal for a robot manipulator. Point-to-point path planning generates a specified path with a sequence of configurations that the manipulator will have to pass. Each point can also be determined with specific constraints for velocity and acceleration. A path can be generated with either a single polynomial or a sequence of interpolating polynomials.

Generating a path with a single polynomial is good because the signal is continuous, but if the path has many points, the order of the polynomial will be large. This makes it hard to calculate and gives problematic oscillations.

Generating a path as a sequence of interpolating polynomials is easier. With cubic polynomials, every point has constraints to velocity, and they are easy to make continuous. Such polynomials are never higher than 3. order, but each segment is only valid from the time determined when calculating the path.

Given constraints to time, position and velocity, each point is given as

$$p_n = (t_n, q_n, v_n) \tag{5.9}$$

A cubic polynomial from p_n to p_{n+1} can then be generated as

$$q(t, t_n) = a_0 + a_1(t - t_n) + a_2(t - t_n)^2 + a_3(t - t_n)^3 \tag{5.10}$$

This polynomial gives a continuous path for the actuator to follow within the time frame given. The a-coefficients are calculated as:

$$\begin{aligned} a_0 &= q_n \\ a_1 &= v_n \\ a_2 &= \frac{3(q_{n+1} - q_n) - (2v_n + v_{n+1})(t_{n+1} - t_n)}{(t_{n+1} - t_n)^2} \\ a_3 &= \frac{2(q_n - q_{n+1}) + (v_n + v_{n+1})(t_{n+1} - t_n)}{(t_{n+1} - t_n)^3} \end{aligned} \tag{5.11}$$

5.4 Dynamics

5.4.1 Newtons' Laws of Motion

Newton's laws of motion are three equations that describe the forces acting on a physical object [32]. They were first described by Sir Isaac Newton and are the basis for classical mechanics. The three equations were paired with statements explaining them:

$$\Sigma F = 0 \tag{5.12}$$

$$F = ma \tag{5.13}$$

$$F_a = -F_b \tag{5.14}$$

Newton's first law states that a body in motion will stay in motion unless a force acts upon it, 5.12. Newton's second law states that the force acting on an abject is equal to its mass times acceleration, 5.13. Newton's third law states that when object A exerts a force upon object B, object B exerts an equal and opposite force on object A, 5.14 [32].

5.4.2 Simple Pendulum in Space

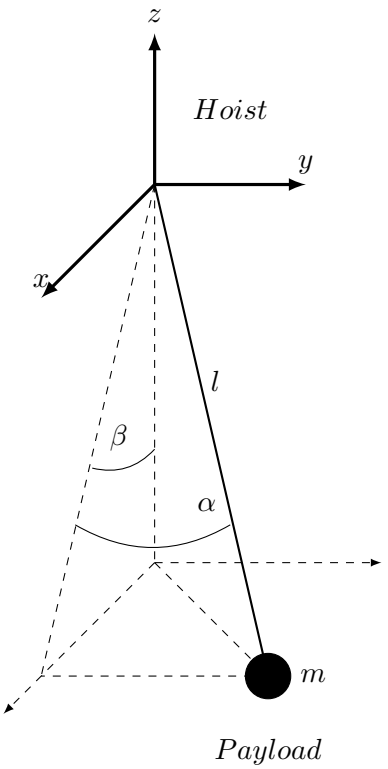

Figure 5.2: Simple pendulum in space.

A pendulum is a classical subject of analysis in mechanical physics. This system consists of a fixed point, a massless cord and a mass attached to the cord. When the pendulum is displaced from its equilibrium position, the force of gravity will accelerate the mass towards its equilibrium position. This will cause oscillations around the equilibrium position, also called sway. T can be expressed as the time constant of an oscillation cycle

$$T \approx 2\pi\sqrt{\frac{l}{g}} \tag{5.15}$$

and can be used to find the frequency of the oscillations.

$$f = \frac{1}{T} \tag{5.16}$$

Physical pendulums are subject to friction, and their amplitude and cycle time will decay over time. To calculate the position of the mass in the coordinate frame of figure 5.2, one can utilise trigonometry as follows.

$$\begin{aligned} x_m &= l\sin(\beta)\cos(\alpha) \\ y_m &= l\sin(\alpha) \\ z_m &= -l\cos\beta\sin(\alpha) \end{aligned} \tag{5.17}$$

5.4.3 Lagrange's Approach

The computations and information presented in this section regarding robot modelling and dynamics are collected from Spong's, Hutcinson's and Vidyasagar's book [31]. Some information is also collected from William's thesis [33].

The Lagrange's equation is used to solve dynamic problems with certain constraints. The Lagrangian is defined as

$$\mathcal{L} = \mathcal{K} - \mathcal{P} \tag{5.18}$$

where $\mathcal{K}$ is total kinetic energy and $\mathcal{P}$ is the potential energy of the system, and $\mathcal{L}$ is the Lagrangian [34]. The kinetic energy depends on the generalised velocities $\dot{q}_n$, and may be written $\mathcal{K} = \mathcal{K}(\dot{q}_1, \dot{q}_1, \dot{q}_1, \ldots, \dot{q}_n)$, and the potential energy may be written as $\mathcal{P} = \mathcal{P}(q_1, q_2, q_3, \ldots, q_n)$, where q_n are the generalised coordinates. From Newton's law only, it is possible to derive Lagrange's equation

$$\frac{d}{dt}\left(\frac{\partial \mathcal{L}}{\partial \dot{q}_i}\right) - \left(\frac{\partial \mathcal{L}}{\partial q_i}\right) = \mathcal{Q}_i \quad i = 1, \ldots, n \tag{5.19}$$

where $\mathcal{Q}_i$ is the generalised force associated to link i.

5.4.3.1 Kinetic Energy

The combined kinetic energy of an n-link manipulator can be expressed as the aggregate of the kinetic energy associated with each individual link.

$$\mathcal{K} = \sum_{i=1}^{n} \mathcal{K}_i \tag{5.20}$$

The individual kinetic energy associated with each link is a sum of two terms, the translational kinetic energy and the rotational kinetic energy, and can be expressed as

$$\mathcal{K}_i = \frac{1}{2} m_i v_i^T v_i + \frac{1}{2} \omega^T \mathcal{I} \omega_i \tag{5.21}$$

where m_i is the mass of the object, v_i is the velocity matrix, ω_i is the angular velocity and $\mathcal{I}$ is the Inertia tensor, a 3×3 symmetric matrix [31]. The Inertia tensor matrix can be expressed as

$$\mathcal{I}_i = R I_i R^T \tag{5.22}$$

where R is the rotation matrix of the rigid body and I is the inertial tensor matrix in the original coordinate system. Linear and angular velocities can be expressed by Jacobian matrices and the derivatives of the joint variables

$$v_i = J_{v_i}(q)\dot{q}, \quad \omega_i = J_{\omega_i}(q)\dot{q} \tag{5.23}$$

where the dimension of the matrices is $3 \times n$. Then the kinetic energy of a manipulator i can be expressed as

$$\mathcal{K} = \frac{1}{2}\dot{q}^T \left[\sum_{i=1}^{n} \{ m_i J_{v_i}(q)^T J_{v_i}(q) + J_{\omega_i}^T R_i(q) I_i R_i(q)^T J_{\omega_i}(q) \} \right] \dot{q} \tag{5.24}$$

Equation (5.24) can be simplified as

$$\mathcal{K} = \frac{1}{2}\dot{q}^T M(q) \dot{q} \tag{5.25}$$

where

$$M(q) = \left[\sum_{i=1}^{n} \{ m_i J_{v_i}(q)^T J_{v_i}(q) + J_{\omega_i}^T R_i(q) I_i R_i(q)^T J_{\omega_i}(q) \} \right] \tag{5.26}$$

5.4.3.2 Potential Energy

The combined potential energy of an n-link manipulator can be expressed as the aggregate of the kinetic energy associated with each individual link.

$$\mathcal{P} = \sum_{i=1}^{n} \mathcal{P}_i \tag{5.27}$$

The potential energy of link i can be computed by

$$\mathcal{P}_i = m_i g^T r_{ci} \tag{5.28}$$

where g is the vector associated with gravity and r_{ci} is the coordinates of the link centre of mass. Then the potential energy of a manipulator i can be expressed as

$$\mathcal{P} = \sum_{i=1}^{n} m_i g^T r_{ci} \tag{5.29}$$

5.4.3.3 Equations of Motions

To compute the equations of motion we can specialise the Lagrange equation presented in section (5.4.3). First, we can express the kinetic energy as a quadratic function of $\dot{q}$ of the form

$$\mathcal{K} = \frac{1}{2}\dot{q}^T M(q) \dot{q} = \frac{1}{2} \sum_{i,j} M_{ij}(q) \dot{q}_i \dot{q}_j \tag{5.30}$$

where $M_{i,j}$ are the entries for the inertia matrix M(q). This matrix is symmetric and positive for each $q \in \mathbb{R}^n$. The potential energy is independent of $\dot{q}$ and can be expressed as

$$\mathcal{P} = \mathcal{P}(q) \tag{5.31}$$

We can then express the Lagrangian in Equation (5.18) with Equation (5.30) and (5.31) as

$$\mathcal{L} = \mathcal{K} - \mathcal{P} = \frac{1}{2}\sum_{i,j} M_{ij}(q)\dot{q}_i\dot{q}_j - \mathcal{P}(q) \tag{5.32}$$

The k^{th} joint velocity is given by the partial derivatives of the Lagrangian

$$\frac{\partial \mathcal{L}}{\partial \dot{q}_k} = \sum_j M_{kj}\dot{q}_j \tag{5.33}$$

and can therefore be expressed as

$$\begin{aligned}\frac{d}{dt}\frac{\partial \mathcal{L}}{\partial \dot{q}_k} &= \sum_j M_{kj}\ddot{q}_j + \sum_j \frac{d}{dt}M_{kj}\dot{q}_j \\ &= \sum_j M_{kj}\ddot{q}_j + \sum_{i,j} \frac{d}{dt}\frac{\partial M_{kj}}{\partial q_i}\dot{q}_i\dot{q}_j\end{aligned} \tag{5.34}$$

Furthermore, the partial derivative with respect to the k_{th} joints position is given by

$$\frac{\partial \mathcal{L}}{\partial q_k} = \frac{1}{2}\sum_{i,j}\frac{\partial M_{ij}}{\partial q_k}\dot{q}_i\dot{q}_j - \frac{\partial \mathcal{P}}{\partial q_k} \tag{5.35}$$

The Euler-Lagrange equation can then be written as

$$\sum_j M_{kj}\ddot{q}_j + \sum_{i,j}\left\{\frac{\partial M_{kj}}{\partial q_i} - \frac{1}{2}\frac{\partial M_{ij}}{\partial q_k}\right\}\dot{q}_i\dot{q}_j + \frac{\partial \mathcal{P}}{\partial q_k} = \mathcal{Q}_i \tag{5.36}$$

We can further interchange the order of summation and use the advantage of symmetry to show that

$$\begin{aligned}\sum_{i,j}\left\{\frac{\partial M_{kj}}{\partial q_i} - \frac{1}{2}\frac{\partial M_{ij}}{\partial q_k}\right\}\dot{q}_i\dot{q}_j &= \sum_{i,j}\frac{1}{2}\left\{\frac{\partial M_{kj}}{\partial q_i} + \frac{\partial M_{ij}}{\partial q_j} - \frac{\partial M_{ij}}{\partial q_k}\right\}\dot{q}_i\dot{q}_j \\ &= \sum_{i,j} c_{ijk}\dot{q}_i\dot{q}_j\end{aligned} \tag{5.37}$$

where c_{ijk} is known as Christoffel symbols and is defined as

$$c_{ijk} = \frac{1}{2}\left\{\frac{\partial M_{kj}}{\partial q_i} + \frac{\partial M_{ij}}{\partial q_j} - \frac{\partial M_{ij}}{\partial q_k}\right\}\dot{q}_i\dot{q}_j \tag{5.38}$$

Finally, if we define

$$g_k = \frac{\partial \mathcal{P}}{\partial q_k} \tag{5.39}$$

the equation of motion can be written as

$$M(q)\ddot{q} + C(q,\dot{q})\dot{q} + g(q) = Q \tag{5.40}$$

where $M(q)$ is the inertia matrix, $C(q, \dot{q})$ is the Coriolis and Centripetal matrix and $g(q)$ is the gravitational matrix.

5.5 System Theory

5.5.1 Linear Systems

A linear system is a system which fulfils two principles: the superposition principle and the homogeneity principle. The superposition principle states that the output response of a system caused by multiple inputs should be the sum of each output caused by each input individually.

$$f(x + y) = f(x) + f(y)$$

The principle of homogeneity states that if the input is scaled by a factor α, the output should be scaled with the same factor α.

$$f(\alpha x) = \alpha x$$

Linear systems are important in automatic control theory, and standard engineering practice is to represent the linear in a state-space representation

$$\begin{aligned} \dot{x}(t) &= Ax(t) + Bu(t) \\ y(t) &= Cx(t) + Du(t) \end{aligned} \tag{5.41}$$

where:

$x(t) =$ is the state vector of time, $x(t) \in \mathbb{R}^n$
$y(t) =$ is the output vector of time, $y(t) \in \mathbb{R}^q$
$u(t) =$ is the control vector of time, $u(t) \in \mathbb{R}^p$
$A =$ is the state matrix, $dim[A] = n \times n$
$B =$ is the input matrix, $dim[B] = n \times p$
$C =$ is the output matrix, $dim[C] = q \times n$
$D =$ is the feed-through matrix, $dim[D] = q \times p$

5.5.2 Non-linear Systems

A non-linear system is a system where either the superposition- or the homogeneity principles are not valid. In essence, it is a system where the change of the output is not proportional to the change of the inputs [35].

$$\begin{aligned} f(x + y) &\neq f(x) + f(y) \\ f(\alpha x) &\neq \alpha f(x) \end{aligned}$$

These systems are more complex to control than linear systems, and are often linearised and presented as a number of linear equations on the state-space form shown in equation 5.41

5.6 Control Theory

5.6.1 Feedback Control

The aim of feedback control is to keep a process value y as close to a reference value r as possible. The most common feedback controller is the PID controller. The PID controller uses the error signal $e = r - y$ and does mathematical operations to this in order to provide an input signal to a system that corrects the error.

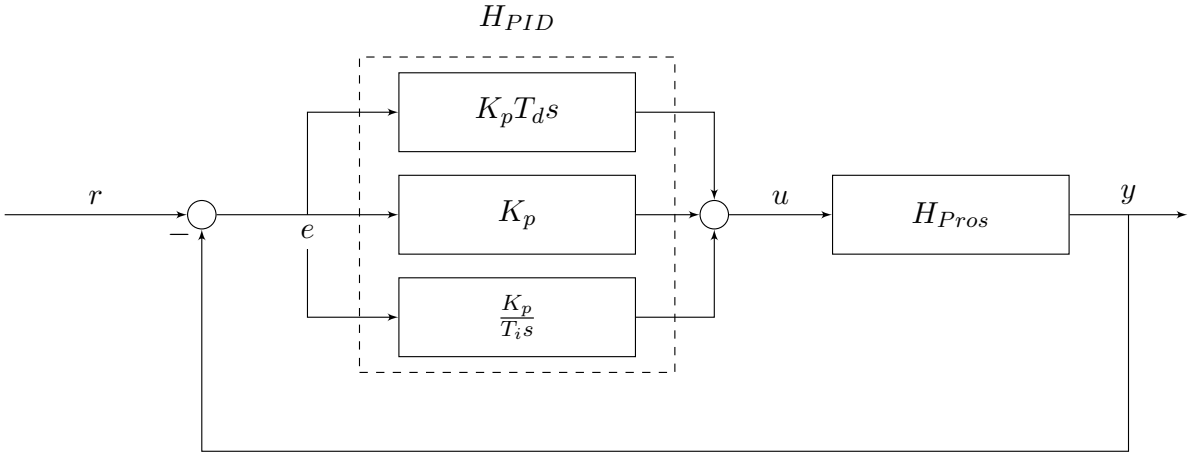

Figure 5.3: Feedback control scheme with PID controller and error signal.

The naming of the PID controller is an abbreviation for its 3 contributing parts, which stand for proportional, integral, and derivative gain. The gain from the controller is calculated by the following function:

$$u(t) = u_0 + K_p \left(e(t) + \frac{1}{T_i} \int_0^t e(t) + T_d \frac{de}{dt} \right) \tag{5.42}$$

The transfer function for the controller can then be calculated as:

$$\begin{aligned} U(S) &= K_p \left(E(s) + \frac{E(s)}{T_i s} + T_d E(s) s \right) \\ U(S) &= K_p E(s) \left(1 + \frac{1}{T_i s} + T_d s \right) \\ \frac{U(s)}{E(s)} &= K_p \left(1 + \frac{1}{T_i s} + T_d s \right) \\ H_{PID} = \frac{U(s)}{E(s)} &= K_p \left(1 + \frac{1}{T_i s} + T_d \frac{N}{1 + N \frac{1}{s}} \right) \end{aligned} \tag{5.43}$$

The final form of the derivative part is approximated with the filter factor N in order to make the transfer function proper, as improper transfer functions are impossible to realise, $s \approx \frac{N}{1+N\frac{1}{s}}$. The balance between the factors K_p, T_i, and T_d is what determines the transient response of the system.

5.6.2 Feedforward Control

Feedback control has some inherent disadvantages. The output of the control unit is based on the error signal, which means perfect tracking is impossible. This problem can be solved with a feedforward controller from the reference signal. If the feedforward transfer function is constructed as $H_{ff} = \frac{1}{H_{pros}}$, then the tranfer function $M(s) = \frac{Y(s)}{R(s)} = \frac{H_{pros}}{H_{pros}} = 1$. This means that if there is no disturbance or limits to the system's gain, the process value should track the reference signal exactly.

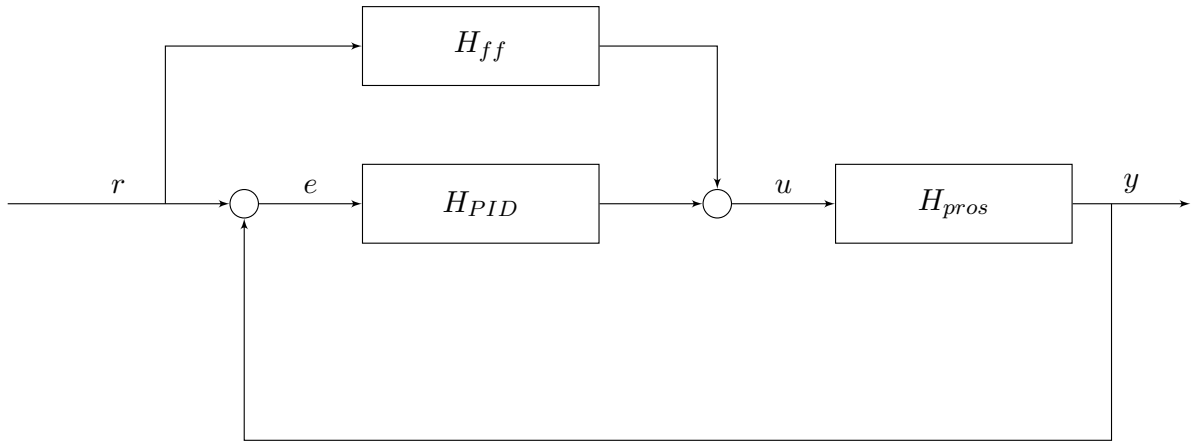

Figure 5.4: Feedforward and feedback control scheme with PID controller and error signal.

Since the model of the system is an approximation and not all disturbances are measured, the feedforward should always be used in combination with feedback control for best results.

5.6.3 Input Shaping

Input shaping is a technique applied in control engineering to reduce vibrations, also referred to as sway. This is an open-loop control strategy and is performed in such a way that the sway angle's natural frequency remains unexcited [36]. When an impulse (A_1)is applied to an under-critically dampened system, the resulting system response is vibrations or sway. The green solid line in figure 5.5 represents the response of the initial impulse, and the solid blue line represents the second impulse A_2, generated by the input shaper. When A_2 is applied with an appropriate amplitude and time location, the second response will suppress the first response. This results in cancellation and zero vibration in the system represented by the red dotted line in Figure 5.5.

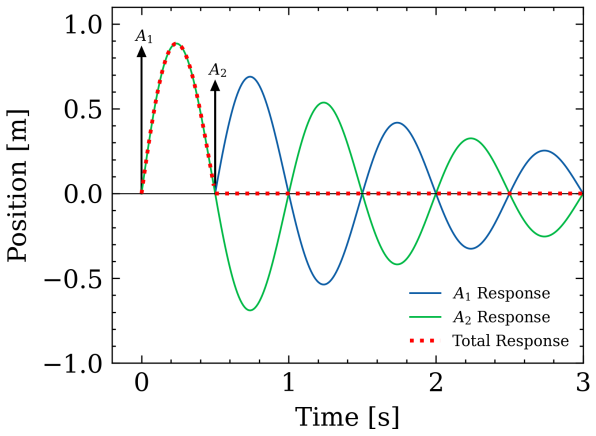

Figure 5.5: Basic concept of input shaping [37].

The principle of convolution is utilised to gain the desired steps in the reference. The principle of convolution is determined as

$$f(t) * g(t) = \int_0^t f(t-\tau)g(\tau)d\tau \tag{5.44}$$

The process is illustrated in figure 5.6, where the desired velocity reference signal is convoluted with a sequence of impulses with a calculated amplitude

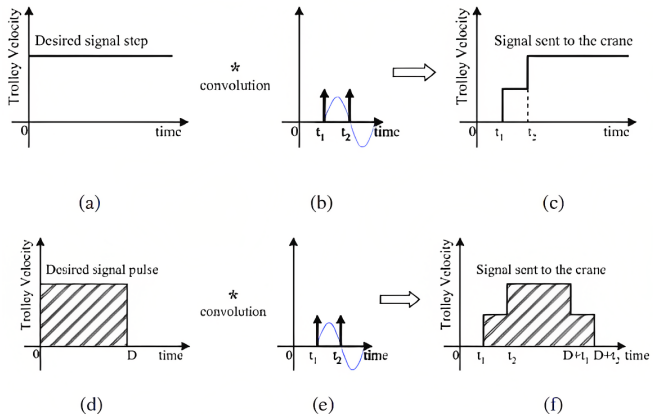

Figure 5.6: (a) is a desired reference velocity step signal, (b) is the calculated sequence of impulses. (c) is signal (a) and (b) convoluted resulting in a shaped command. (d) is the initial signal, (e) is the input shaper and (e) is the shaped signal.

To derive the necessary equations to compute the amplitude A_1 and the time location t_i the following closed-loop transfer function introduced by D. Yuan and T. Chang [38] is considered

$$G(s) = \frac{\omega_n^2}{s^2 + 2\zeta\omega_n s + \omega_n^2} \tag{5.45}$$

where ζ is the dampening ratio and ω_n is the natural frequency derived from

$$w_n = \sqrt{\frac{g}{l}} \tag{5.46}$$

Furthermore, the impulse response of 5.45 is given by

$$y(t) = \frac{\omega_n}{\sqrt{1-\zeta^2}} e^{-}\zeta\omega_n(t-t_0)\sin\left[(\omega_n\sqrt{1-\zeta^2})(t-t_0)\right]u(t-t_0) \tag{5.47}$$

where t_0 is the impulse time instance and u(...) is the unit step function [38]. The unit step function is constructed by a series of impulses $A_i\delta(t-t_i)$ where A_i is the amplitude and t_i is the time locations of the impulse inputs. Further, can the total impulse response be derived as

$$y(t) = \sum_{i=1}^{n} y_i(t) \tag{5.48}$$

where n is the number of impulses. Furthermore, the total impulse response is given as

$$y_i(t) = \frac{A_i\omega_n}{\sqrt{1-\zeta^2}} e^{-\zeta\omega_n(t-t_0)}\sin\left[(\omega_n\sqrt{1-\zeta^2})(t-t_i)\right]\delta(t-t_0) \tag{5.49}$$

To further develop this equation it is necessary to compute the total response at the settling time of the vibrations $t = t_N$

$$y(t_N) = \sum_{i=1}^{n} \frac{A_i\omega_n}{\sqrt{1-\zeta^2}} e^{-\zeta\omega_n(t-t_0)}\sin\left[(\omega_n\sqrt{1-\zeta^2})(t-t_i)\right]\delta(t-t_0) \tag{5.50}$$

and further as

$$y(t_N) = \sum_{i=1}^{n} B_i \sin(\omega_d t_n - \omega_d t_i) \tag{5.51}$$

where

$$\omega_d = \omega_n \sqrt{1-\zeta} \tag{5.52}$$

and

$$B_i = \frac{A_i \omega_n}{\sqrt{1-\zeta}} e^{\zeta \omega_n t_N} e^{\zeta \omega_n t_i} \tag{5.53}$$

By using trigonometric identity [39]

$$K_1 \sin(\alpha t + \phi_1) + ... + K_n \sin(\alpha t + \phi_n) = A_{amp} \sin(\alpha t + \psi) \tag{5.54}$$

where A_{amp} can be written as

$$A_{amp} = \sqrt{\left(\sum_{i=1}^{n} K_i \cos(\phi_i)\right) + \left(\sum_{i=1}^{n} K_i \sin(\phi_i)\right)} \tag{5.55}$$

$$\psi = \tan^{-1} \frac{\sum_{i=1}^{n} K_i \cos(\phi_i)}{\sum_{i=1}^{n} K_i \sin(\phi_i)} \tag{5.56}$$

From Equations 5.55 and 5.56 it is possible to write the vibration amplitude as

$$A_{\sum} = \frac{A_i \omega_n}{\sqrt{1-\zeta^2}} e^{-\zeta \omega_n (t-t_0)} \sqrt{(\sum_{i=1}^{n} A_i e^{\zeta \omega_n t_i} \cos(\omega_d t_i)) + (\sum_{i=1}^{n} A_i e^{\zeta \omega_n t_i} \cos(\omega_d t_i))} \tag{5.57}$$

To construct a non-dimensional vibration amplitude, Equation 5.57 is divided by the amplitude of a single impulse. The Amplitude of a single impulse is [40]

$$A_{single} = \frac{\omega_n}{\sqrt{1-\zeta}} \tag{5.58}$$

To compute the residual Equation 5.57 is divided by 5.58

$$V(\omega_n, \zeta) = e^{-\zeta \omega_n t_n} \sqrt{C(\omega_n, \zeta)^2 + S(\omega_n, \zeta)^2} \tag{5.59}$$

where

$$\begin{aligned} C(\omega_n, \zeta) &= \sum_{i=1}^{n} A_i e^{\zeta \omega_n t_i} \cos(\omega_d t_i) \\ S(\omega_n, \zeta) &= \sum_{i=1}^{n} A_i e^{\zeta \omega_n t_i} \sin(\omega_d t_i) \end{aligned} \tag{5.60}$$

where ω_d is the natural damped frequency. It is also important to avoid trivial solutions and it is, therefore, necessary to obtain

$$\sum_{i=1}^{n} A_i = 1, \quad i = 1, ..., n \tag{5.61}$$

At last, it is also important that the input shaper is robust to errors in the natural frequency. It is

therefore necessary to fulfil this constraint

$$\frac{d^i}{d\omega^i} V(\omega, \zeta, t_N) = 0. \tag{5.62}$$

Chapter 6

Modelling of crane dynamics

The motivation for developing a dynamical model of the SU-M4-MUN-M60 crane in Casthouse Sunndal arose from the need of a framework for testing various control strategies. Conducting tests on the actual crane would have been both impractical and undesirable. Implementing software changes and running tests on a full-scale system would represent a safety hazard and disrupt production. It was therefore desierable to build a simulation enviornment. This would enable the ability to experiment with different implementations and parameters without requiring physical testing on the actual crane. The model was developed using MATLAB and MATLAB's Simulink using information collected from the crane's datasheet (A9). To ensure the accuracy of the dynamics, the model was verified using the measurements and videos from the visit to Casthouse Sunndal.

6.1 Approximations and Neglected Dynamics

In order to make this project feasible, it was necessary to make certain approximations concerning the development of the dynamics and the surrounding environments. This need arose from a combination of familiarity with the field of system theory, available data, and the project's timeframe.

1. Neglected Disturbances:
   (a) friction between bridge and rails, and trolley and rails,
   (b) mechanical errors in actuators causing static or dynamic backlash, or jerks,
   (c) noisy measurements from sensors,
2. Neglected dynamics:
   (a) motor dynamics,
   (b) cable's flexibility,
   (c) single cable instead of eight cables,
   (d) payload rotation,
   (e) trolley dynamics (the trolley is assumed as a lumped mass)
   (f) flexibilities in the trolley and bridge supporting rails

Numerous measurements of the overhead crane's dynamics were conducted during testing in Casthouse Sunndal, and indicated that the crane did not oscillate as much as originally anticipated. This discovery made it possible to simplify some of the aspects related to dynamic design, and still get a representative model.

6.1.1 Motor Dynamics

The first approximation regards the dynamics associated with the overhead crane's motors. An accurate model would account for all aspects associated with the electrical circuitry, mechanical and thermal components. Given the project's timeframe and the lack of impact on the pendulum dynamics, modelling in such a manner was considered unnecessary. In this model, the motor is a gain from -100% to 100%, which directly corresponds to the speed of the crane. To control acceleration, a rate limiter is implemented, while a saturation block is utilised to constrain the speed. This is shown in figure 6.1.

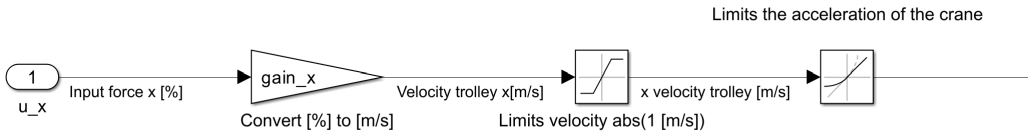

Figure 6.1: Motor dynamics in Simulink.

6.1.2 Pendulum Dynamics

Another approximation is treating the system as a single spherical pendulum with a point mass. In reality, the system consists of one pendulum system from the trolley to the hook, another from the hook to the yoke, and if there is a load multiple pendulum systems from the yoke and to each ingot. The simplification has been deemed suitable because the pendulum between the hook block and lifting yoke, as well as the pendulum between the lifting yoke and extrusion ingots, are observed to seldom deviate from parallel orientation. Therefore the payload with and without ingots attached is seen as one point mass with various masses. This simplification poses a challenge because the ingots exceed 7 meters in length, meaning even a small angle can cause a significant offset. Figure 5.2 displays the system on which the dynamics are founded, and are described in section 5.4.2.

6.1.3 Damping Coefficient

To bring the oscillations of the pendulum system to a halt, the model required a damping coefficient. The damping coefficient accounts for both the impact of air resistance and the fact that the system is simplified by using only one wire, whereas in reality, eight wires support the load.

The damping coefficient, represented by the variable b, has been modelled in a manner analogous to the modelling of friction. It is proportional to the speed of the load, $F_b = -b\dot{x}$. The value of b was obtained by examining the differential equation governing the angle θ.

$$\begin{aligned} -mgl\sin\theta - bl\dot{\theta}l &= ml^2\ddot{\theta} \\ \ddot{\theta} + \frac{b}{m}\dot{\theta} + \frac{g}{l}\sin\theta &= 0 \\ \ddot{\theta} + \frac{b}{m}\dot{\theta} + \frac{g}{l}\theta &= 0 \end{aligned} \tag{6.1}$$

The sine function can be simplified as $\sin\alpha \cong \alpha$, due to the minuscule angles involved. Then the differential equation is solved:

$$\begin{aligned} \theta(t) &= \theta_0 l^{-\frac{b}{2m}t}\cos\left(\omega t + \phi\right) \\ \omega &= \sqrt{\omega_0 - \left(\frac{b}{2m}\right)^2} \\ \omega_0 &= \sqrt{\frac{g}{l}} \end{aligned} \tag{6.2}$$

A formula can further be derived where the only unknown is the dampening coefficient

$$\begin{aligned} \omega &= \sqrt{\omega_0^2 - \left(\frac{b}{2m}\right)^2} = \sqrt{\frac{g}{l} - \left(\frac{b}{2m}\right)^2} \\ \omega &= \frac{2\pi}{T} \\ T &= \frac{2\pi}{\omega} \\ T &= \frac{2\pi}{\sqrt{\frac{g}{l} - \left(\frac{b}{2m}\right)^2}} \end{aligned} \tag{6.3}$$

By algebraic manipulation, the formula for the dampening coefficient is

$$b = 2m\sqrt{\frac{g}{l} - \left(\frac{2\pi}{T}\right)^2} \tag{6.4}$$

Through the use of this formula, a damping coefficient has been derived. This formula gives a good estimate for the dampening force. A limitation of this formula is that it necessitates the determination of the period time T for systems with varying lengths and masses, which is achievable but time-consuming.

During the verification of the simulation model's coefficient, it became evident that the magnitude of the coefficient was excessively large. By comparing the results from the simulation with the videos aquired at the casthouse, it was noted that the payload oscillations decayed too quickly with this value. By trial and error, the value was decreased to better align with the oscillations of the system.

6.2 Kinematics

6.2.1 Forward Kinematics

Forward kinematics is employed to determine the position of the load. Once the position of the trolley is known, the load's position in relation to the trolley must be determined, and subsequently added to the trolley position for the derivation of its position in the inertial frame. Everything needed to find the position of the load in relation to the trolley is the length of the hoist and the angles α and β. Trigonometry can be used to find the positions. To initiate the

kinematics, both the sin and cos functions for both α and β are written.

$$\begin{aligned} \sin(\alpha) &= \frac{y_1}{l} \\ \cos(\alpha) &= \frac{x_2}{l} \\ \sin(\beta) &= \frac{x_1}{x_2} \\ \cos(\beta) &= \frac{z_1}{x_2} \end{aligned} \tag{6.5}$$

The desired outputs of the equations are the x_1, y_1 and z_1, while l, α and β are the known variables. By applying algebraic techniques, the equations from 6.5 can be transformed into the following set of equations, allowing for the determination of x_1, y_1 and z_1.

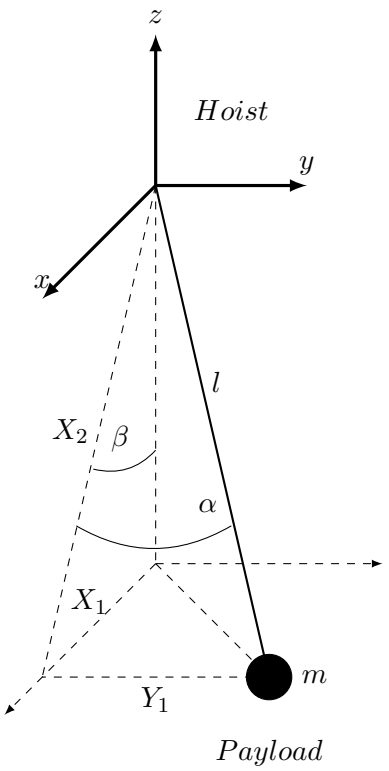

$$\begin{aligned} x_1 &= l\cos\alpha\sin\beta \\ y_1 &= l\sin\alpha \\ z_1 &= -l\cos\alpha\cos\beta \end{aligned} \tag{6.6}$$

Figure 6.2: Kinematics from trolley to payload.

These equations represent the relationship between the position of the trolley and the position of the load. To get the position of the load in the inertial frame, the position of the load in relation to the trolley must be added to the position of the trolley.

$$\begin{aligned} x_{load} &= x_{trolley} + l\cos(\alpha)\sin(\beta) \\ y_{load} &= y_{trolley} + l\sin(\alpha) \\ z_{load} &= -l\cos(\alpha)\cos(\beta) \end{aligned} \tag{6.7}$$

The overhead crane can be considered a prismatic robot with 3 controllable degrees of freedom (DOF):

1. The bridge can move forward and backwards along our defined x-axis.
2. The trolley can move between the two girders along our defined y-axis.
3. The hoist can lift and lower objects attached to the hook.

By using the forward kinematics derived in (5.2.1) the following DH convention table can be constructed

Link	$\mathbf{a_i}$	$\alpha_\mathbf{i}$	$\mathbf{d_i}$	$\theta_\mathbf{i}$
1	0	90°	d_1^*	90°
2	0	90°	d_2^*	−90°
3	0	0	d_3^*	0

Table 6.1: Denavit Hartenberg Table of overhead crane with 3 DOFs.

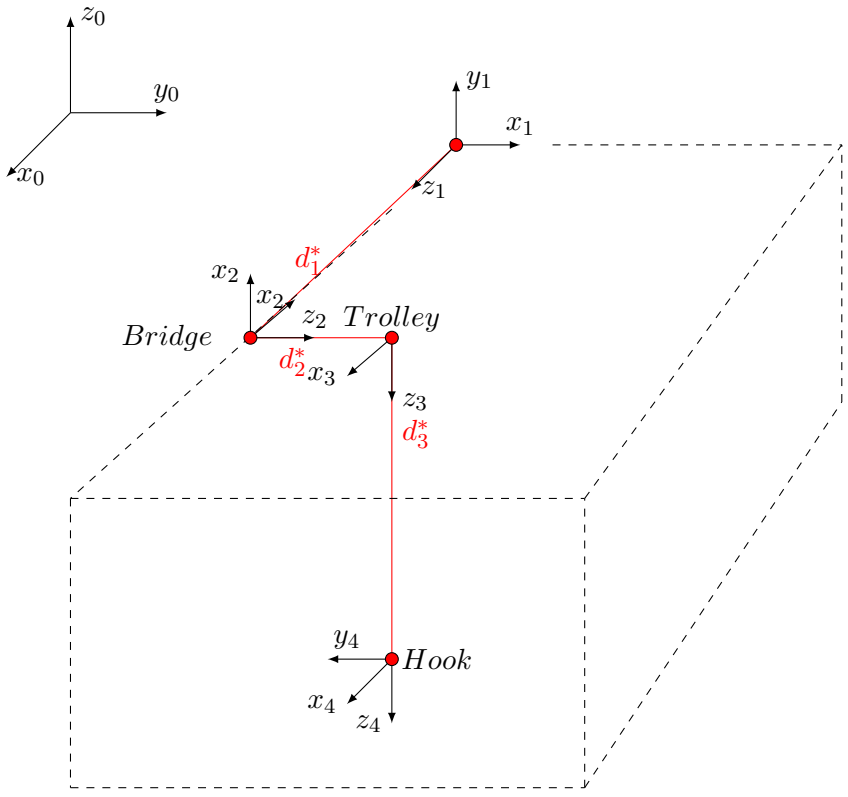

Figure 6.3: Forward kinematics of overhead crane.

Furthermore, the homogeneous transformation matrices can be derived using Table 6.1 as

$$A_1 = \begin{bmatrix} 0 & 0 & 1 & 0 \\ 1 & 0 & 0 & 0 \\ 0 & 1 & 0 & d_1^* \\ 0 & 0 & 0 & 1 \end{bmatrix}, \; A_2 = \begin{bmatrix} 0 & 0 & -1 & 0 \\ -1 & 0 & 0 & 0 \\ 0 & 1 & 0 & d_2^* \\ 0 & 0 & 0 & 1 \end{bmatrix}, \; A_3 = \begin{bmatrix} 1 & 0 & 0 & 0 \\ 0 & 1 & 0 & 0 \\ 0 & 0 & 1 & d_3^* \\ 0 & 0 & 0 & 1 \end{bmatrix} \tag{6.8}$$

where the robot has the following forward kinematics

$$T_1^3 = A_1(q_1)A_2(q_2)A_3(q_3) = \begin{bmatrix} 0 & 1 & 0 & d_2^* \\ 0 & 0 & -1 & -d_3^* \\ -1 & 0 & 0 & d_1^* \\ 0 & 0 & 0 & 1 \end{bmatrix} \tag{6.9}$$

where $q_1 = d_1^*$, $q_2 = d_2^*$ and $q_3 = d_3^*$. To further orientate the robot in relation to the inertial coordinate frame x_0, y_0, z_0 a homogenous must be applied to T_1^3 as T_0^1

$$\begin{aligned} T_0^3 = T_0^1 * T_1^3 &= \begin{bmatrix} 0 & 0 & 1 & 0 \\ 1 & 0 & 0 & 0 \\ 0 & 1 & 0 & 0 \\ 0 & 0 & 0 & 1 \end{bmatrix} \begin{bmatrix} 0 & 1 & 0 & d_2^* \\ 0 & 0 & -1 & -d_3^* \\ -1 & 0 & 0 & d_1^* \\ 0 & 0 & 0 & 1 \end{bmatrix} \\ &= \begin{bmatrix} 0 & 1 & 0 & d_1^* \\ 0 & 1 & 0 & d_2^* \\ 0 & 0 & -1 & -d_3^* \\ 0 & 0 & 0 & 1 \end{bmatrix} \end{aligned} \tag{6.10}$$

6.2.2 Inverse Kinematics

In order to derive the inverse kinematics for the system, a simplified approach has been used. By considering the hoist as a rigid body, the crane can be classified as a cartesian robot. It makes sense to do the inverse kinematics this way because the wanted position of the load is with both angles at zero. The inverse kinematics of such a cartesian robot is simple, the position of the load is the same as the value of each actuator along the axis.

$$P_0 = \begin{bmatrix} x_0 \\ y_0 \\ z_0 \end{bmatrix} = \begin{bmatrix} d_1^* \\ d_2^* \\ d_3^* \end{bmatrix} \tag{6.11}$$

6.3 Mathematical Modeling with Newtons Laws of Motion

The dynamics of the crane have been derived to create a model of the overhead crane. Such a model can be used to test different features, such as the implementation of trajectory planning and anti-sway algorithms. The system dynamics are developed in MATLAB's Simulink tool, based on the forward kinematics described in section 6.2.1, and Newtons Laws of otion described in 5.4.1 and 6.3.1. Simulink has been utilised, as it makes the model organised and easy to implement changes to the dynamics. Furthermore, the way the program is structured allows the simulation of various inputs, making it simple to observe changes in the dynamic outputs.

6.3.1 Dynamic Representation

In order to simulate the system with Simulink, the dynamics of the system were derived using Newton's Laws of Motion (5.4.1). By applying Newton's second law of motion, the acceleration of the load can be determined in each direction.

6.3.1.1 Dynamic in X Direction

To calculate the force in the x direction, Newton's Laws of Motion and trigonometry were utilised. The gravitational force is equalised by the tension force in the cable ensuring that the load remains stationary, $G = S_y$. If the load is suspended at an angle, the tension force of the cable must be sufficient to balance out the gravitational force. This causes a portion of the tension force in the cable to accelerate the load along the x-axis.

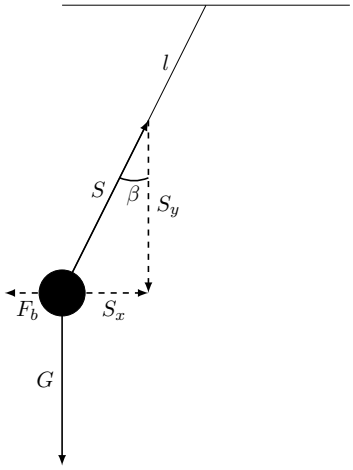

Figure 6.4: Forces on the payload of a simple pendulum.

Since the only known force on the mass is the force pulling the load down, the tangent function of the angle β has to be used in order to find the magnitude of the force pulling the load along the x-axis, this force is labelled F_β.

$$F_\beta = S_x = G\tan(\beta) = mg\tan(\beta) \tag{6.12}$$

In practical applications, the angles of α and β will be determined using sensors. In Simulink, the angles were determined using trigonometry. In order to collect equation 6.12, the angle β needs to be determined. $\sin(\beta)$ is found by the following trigonometric and algebraic equations:

$$\sin(\beta) = \frac{x_1}{x_2} = \frac{x_1}{l\cos\alpha} = \frac{x_{trolley} - x_{load}}{l\cos\alpha} \tag{6.13}$$

Subsequently, the angle is determined using the arcsine function, followed by the calculation of the force magnitude using the tangent function. The angle α is found in 6.3.1.2.

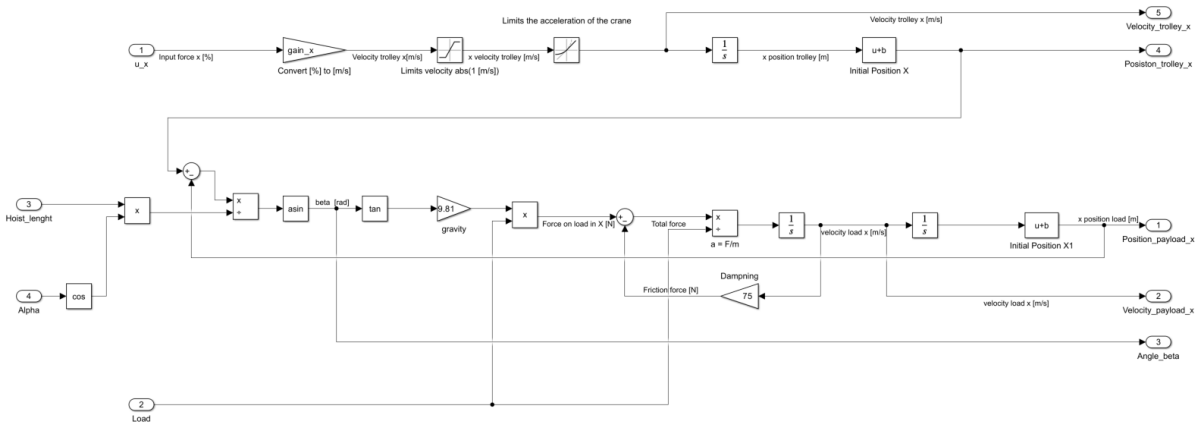

Figure 6.5: Simulink representation of dynamics in x direction.

At the top of the subsystem in figure 6.5, the input signal u_x is converted to the trolley's velocity with a gain and saturation block to simulate the velocity and position of the trolley. A rate limiter block was used to prevent the model from having infinite acceleration and constrained the acceleration of the bridge. The rest of the system is represented in Simulink and is the equivalent of Newton's Second Law of Motion.

$$\begin{aligned} \Sigma F_x &= 0 \\ F_x &= F_\beta - F_b \\ F_x &= mg\tan(\beta) - \dot{x}_{load} b \end{aligned} \tag{6.14}$$

Using this equation, the force along the x-axis can be determined. The acceleration in the same direction can then be derived using $a = \frac{F_x}{m}$. The velocity and position along this axis can then be found by integrating once and twice respectively. The dampening force F_b is described in 6.1.3

6.3.1.2 Dynamic in Y Direction

The forces in the y direction are analogous to the forces in the x direction. The only difference is that F_α is independent of β. The force in this direction, caused by the angle α, can therefore be described by:

$$F_\alpha = mg\tan(\alpha) \tag{6.15}$$

In order to find the angle α, the expression $\sin\alpha$ was derived by the trigonometric equation described in 6.2.1:

$$\sin(\alpha) = \frac{y_1}{l} = \frac{y_{trolley} - y_{load}}{l} \tag{6.16}$$

An arcsine function is then used to find the angle, and then a tangent function to find the

magnitude of the force, F_α. All the forces that act in this direction are the force caused by an angle α and the dampening force. The sum of all forces can then be written as:

$$\begin{aligned} \Sigma F_y &= 0 \\ F_y &= F_\alpha - F_b \\ F_y &= mg\frac{y_{trolley} - y_{load}}{l} - \dot{y}_{load}b \end{aligned} \tag{6.17}$$

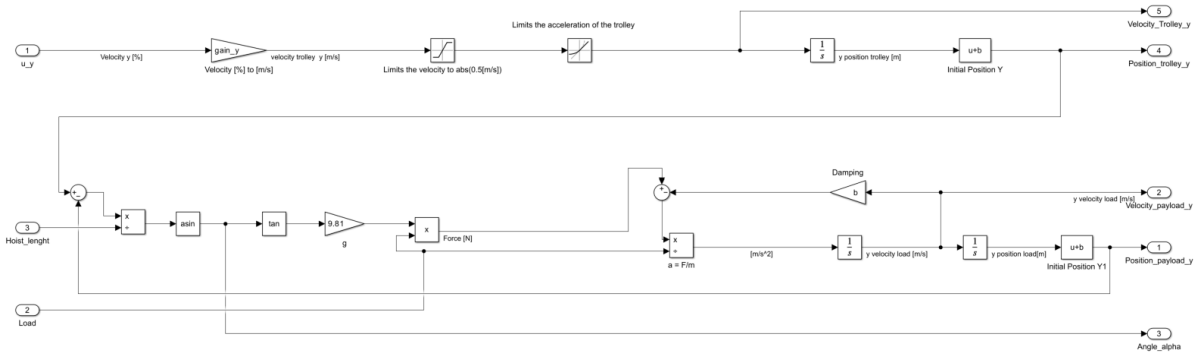

Figure 6.6: Simulink representation of dynamics in y direction.

By finding the total force, the acceleration can be found with $a = \frac{F_y}{m}$. This can in turn be used to find the velocity and position of the load in the Y direction.

6.3.1.3 Dynamic in Z Direction

The height of the load is determined by the angles alpha and beta and the length of the cable. If there is no angle, the length of the cable is equal to the opposite of the position, in regard to how the inertial frame is defined.

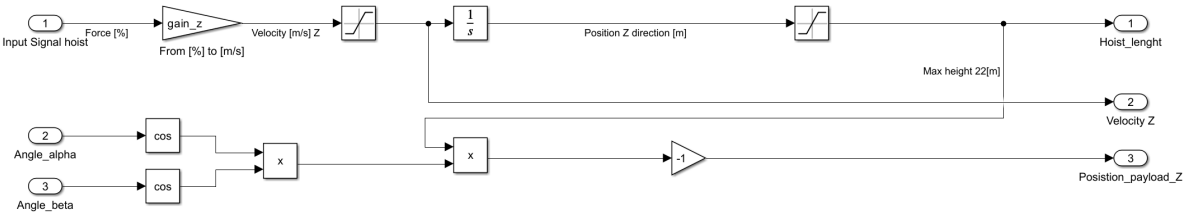

Figure 6.7: Simulink representation of dynamics in z direction.

The input signal is converted to velocity in the same way as in X and Y directions at the top of the subsystem. The position of the load is calculated with the equation: $P_z = -l\cos\alpha\cos\beta$, which is displayed in figure 6.7. The angles alpha and beta are found in the X and Y dynamics subsystems.

6.4 Simulink Structure

The Simulink program has been structured into several subsystems, each handling a part of the dynamics. This results in a clear overview of which inputs and outputs correspond to different system parts. The program has been organized in a user-friendly manner to facilitate ease of use and simplicity of understanding. Breaking down the dynamic into multiple subsystems makes it easy to identify potential areas for improvement, which can lead to better performance and accuracy over time.

6.4.1 Main Subsystem

Figure 6.8 shows the primary subsystem, which encompasses all the dynamics pertaining to the overhead crane. The subsystem receives force and payload weight as inputs and generates outputs that correspond with the system dynamic. These outputs can be utilised in developing trajectory planning as well as anti-sway algorithms. The dynamics inside the subsystem are described in section 6.3.1.

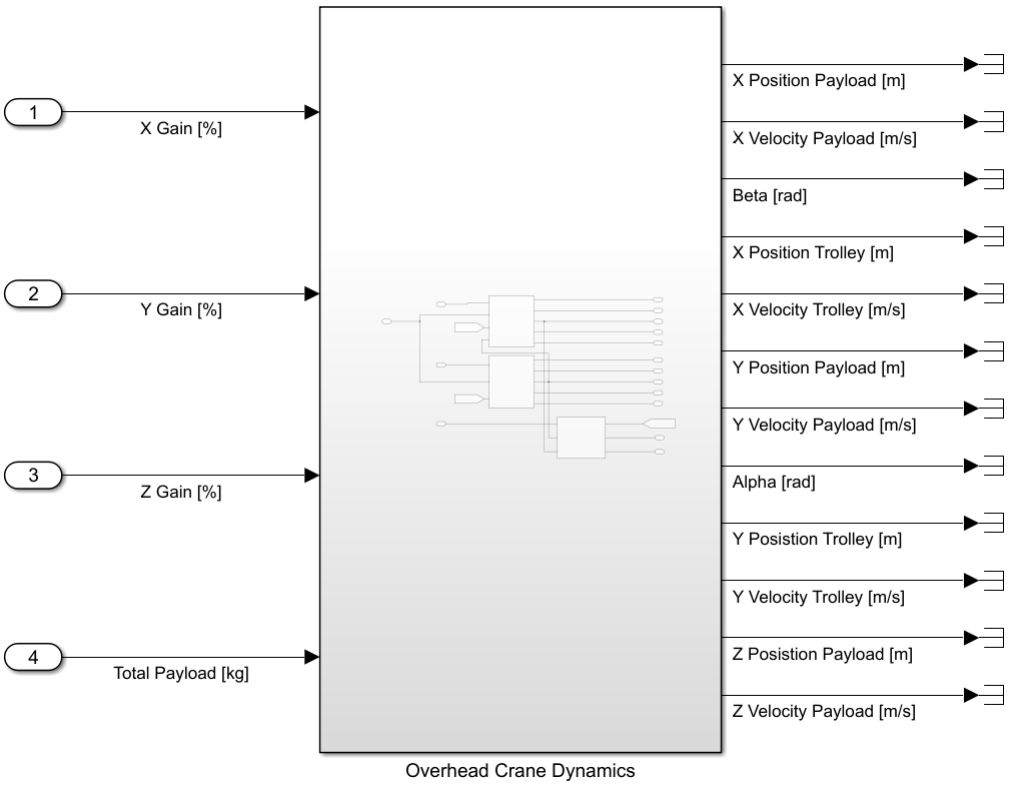

Figure 6.8: Main Dynamic Subsystem.

6.4.2 Dynamic Subsystems

Figure 6.9 depicts three interdependent subsystems that encompass the dynamics of the overhead crane. The length of the cable, and the angles α and β influence the dynamics along each axis. This relationship is illustrated in the figure through the use of "Hoist_length" tags. Each subsystem contains the dynamics related to the directions of the coordinate X, Y, and Z,

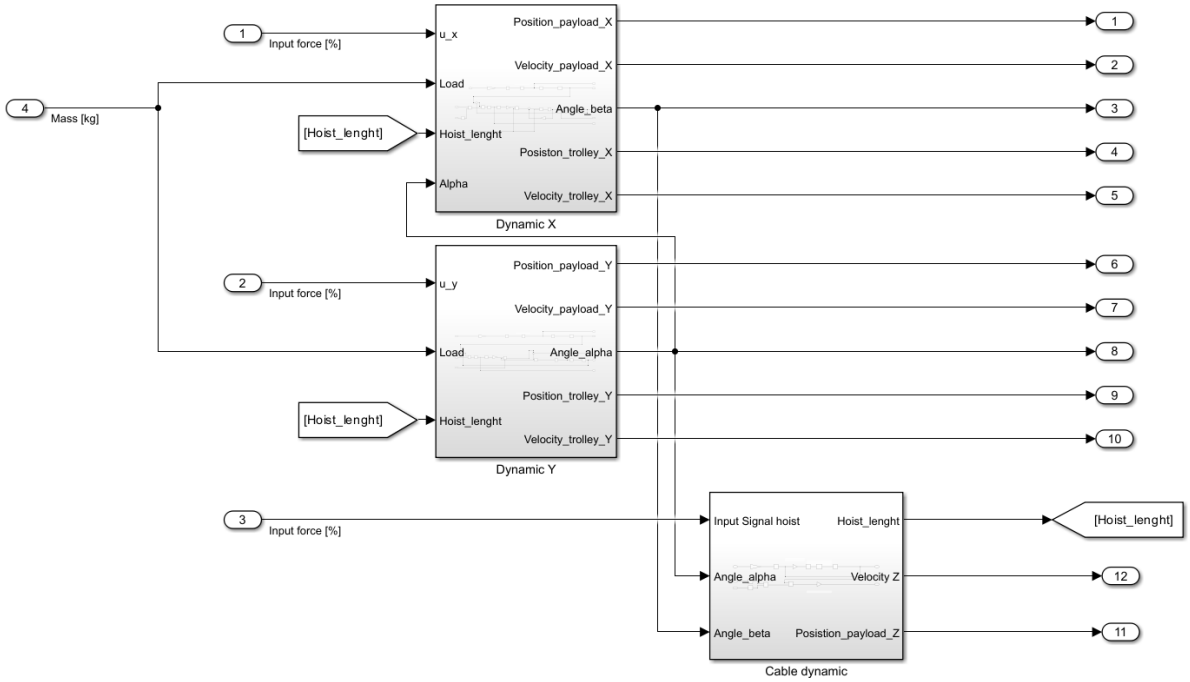

Figure 6.9: Simulink representation of dynamic subsystem.

6.5 Model Verification

In order to verify that the model of the system exerts the same dynamics as the actual system, tests had to be made to ensure the responses of the simulation match those of the real system. By comparing the footage taken during the visit at Casthouse Sunndal with the responses shown in the simulation, the simulation could be verified.

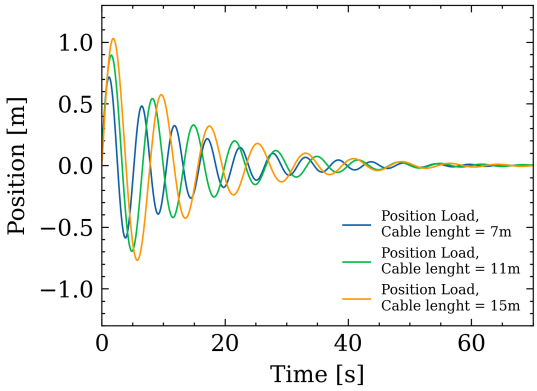

(a) Dampning in x direction with different cable lengths.

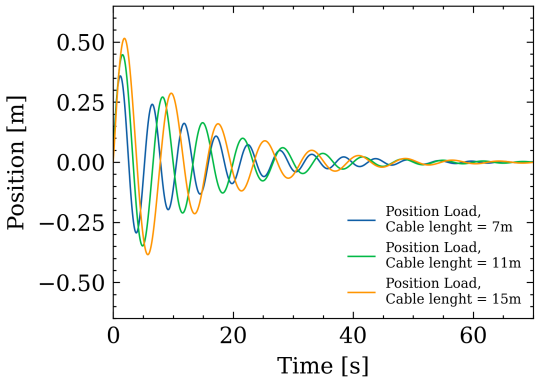

(b) Dampning in y direction with different cable lengths.

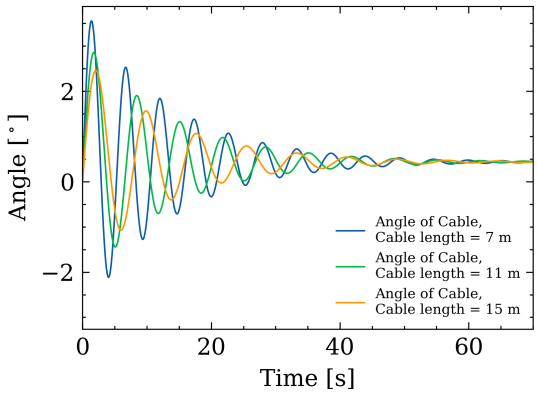

(c) Sway angle in x direction with different cable lengths.

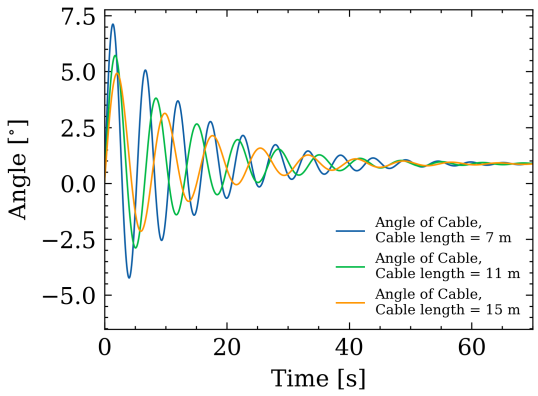

(d) Sway angle in y direction with different cable lengths.

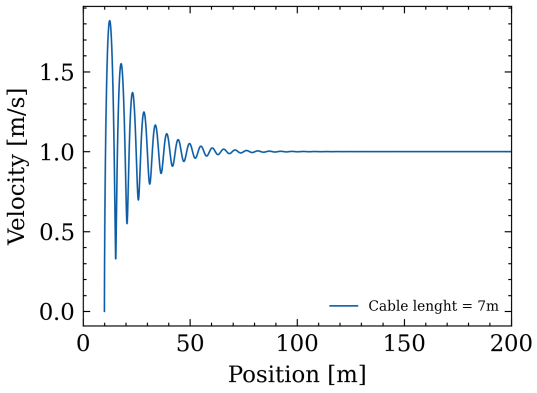

(e) Phase plot of payload position and speed in x direction.

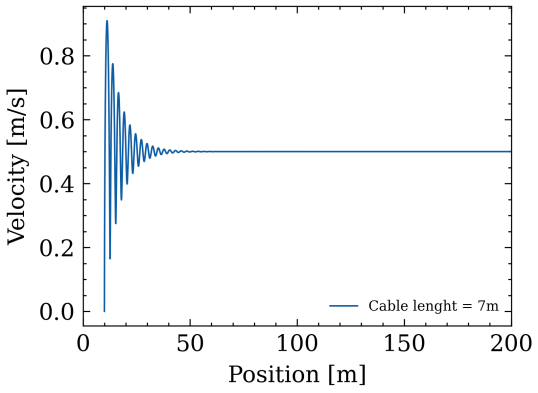

(f) Phase plot of payload position and speed in y direction.

Figure 6.10: Model verification test results

The results from the tests are presented in figure 6.10. The tests were carried out by moving the trolley at 100% speed until the payload stabilised behind the trolley at a constant speed, as shown in 6.10e and 6.10f. The tests were conducted in this manner because using a short pulse or Dirac as input resulted in errors caused by the system's varying resonance frequencies with different cable lengths. The tests were carried out with an empty lifting yoke, and having an extra would prolong the oscillations. The frequency would however be the same because the frequency depends on the length of the hoist.

Figure 6.10a and 6.10b show how the payload oscillates around the position of the trolley it comes to rest. The test was carried out with different cable lengths in order to verify the dynamics for different operating conditions. The tests showed that a larger hoist length resulted in slower oscillations and larger angles α and β, thereby a greater error between the trolley and payload. These results are in line with what is expected of such a system.

In order to get a more accurate model, more time should be given to model an accurate dampening for the system. Most of the dampening is caused by the multi-cable configuration of the hook block, which impacts the dampening differently for different loads.

6.6 Mathematical Modeling with Lagranges Equations of Motion

The computation in this section regarding the dynamics is based on the report by Andrei Aksjonov "3D KRAANA JUHTIMISSÜSTEEM" [41]

The dynamics of the crane can be modelled using Newton's Law of Motion as described in section 6.3, or with the use of the Lagrangian theory explained in section 5.4.3. While the Lagrangian approach was initially attempted in this project, it was found impractical for achieving an accurate model and was therefore replaced by the model derived from Newton's Laws of Motion. However, it is worth noting that the model based on Lagrangian is still relevant for certain control strategies, such as the Linear Quadratic Regulator (LQR), which require the model to be represented in state-space form. Although the full computation of the Lagrangian model is not included in this report, it can be found in the report written by Andrei Aksjonov [41].

6.6.1 Mathematical Representation

The Lagrangian approach is defined as the kinetic energy ($\mathcal{K}$) of the pendulum, minus the potential energy ($\mathcal{P}$), as shown in equation 6.18. The Kinetic energy and Potential energy are described with equation 6.19 and 6.20, for further description see section 5.4.3. This model does not account for friction.

$$\mathcal{L} = \mathcal{K} - \mathcal{P} \tag{6.18}$$

$$\mathcal{K} = \frac{1}{2}mv^2 \tag{6.19}$$

where m is the mass of the payload, and v is the velocity.

$$\mathcal{P} = mgl \tag{6.20}$$

where m = mass, g = acceleration of gravity and l = length of hoist. Using the theory explained in section 5.4.3, the dynamics of the crane are represented with the equations below, and the variables are explained in table 6.2.

Symbol	Description
m_{trolley}	Mass of the trolley
m_{payload}	Mass of the payload
m_{bridge}	Mass of the bridge
l	Length of the hoist
u_x	Input force x direction
u_y	Input force y direction
u_z	Input force z direction
β	Angle β
α	Angle α
g	Gravitational force
x_{t}	trolley position x direction
y_{t}	trolley position y direction

Table 6.2: Dynamic parameters description

$$\ddot{x} = \frac{1}{m_{\text{trolley}} + m_{\text{bridge}} + m_{\text{payload}}} u_x + \frac{m_{\text{payload}} g}{m_{\text{trolley}} + m_{\text{bridge}} + m_{\text{payload}}} \beta$$
$$\ddot{y} = \frac{1}{m_{\text{trolley}} + m_{\text{payload}}} u_y + \frac{m_{\text{payload}} g}{m_{\text{trolley}} + m_{\text{payload}}} \alpha$$
$$\ddot{\beta} = -\frac{1}{l(m_{\text{trolley}} + m_{\text{bridge}} + m_{\text{payload}})} u_x - \frac{g(m_{\text{trolley}} + m_{\text{bridge}} + 2m_{\text{payload}})}{l(m_{\text{trolley}} + m_{\text{bridge}} + m_{\text{payload}})} \beta$$
$$\ddot{\alpha} = -\frac{1}{l(m_{\text{trolley}} + m_{\text{payload}})} u_y - \frac{g(m_{\text{trolley}} + 2m_{\text{payload}})}{l(m_{\text{trolley}} + m_{\text{payload}})} \alpha$$
$$\ddot{l} = \frac{1}{2m_{\text{payload}}} u_z$$

The equations can be expressed as a state-space model, with x^0 representing the steady-state vector:

$$x^0 = [x^0 \; \dot{x^0} \; y^0 \; \dot{y^0} \; \beta^0 \; \dot{\beta^0} \; \alpha \; \dot{\alpha^0} \; l^0 \; \dot{l^0}]^T = [0\,0\,0\,0\,0\,0\,0\,0\,0\,0]^T \tag{6.21}$$

The system's input is represented by a force vector, $u = [u_x \; u_y \; u_z]^T$. This gives us the following state-space model:

$$\dot{x}_1 = \dot{x}_w = x_2 \tag{6.22}$$
$$\dot{x}_2 = \ddot{x}_w = \frac{1}{m_{trolley} + m_{bridge} + m_{payload}} u_x + \frac{m_{payload} g}{m_{trolley} + m_{bridge} + m_{payload}} \beta \tag{6.23}$$
$$\dot{x}_3 = \dot{y}_w = x4 \tag{6.24}$$
$$\dot{x}_4 = \ddot{y}_w = \frac{1}{m_{trolley} + m_{payload}} u_y + \frac{m_{payload} g}{m_{trolley} + m_{payload}} \alpha \tag{6.25}$$
$$\dot{x}_5 = \dot{\beta} = x_6 \tag{6.26}$$
$$\dot{x}_6 = \ddot{\beta} = -\frac{1}{l(m_{trolley} + m_{bridge} + m_{payload})} u_x - \frac{g(m_{trolley} + m_{bridge} + 2m_{payload})}{l(m_{trolley} + m_{brigde} + m_{payload})} \beta \tag{6.27}$$
$$\dot{x}_7 = \dot{\alpha} = x_8 \tag{6.28}$$
$$\dot{x}_8 = \ddot{\alpha} = -\frac{1}{l(m_{trolley} + m_{payload})} u_y - \frac{g(m_{trolley} + 2m_{payload})}{l(m_{trolley} + m_{payload})} \alpha \tag{6.29}$$
$$\dot{x}_9 = \dot{z}_w = x_1 0 \tag{6.30}$$
$$\dot{x}_{10} = \ddot{z}_w = \frac{u_z}{2m_l} \tag{6.31}$$

This will be represented in A, B, C and D matrices. The A matrix characterises how the system evolves over time, considering the current state of the system and the influence of the input forces at that specific time. The B matrix describes how the inputs are incorporated into the system and which states of the system they are affecting. Matrix C presents how the states are combined to get the outputs, and the D matrix captures the direct influence of the inputs on the

outputs.

The MATLAB implementation of the mathematical model is shown in the appendix A8.

6.7 Discussion

The primary goal of making a mathematical model of the crane's dynamics was to create a simulation environment that could be used in the development of a control system. Initially, an attempt was made to create a model with the use of the Lagrangian approach, as described in section 6.6. However, during the project, it became evident that a model based on Newton's Laws of Motion was more suitable for the crane's dynamics. This decision was based on the project's timeline as well as the team's familiarity with the Lagrangian theory.

The model based on Newton's Laws of Motion was subsequently utilised for the creation of the system dynamics, as detailed in section 6.3. During the development of the model, it became clear that certain approximations had to be made due to available technical information and timeframe. Firstly, a gain between -100% and 100% corresponds to the real speed of the crane. This approximation was acceptable, as the focus was on the pendulum dynamics, which can be modelled without the knowledge of the motor dynamics. Secondly, and the most significant approximation made, which may affect the dynamics to some extent, is the representation of the pendulum dynamics as a single spherical point mass system. When in reality the system consists of two spherical pendulums with torsion, along with a spherical pendulum for each ingot. In addition to this, the ingots are over 7 meters long, thus making a small angle on the hoist gives a significantly larger error in the position of the ingots. However, the simplified model was sufficient for further project development. Investing more time in a more accurate model would have come at the expense of other aspects of the project. Another approximation is the friction force caused by cable dynamics and the friction suspension system, which were modelled just by applying a damping coefficient as described in section 6.1.3. A more accurate model can be derived by utilising a cable model by SINTEF, as demonstrated in the master thesis written by P.Syvertsen [42]. Nevertheless, the simplified model appeared to be sufficient for further project development, highlighting that this remains a feasibility study.

Chapter 7

Control of Overhead Crane

7.1 Control Objectives

Today, Hydro's overhead cranes are operated under manual control. Although the pit-stripping process requires a high degree of precision, the task is highly repeatable. The objectives are therefore to develop a control system that covers

1. Trajectory planning.
2. Precise payload positioning in space.
3. Payload sway compensation.

Trajectory planning will be implemented as an algorithm computing trajectories in real-time. The precise position control system will be constructed by a closed-loop feedback controller, as well as a feedforward controller to control the movement in space relative to its planned trajectories. To compensate for the payload swing, an input shaper will be implemented into the simulation system.

An input shaper also has the potential to reduce payload swing when the crane is controlled manually. This will benefit the few but precise tasks operators are performing, which are often with a significantly larger payload. This is done with a modification of the joy stick signals through a control shaping algorithm. Such an algorithm will also reduce the hazard of these type of operations, which often requires more interaction with the payload in man-demanding operations.

7.2 Trajectory Planning

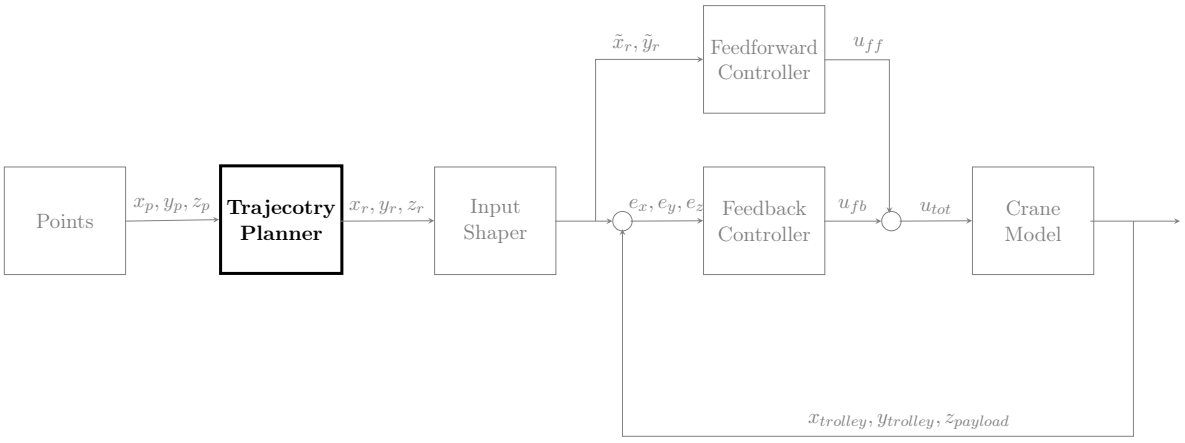

Figure 7.1: Block scheme of the control system, where trajectory planner is highlighted.

In order to control the crane's movement, a reference signal has to be generated. This can be achieved by point-to-point (PTP) trajectory generation derived in section 5.3.1. In order to generate these trajectories, each point has to be determined, as well as the specified time of departure and arrival. For the simulated environment, the points were roughly approximated, while in the physical system, the coordinates of the points would have to be calibrated with the installed sensors. PTP trajectory planning generates smooth curves, which make for slow changes in speed and no jumps in acceleration. It is also significant that both the trolley and bridge are stationary at their designated final positions as well as minimizing the sway of the hoist, which smooth polynomials contribute to. An example of a reference trajectory can be seen in figure 7.2.

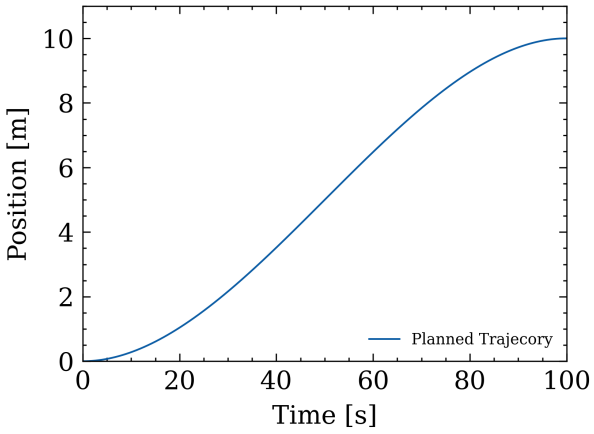

Figure 7.2: Example trajectory with PTP trajectory planning.

In order to generate the trajectories, a MATLAB algorithm has been made. The algorithm is implemented in Simulink, using a MATLAB function block. The inputs of this block are the time t, and the sequence of points $p_n(q_n, v_n, t_n)$ represented by a matrix with $[n \times 3]$ dimension for each direction. Using these points, the script automatically calculates the trajectories. This makes it easy to make different paths and long paths with numerous points. In algorithm 1, the pseudocode for the trajectory planner is shown.

Algorithm 1 Real-time trajectory planning algorithm

Input : Time, viapoints in space with initial velocity and initial start-time
Output : Planned trajectory in realtime
Initialize : Number of segments, initial segment
if *current segment <= number of segments* **then**
  if *start-time for current segment < time < start-time for next segment* **then**
    Calculate trajectory
  else
    move on to next segment
  end
end

The timing between points was calculated based on the maximum velocity of the trolley in each direction. The distance from the casting pit to the lay-down station is approximately 24 meters

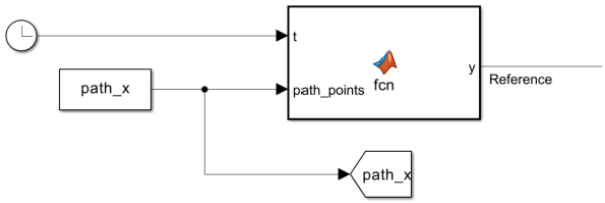

Figure 7.3: Trajectory planning function block.

in the x direction, and the maximum velocity of the actuator (the bridge) in this direction is $1.0\frac{m}{s}$. The distance can be covered in 24 seconds at a maximum speed, but to provide soft accelerations for the system, extra time was allocated for each path. If multiple actuators move simultaneously, for example, both the X and Y actuators, the timeframe is given by considering the direction that would take the longest.

Due to the fact that this only is a simulation, external factors that could affect the process are hard to foresee. Because there is no communication between the position along each coordinate axis, a system should be developed to ensure that the load is in the correct position before the following sequence can begin. An example of such a system could be that each coordinate has to be within 50mm of the reference point for at least 5 seconds before the next sequence could begin. This measure would ensure that the load is properly positioned and has minimal oscillations.

7.2.1 Alternative Path Planning

Given that the full path for extracting a cast will involve numerous waypoints, point-to-point path planning is a suitable option. In order to solve the path planning problem, two methods have been considered. The two methods are cubic polynomial and spline interpolation, which both can generate the same path. The decision between the two options came down to how the system was going to follow the path. The cubic polynomial method generates a path based on time, while spline interpolation generates a path based on τ. The spline interpolation method will be referred to as the tau method.

The method that was ultimately adopted as the solution was point-to-point path planning with a cubic polynomial, over the alternative. The deciding factor was that the path of the crane in space is relatively straightforward, therefore the easiest method was implemented (PTP). The tau method is suitable for more complex control and further work. Taking a closer look at the tau method is recommended because it gives more freedom when making the control system. Given the following general path from the tau method [43]:

$$q(\tau) = (1-\tau)y_0 + \tau y_1 + \tau(1-\tau)((1-\tau)a - \tau b) \tag{7.1}$$

This generates a path from y_0 to y_1 during which $0 < \tau < 1$, where a and b are restrictions of velocity. This gives freedom to choose a function for τ so that the actuator moves at a desired

velocity. An example is

$$\tau(t) = \frac{t - t_0}{t_1 - t_0} \tag{7.2}$$

Here, t_0 is the time the sequence starts, and t_1 is the time when it ends. This makes tau grow at a linear rate, thereby constant speed between y_0 and y_1. Other options include setting a limit on $\dot{\tau} = u$ to control oscillations and so on, as an alternative for sway control. Although the limited timeframe of this project precluded further work on such a solution, its potential merits further investigation.

7.3 Path Following

In order to follow the trajectory path given, feedback control and feedforward control have been implemented.

7.3.1 Feedback Control

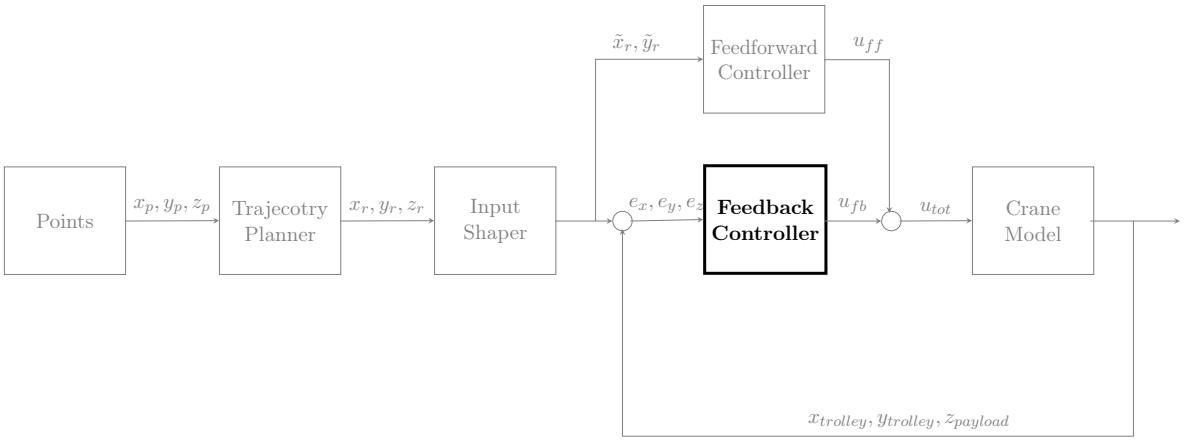

Figure 7.4: Block scheme of the control system, where feedback controller is highlighted.

In order to control the error between the reference signal and the process value, a PID controller is used. Unless an external force acts upon the system, an integral process such as this will never have any steady state error while using a proportional controller. In case of any unforeseen external forces or a steady-state error, a small integral gain is advised. In order to find the parameters for the PID controller, the Ziegeler-Nichols method was utilised [44]. It is important to note that the function for the controller used in this method is

$$u(t) = K_p \left(e(t) + \frac{1}{T_i} \int_0^t e(t)dt + T_d \frac{de(t)}{dt} \right) \tag{7.3}$$

This corresponds to the PID controller in Simulink on "Ideal form", where in Simulink, $P = K_p$, $I = \frac{1}{T_i}$, and $D = T_d$. Ziegeler-Nichols method uses a proportional controller and increases the gain until the system outputs standing oscillations. Despite applying increased gain, utilising the trolley position for feedback did not result in any oscillations. Consequently, in order to induce oscillations, the load's process value was employed. However, during actual system control, the

position of the trolley is utilised. With these oscillations, the critical gain of the system had been found, and by looking at the time between the oscillating peaks, the critical period time had been determined. For this system in the x direction, the critical gain is $K_k = 15$ and the critical period time is $T_k = 6.3$.

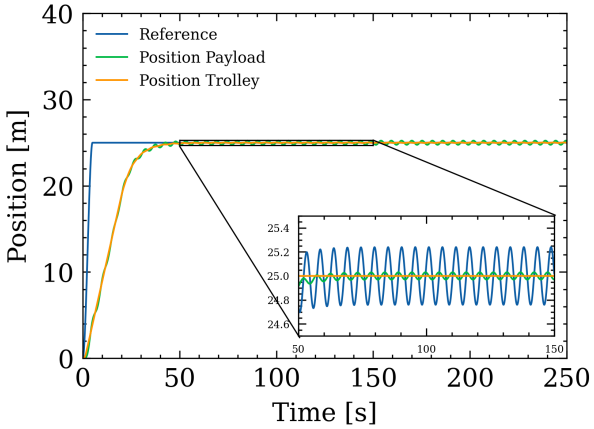

Figure 7.5: Standing oscillations with proportional regulator, $K_p = 15$.

Using the Ziegler-Nichols method, a table is used to find the suggested parameters for a PID controller. These parameteres can be calculated as follows: $K_p = K_k \cdot 0.65$, $T_i = 0.5 \cdot T_k$ and $T_d = T_k \cdot 0.12$. This was of course just a suggestion and needed to be adjusted for this specific system. Testing showed that minimal derivative gain, small integral gain, and huge proportional gain yielded the best results, upward to $K_p = 1000$. These numerical parameters were initially utilised, and subsequently fine-tuned in unison with the feedforward controller, in order to achieve the intended path following(7.3.3). The same method was used to find parameters for the PID controller in the y direction.

The following plot was made to see how accurately the trolley could track a reference trajectory with only feedback control. This was done by putting in huge proportional gain. Due to the system's slow response and constricted capacity for acceleration, a proportional controller with a large gain worked well.

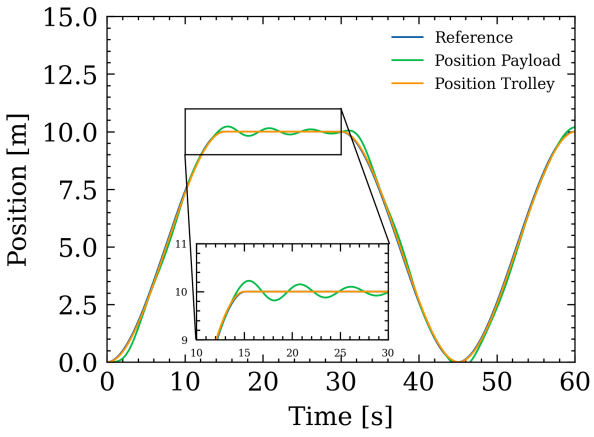

Figure 7.6: Feedback control of the trolley and load positions in response to a reference signal.

However, perfect path-following with just feedback control is by definition impossible due to the fact that the gain from the controller comes directly from the error between the reference and the process value. Figure 7.6 displays that path-following with such a controller follows the path efficiently, but there is significant sway on the load.

7.3.2 Feedforward Control

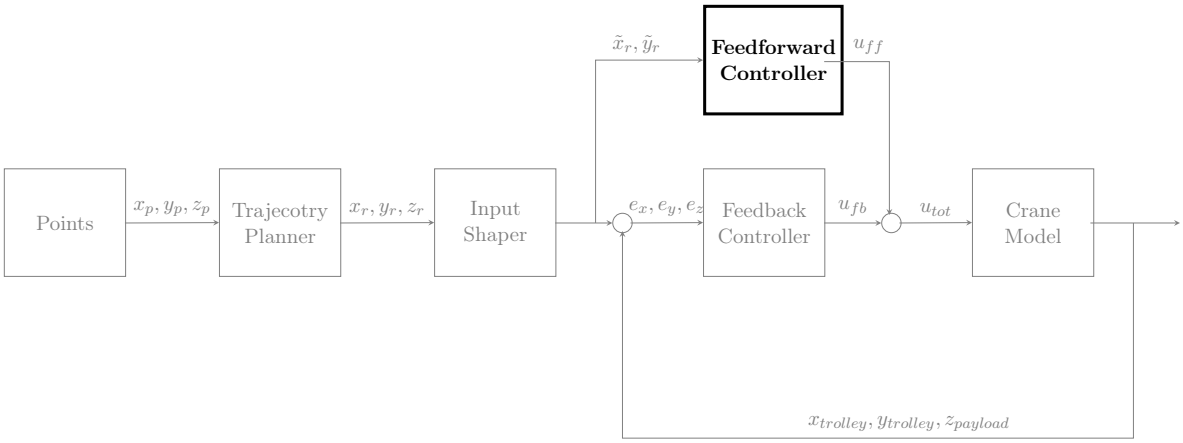

Figure 7.7: Block scheme of the control system, where feedforward controller is highlighted.

Because of how to feedforward controller is designed, the transfer function of the system in each direction had to be found. The system is an integrator with different velocities in each direction. In order to find the transfer function of the process, the step response method was used.

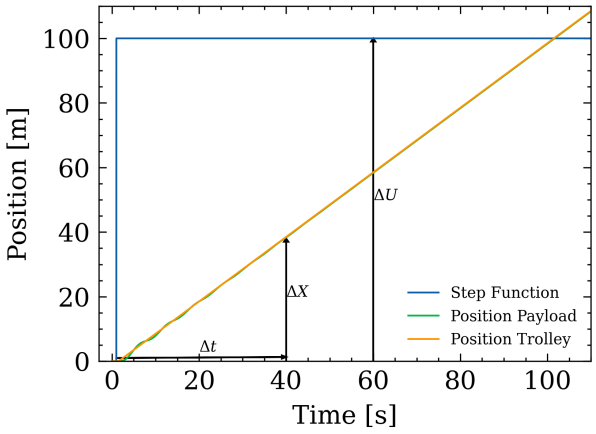

Figure 7.8: Step response method for calculation of transfer function.

The transfer function for an integrating process is $H(s) = \frac{1}{T_p s}$ where T_p is calculated as $T_p = \frac{\Delta U}{\Delta X}\Delta t$ [44]. For the X direction, the step response method gave the values $T_p = \frac{100}{40}40 = 100$ which in turn gives the transfer function $H_x(s) = \frac{1}{100s}$. This translates to the fact that the system moves at a rate of 1 meter per second for a gain of 100%. However, it should be noted that this representation is not entirely precise. In reality, the acceleration to initialise the step response is smooth, and the load has oscillations. It is however a good approximation for the response of the trolley.

The same method was used to find the transfer function of the system in the y direction, with the result being $H_y(s) = \frac{1}{200s}$. The only difference here is that the actuator moves slower in this direction, at a rate of half a meter per second at 100% gain.

Since the feedforward block is $H_{ff} = \frac{1}{H_{pros}}$, the feedforward transfer function for the y direction is 200s. This is an improper transfer function and is impossible to implement in reality, it can however be approximated as [45]:

$$\begin{aligned} H_{ff} &= 200s \cdot \frac{1+s}{1+s} \\ H_{ff} &= \frac{200s + 200s^2}{1+s} \\ H_{ff} &= \frac{200s}{1+s} \end{aligned} \tag{7.4}$$

Hence, the transfer function for the feedforward controller used for this project is represented as:

$$H_{ff} = \frac{T_n s}{T_d s + 1} \tag{7.5}$$

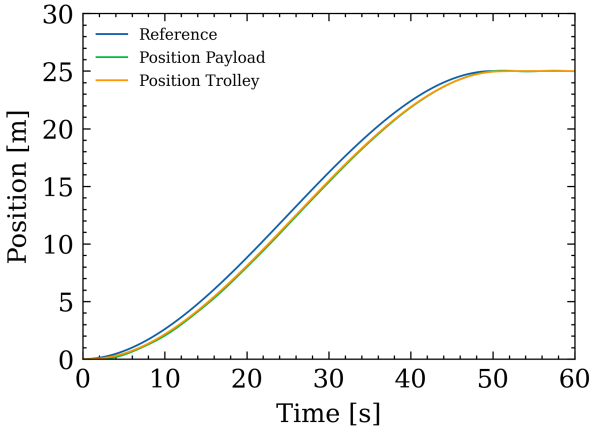

Figure 7.9: Feedforward control without feedback loop.

In figure 7.9, it can be seen how the trolley follows the generated path, without feedback control. While feedback control is crucial for compensating for unforeseen dynamics, the figure effectively demonstrates the accuracy achieved by this approximation.

7.3.2.1 Alternative Implementation of Feedforward Controller

The feedforward controller was implemented as a proper transfer function. The reason for this is that an improper function is impossible to implement in reality. The impracticability of implementing a real-time improper transfer function stems from its derivative nature, which requires knowledge about future values. However, since the feedforward controller is based on the reference signal, and the reference signal is known from start to finish, the feedforward controller can be implemented as an improper transfer function. Due to trouble with implementing this in

the simulation environment, this has not been done in this project. However, it is recommended to explore and incorporate this aspect in future development endeavours.

7.3.3 Controller Parameter Tuning Strategies

The two controllers that were described in section 7.3.1 and 7.3.2, can be seamlessly integrated together into one control system, as depicted in the accompanying figure 7.10. This gives a robust control system that compensates for reference errors, as well as quick changes in the reference.

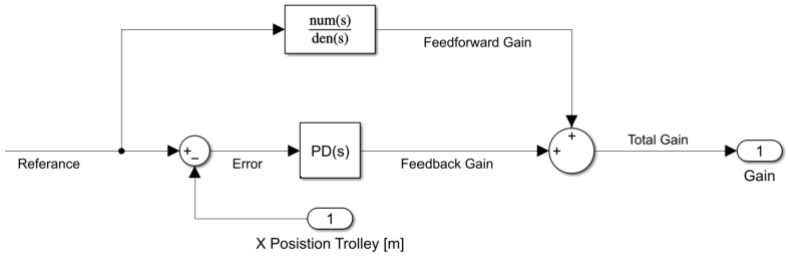

Figure 7.10: Control loop with feedforward and feedback control.

The design of this control system makes it possible to follow the path with little to almost negligible oscillations on the payload, depending on the specific time-frame requirements. If a rapid process is desired, there is a trade-off with increased oscillations, and a slow process gives us fewer oscillations. This is shown in figure 7.11a and 7.12a.

7.3.3.1 Fast Response Controller Tuning

To achieve a rapid control system, the controllers must be tuned to generate a sufficient response to deviations from the reference. However, the trade-off with a rapid control system, is bigger oscillations in the payload, as illustrated in figure 7.11a. The regulator parameters have been determined based on the Ziegler and Nichols and step-response method, which were derived in section 7.3.1 and 7.3.2. However, these parameters have been adjusted to make the system faster and with fewer oscillations.

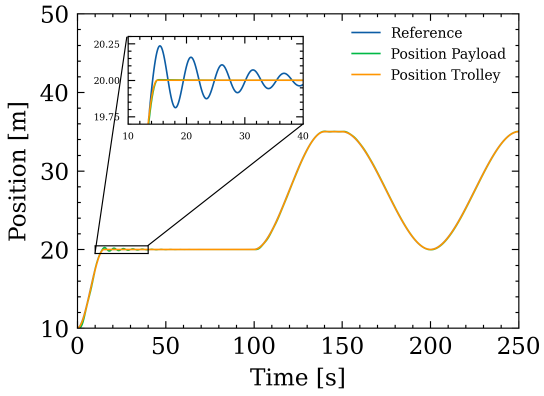

(a) Pathfollowing with fast response.

PID controller	P	1000
	I	0.05
	D	0.07
Feedforward	T_n	100
	T_d	0.1

(b) Parameters for controllers.

Figure 7.11: Fast response controller tuning with fitted parameters.

To enhance the responsiveness of the controllers towards deviations from the reference, there was applied some adjustments to the controllers. The feedforward controller is a transfer function based on the crane dynamics, as described in section 7.3.2. To increase the response of the controller, the transfer function was modified by decreasing the denominator. This is done to make the crane dynamic appear faster than it really is, which makes the feedforward controller more responsive. Decreasing the denominator makes the feedforward act faster, and gives a slightly increased gain. Decreasing the numerator of the feedforward controller makes the feedforward give less gain so that the process value doesn't overshoot the reference. The PID controller gains responsiveness by simply increasing the proportional gain and decreasing the deviation gain.

7.3.3.2 Stability-Driven Controller Tuning

The opposite is done to make the controllers respond more passively to deviations from the reference. Regarding the feedforward controller, the transfer function is modified to make the crane dynamic appear slower compared to reality, to make the controller respond more mildly. This is done by decreasing the numerator and increasing the denominator.

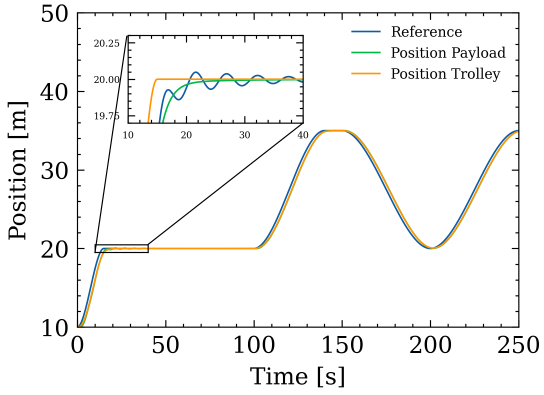

(a) Pathfollowing with stability driven tuning.

PID controller	P	9.75
	I	0.05
	D	0.756
Feedforward	T_n	85
	T_d	1.65

(b) Parameters for controllers.

Figure 7.12: Stability driven controller tuning with fitted parameters.

This tuning causes the process value to have to chase the reference the entire way, because of the feedforward controller adjustment. This however results in smaller oscillations.

7.3.4 Controller Parameters

Although many of the parameters suggested will be inaccurate when implementing an actual automatic system, the suggestions on how it should be controlled, and how the parameters were adjusted can be applied in practical use. The trolley system being an integrator makes it easy to model. Deviation from the datasheet to the actual physical system makes it necessary to do accurate testing on the system in order to create a good model, while these parameters are from a model based on the datasheet.

For the PID controller, simulations showed that a proportional controller with high gain yielded good results. For the x and y directions, the position was controlled based on the position of the trolley. This means that any sway would not be compensated for, although control with minimal sway was attempted without input shaping in 7.3.3.2 by adjusting the parameters to act less aggressively.

Making the controller output proportional to the error with a gain of 1000 makes the actuators give 100% when the error is 100mm or more. Simulating this gives good results. The Ziegler-Nichols method for tuning the controller gave suggestions, but further simulating showed that a much higher gain showed quicker control, and since the system is so slow, with a maximum velocity of $1\frac{m}{s}$, there is no overshooting caused by the P controller. With such a high gain, stability problems can occur. For instance, when the process value is close to the reference, utilising a high gain can lead to overcompensation, resulting in frequent overshooting and oscillation. This phenomenon is commonly referred to as actuator hunting, where the actuator struggles to attain the precise position required. The solution for a system such as this is that most of the gain into the process comes from the feedforward controller, and as long as this controller keeps the process value within 100mm of the reference, the P controller only corrects for small deviations, as shown in figure 7.13. As well as this system is so slow that it has a hard time overshooting with just a proportional controller. Since the system is so easy to model, the feedforward controller should not have any problems keeping the process value close to the reference.

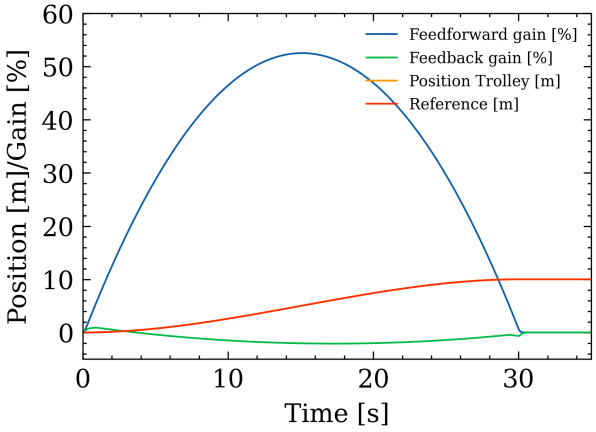

Figure 7.13: Gain from feedback and feedforward controllers while following a simple path.

If actuator hunting is a problem when implementing the system, a possible solution is modifying the output from the controller. By limiting the controller gain to multiples of 10, thereby limiting its output to 10%, 20%, and so on, the actuator can remain motionless as long as it is sufficiently close to its reference. Decreasing the gain is not recommended as it leads to an increase in settling time, it can however be another solution for actuator hunting if it is still a problem.

7.3.5 Alternative Trolley Control Systems

Numerous control systems can be applied to control the crane, including Model Predictive Control (MPC), Linear Quadratic Regulator (LQR) and Cascade with PID control.

7.3.5.1 Model Predictive Control

MPC is an advanced control strategy that is based on a mathematical model of a system, where it is used to predict the system's future behaviour and optimise its gain over a time horizon. The gain is computed by solving an optimisation problem with respect to the current state, the predicted future, and the desired result [46]. While MPC control can be a very effective and good approach, it was not suitable to implement in this project. The dynamics of a crane system are nonlinear and difficult to model precisely, which can lead to an inferior and unstable control system. MPC is also highly complex and needs a substantial amount of computing resources, this can result in delays and make the control response slower, especially in a real-time system such as a crane.

7.3.5.2 Linear Quadratic Regulator

The Linear Quadratic Regulator is a feedback control technique designed to manage linear dynamic systems or locally for nonlinear systems [36], where the goal is to operate the system at minimum cost. The cost is based on a quadratic function, which is called the LQ problem [47]. The tuning of the controller is based on weighting factors (Q and R), which serve to quantify the importance of the states within the system [48]. Based on the weighting factors, a mathematical algorithm chooses the output that results in minimum cost. In this project, the weighing factors

could have been implemented with a dynamic model in state space form, where position and angle would have been considered as states. However, the LQR is mainly designed for linear systems, although it could be used locally for nonlinear systems, the performance of the controller may become unstable as the system deviates from its linear approximation. The controller also requires a good and accurate dynamic model, and therefore might not be suitable for the approximated model that was derived in this project. Another challenge is proper tuning, as it necessitates an in-depth understanding of system theory.

7.3.5.3 Cascade Control

Cascade control is a control method that utilises two control loops in order to control the process value of the system. Research on this was done in order to find out if this could be a solution to controlling the sway of the system. A criterion for cascade control is that the time constants of the inner loop are at least three times faster than those of the outer loop [49].

In cascade control, the output of the first controller is used as a reference for the inner controller. The output from the second controller is the actual output to the system, thereby making the outer control loop a suggestion, and the inner loop the actual control unit. This method requires a measurement of a second variable to use in the inner loop.

The problem with applying cascade control to a system such as this is finding an appropriate measurable second variable. Attempts were made by using the angle in the hoist, or the difference in speed between the trolley and the load. The problem with this was that the states are proportional to each other.

7.4 Input Shaping as Sway Control

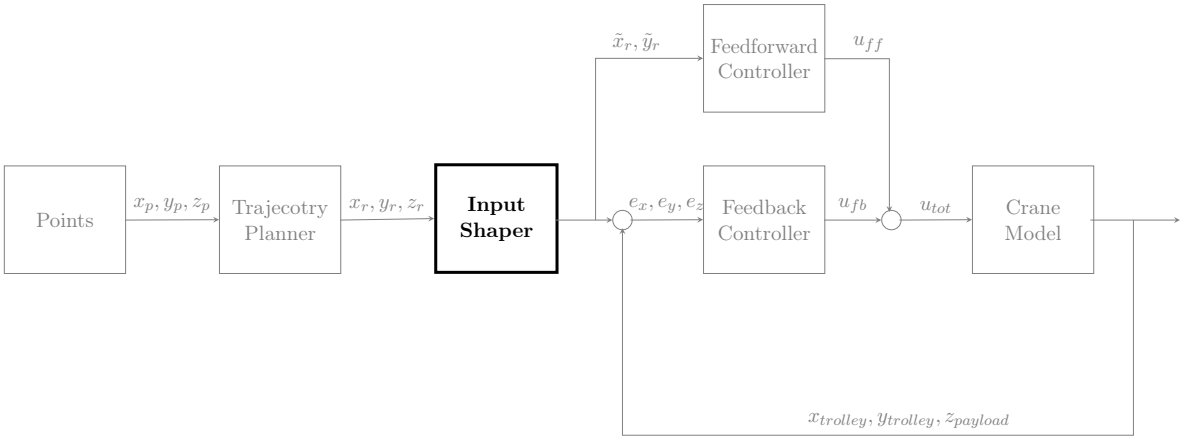

Figure 7.14: Block scheme of the control system, where input shaper highlighted

As a step toward fully automating the extraction process, semi-automated solutions such as input shaping could be of interest. As of now, Hydro's overhead cranes are only controlled by human operators who use a remote control crane joystick. If the operator alters the bridge or

trolley velocities, the bridge or trolley will move a finite distance before it comes to rest [42]. The payload however is not guaranteed to come to rest but may oscillate due to the forces applied.

As described earlier in this thesis, operators use their experience to reduce the sway, but when the load is extensive, even the experienced operators may struggle to remove the sway. Input shaping can therefore be an important strategy to semi and fully automate this process.

The theory behind input shapers is introduced in chapter 5.6.3

7.4.1 Zero Vibration Shaper

Zero Vibration Shaper, also known as ZV Shaper, is the simplest form for the input shaping method presented in this thesis. The ZV shaper is constructed of two ($n = 2$) impulses A_1 and A_2. For simplicity reasons, the time of the first response, t_1, is set to zero. The problem is therefore to compute t_2, A_1 and A_2. The amplitude of these impulses is calculated as follows

$$A_1 + A_2^{\zeta\omega t_2} cos(\omega_d t_2) = 0, \tag{7.6}$$

$$A_2^{\zeta\omega t_2} sin(\omega_d t_2) = 0, \tag{7.7}$$

$$A_1 + A_2 = 1 \tag{7.8}$$

Equation 7.8 is only satisfied when

$$\omega_d t_2 = n\pi \rightarrow t_2 = \frac{n\pi}{\omega_d} \quad n = 1, 2, ... \tag{7.9}$$

t_2 is chosen as

$$t_2 = \frac{\pi}{\omega_d} \tag{7.10}$$

to cancel vibrations. Equation 7.8 and 7.10 can now be rewritten as

$$A_2 - (1 - A_2) = e^{\zeta\omega\frac{\pi}{\omega_d}} = 0 \tag{7.11}$$

A_2 can then be rewritten as

$$A_2 = \frac{e^{\frac{\zeta\pi}{\sqrt{1-\zeta^2}}}}{1 + e^{\frac{\zeta\pi}{\sqrt{1-\zeta^2}}}} = \frac{K}{1+K} \tag{7.12}$$

where $K = e^{\frac{\zeta\pi}{\sqrt{1-\zeta^2}}}$. All impulses and their designated points can be presented as

$$\begin{bmatrix} A_i \\ t_i \end{bmatrix} = \begin{bmatrix} \frac{1}{1+K} & \frac{K}{1+K} \\ 0 & \frac{\pi}{\omega_d} \end{bmatrix} \tag{7.13}$$

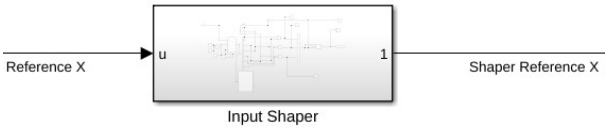

Figure 7.15: Simulink representation of Input shaper.

These equations are implemented in MATLAB Simulink as a subsystem, presented in Figure 7.15, and the fitted parameters are computed. The solution is simulated and presented in Figure 7.16.

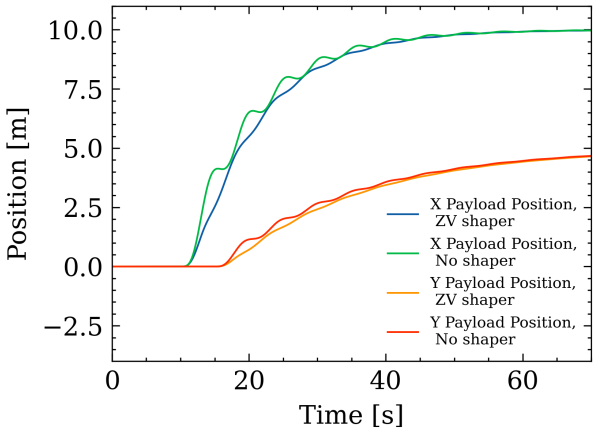

Figure 7.16: Payload Position with and without continuous ZV input shaper.

The ZV input shaper reduces vibrations, although it introduces a time delay to the system. This delay is important to consider when choosing the shaper method. In Figure 7.17 the error between the payload position and trolley position is plotted. This plot shows a decrease in error both in x and y directions, from $\pm 0.8m$ to $\pm 0.4m$ and from $\pm 0.2m$ to $\pm 0.1m$.

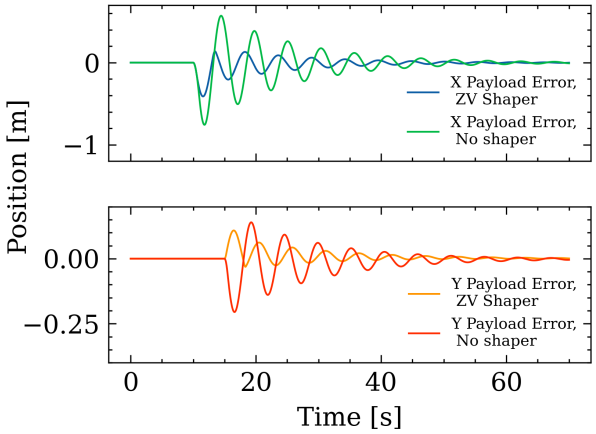

Figure 7.17: Payload position error with and without continuous ZV input shaper.

In Figure 7.18 the sensitivity curve for the ZV shaper is presented. This surface is designed by calculating Equation 5.60 and 5.59, where A_i and t_i are calculated to the crane's dynamics with Equation 7.13. The result is a surface which displays the correlations between the damping ratio

ζ, the relationship between the actual frequency ω and the calculated normalised frequency ω_n, and the residual Vibrations $V(\omega_n, \zeta)$. A change in the relationship $\frac{\omega}{\omega_n}$, caused by a modelling error, results in a significant increase in residual vibration. An increase in the damping ratio also results in an increase in residual vibrations. Such a plot will give adequate knowledge of how a modelling error in the crane dynamic will influence the residual vibration, and what input shaper to choose. Therefore the ZV input shaper is suitable for systems where perfect knowledge is obtained.

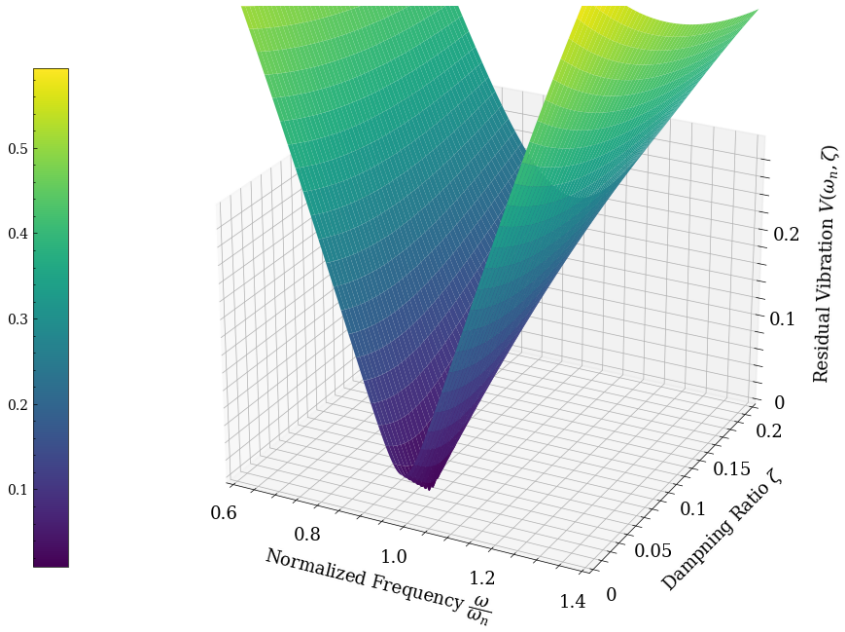

Figure 7.18: Three-dimensional sensitivity curve for ZV input shaper.

7.4.2 Zero Vibration Derivative Shaper

As mentioned in the section above, the ZV shaper proved to be sensitive to modelling errors in the crane's dynamics. In response to this, a more robust input shaper has been developed, named Zero Vibration Derivative Shaper consisting of 3 impulses A_1, A_2 and A_3, where $n = 3$. This type of input shaper also satisfies the robustness constraint

$$\frac{d^3}{d\omega^3} V(\omega, \zeta, t_N) = 0 \tag{7.14}$$

The unknown variables t_2, t_3, A_1, A_2 and A_3 are found using the same method as the ZV shaper

$$\begin{bmatrix} A_i \\ t_i \end{bmatrix} = \begin{bmatrix} \frac{1}{1+2K+K^2} & \frac{2K}{1+2K+K^2} & \frac{K^2}{1+2K+K^2} \\ 0 & \frac{\pi}{\omega_d} & \frac{2\pi}{\omega_d} \end{bmatrix} \tag{7.15}$$

These equations are also implemented in MATLAB Simulink as a subsystem, and the fitted parameters are computed. The solution is also simulated and presented in Figure 7.19.

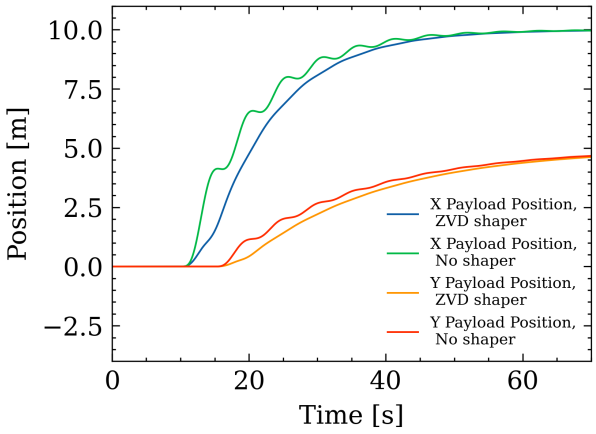

Figure 7.19: Payload Position with and without continuous ZVD input shaper.

After discussing the response with experienced operators, it is concluded that the timing of acceleration is similar to the movement when operated manually. The ZVD input shaper reduces vibrations compared to the ZV shaper, although it introduces a larger time delay. In Figure 7.20 the error between the payload position and trolley position is plotted. The plot shows a decrease in error both in the x and y directions, from $\pm 0.8m$ to $\pm 0.2m$ and from $\pm 0.2m$ to $\pm 0.05m$.

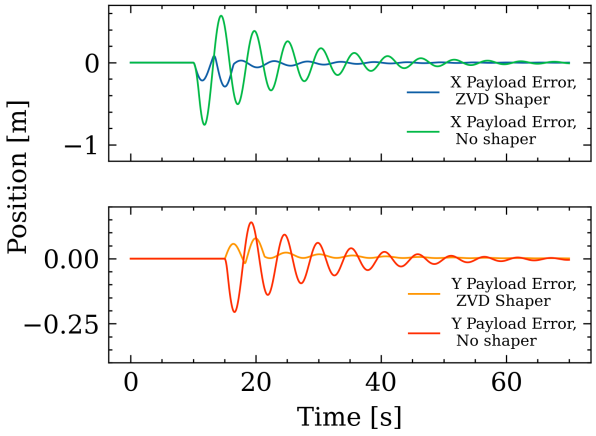

Figure 7.20: Payload position error with and without ZVD input shaper.

In Figure 7.21 the sensitivity curve for the ZVD shaper is shown. This surface is the result of Equation 5.59 and 5.60, where A_i and t_i are derived from the crane dynamics and Equation 7.15. The outcome is a visual representation that demonstrates the relationships among the damping ratio ζ, the actual frequency ω, the calculated normalised frequency ω_n, and the residual Vibrations $V(\omega_n, \zeta)$. A change in the relationship $\frac{\omega}{\omega_n}$, caused by a modelling error, results in a moderate increase in residual vibration compared to the ZV shaper. Compared to the ZV input shaper, the ZVD shaper is more robust due to its moderate increase in residual vibrations. Therefore the ZVD input shaper is suitable for systems where one can not obtain full knowledge of the system modelled.

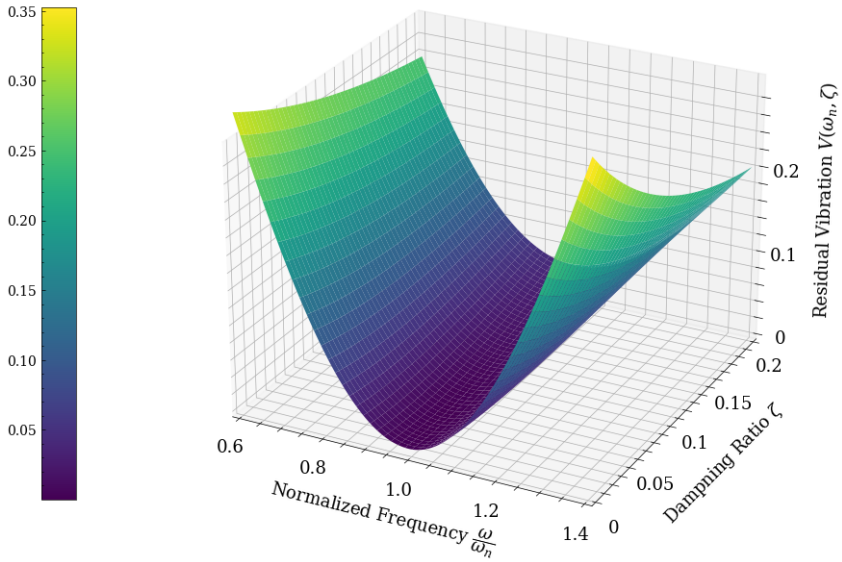

Figure 7.21: Three-dimensional sensitivity curve for ZVD input shaper.

7.4.3 Zero Vibration Derivative Derivative Shaper

As proved earlier, the ZV and ZVD input shapers have some weaknesses regarding errors in the modelling of the crane's dynamics. There is therefore developed an even more robust input shaper, named Zero Vibration Derivative Derivative Shaper consisting of 4 impulses A_1, A_2, A_3 and A_4, where $n = 4$. This type of input shaper also satisfies the robustness constraint

$$\frac{d^4}{d\omega^4} V(\omega, \zeta, t_N) = 0 \tag{7.16}$$

The unknown variables t_2, t_3, A_1, A_2 and A_3 are found using the same method as the ZV shaper and the ZVD shaper

$$\begin{bmatrix} A_i \\ t_i \end{bmatrix} = \begin{bmatrix} \frac{1}{1+3K+3K^2+K^3} & \frac{3K}{1+3K+3K^2+K^3} & \frac{3K^2}{1+3K+3K^2+K^3} & \frac{3K^3}{1+3K+3K^2+K^3} \\ 0 & \frac{\pi}{\omega_d} & \frac{2\pi}{\omega_d} & \frac{3\pi}{\omega_d} \end{bmatrix} \tag{7.17}$$

These equations are implemented in MATLAB Simulink as a subsystem, and the fitted parameters are computed. The solution is also simulated and presented in Figure 7.19.

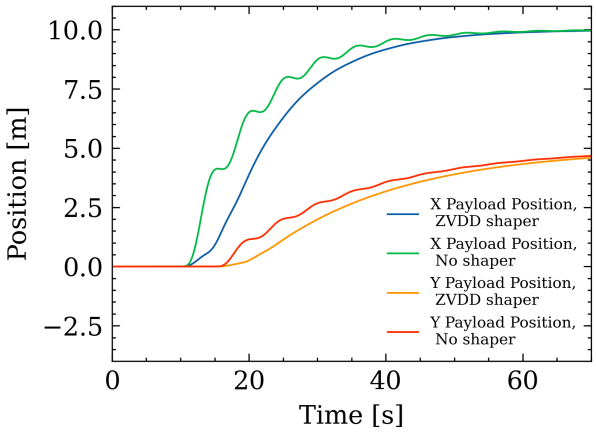

Figure 7.22: Payload position with and without continuous ZVDD Input Shaper

The ZVDD input shaper reduces vibrations better than both to the ZV and ZVD-shaper, although it introduces a larger time delay to the system. In Figure 7.23 the error between the payload position and trolley position is plotted. The plot shows a decrease in error both in x and y directions, from $\pm 0.8m$ to $-0.2m$ in x direction and $\pm 0.2m$ to $-0.075m$ in y directions. The movement of the load is like

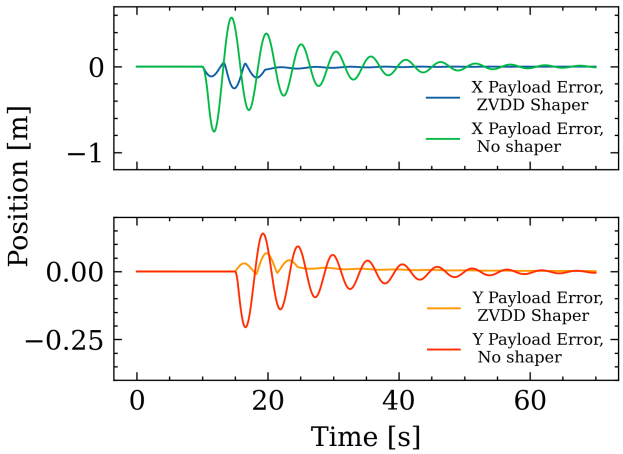

Figure 7.23: Payload position error with and without continuous ZVDD input shaper.

In Figure 7.24 the sensitivity curve for the ZVDD shaper is shown. This surface is designed by calculating Equation 5.60 and 5.59, where A_i and t_i are calculated to the crane's dynamics. The result is a surface which displays the correlations between the damping ratio ζ, the relationship between the actual frequency ω and the calculated normalised frequency ω_n, and the residual Vibrations $V(\omega_n, \zeta)$. A change in the relationship $\frac{\omega}{\omega_n}$, caused by a modelling error, results in an insignificant increase in residual vibration. An increase in the damping ratio also results in an increase in residual vibrations. Compared to the ZV and ZVD input shaper, the ZVDD offers an even more robust solution, and will therefore fit systems where modelling errors are likely.

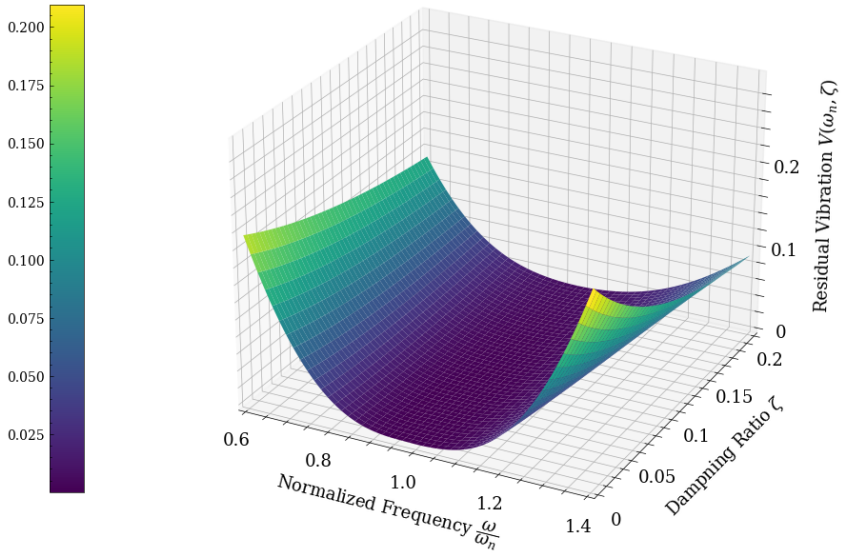

Figure 7.24: Three-dimensional sensitivity curve for ZVDD input shaper.

7.4.4 Discussion

As demonstrated in this section, the application of ZV, ZVD, and ZVDD input shapers yields a noteworthy reduction in sway, albeit with certain limitations. The ZV input shaper reduces the sway with 50%, the ZVD input shaper with 75% and the ZVDD input shaper with 75% as well as the settling time and number of oscillations. It is worth noting, however, that a precise model of the natural frequency of the system is required, and modelling errors may compromise the robustness of the input shaper.

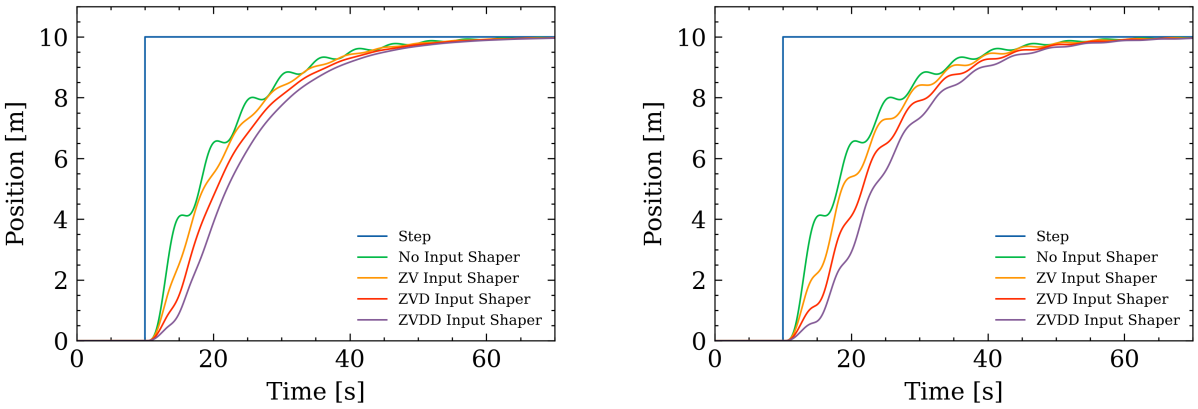

(a) All inputs shapers compared with the correct ω_n.

(b) All inputs shapers compared with the incorrect ω_n.

Figure 7.25: Comparison of input shapers with and without modelling error. Blue is the step in reference, green is the payload position without input shaper, the orange is the position with ZV input shaper and the purple line is the position with ZVDD input shaper.

Moreover, the robustness of the input shapers varies, as evidenced in this thesis. Specifically, the ZVDD input shaper exhibits the highest degree of robustness, whereas the ZV shaper exhibits

the lowest degree of robustness. This must be taken into account when selecting an appropriate input shaper. Furthermore, the delay introduced by the input shaper must also be considered, as greater robustness results in greater delay. Figure 7.26 and 7.25b present sensitivity curves and a simulation test with modelling errors, highlighting that the ZVDD shaper is the most robust due to its ability to cancel a larger range of frequencies.

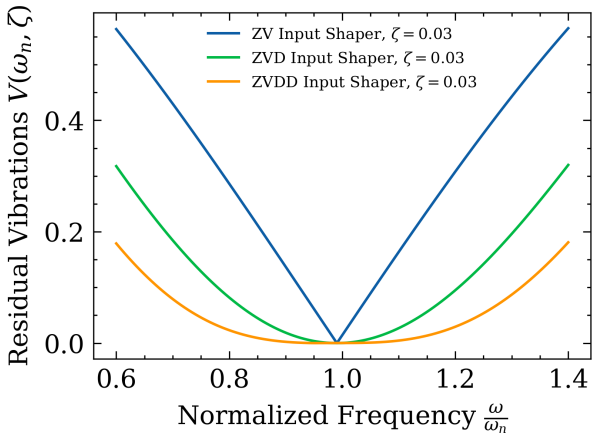

Figure 7.26: Two-dimensional sensitivity curves for ZV, ZVD and ZVDD input shapers with the cranes calculated $\zeta = 0.03$.

There also exist other input shapers that could produce the same results. Examples are the extra insensitive shaper (EI), the unity magnitude zero vibration shaper (UM-ZV), and the specified intensity shaper (SI).

Such solutions have the potential to enable operators to transport payloads with reduced sway, thereby representing critical advancements towards full process automation. Implementing such technological enhancements can facilitate testing, revision, and further development of automated systems.

The simulation results indicate that the ZVD input shaper exhibited the highest level of performance, as evidenced by its robustness, minimal delay, and a reduction of vibrations by 75%. A study performed by *Piedrafita.R*, *Comín.D*, and *Beltraán. J.R* where the ZV, ZVD, and ZVDD input shaper was tested on an industrial overhead crane with promising results [50]. However, it should be noted that alternative control methods may be better suited for more intricate systems, where mitigating modelling errors may prove challenging.

7.5 Alternative Sway Controls

There exist a large amount of literature and studies on different control methods for anti-sway control of overhead cranes. A great part of these studies are only tested on small-scale cranes, and not in industrial conditions. They are although great for proving their concept. A large part of the information regarding the control methods below are collected from *Modelling and control of overhead cranes: a survey* [36].

7.5.1 Sway Control using Cable Length Manipulation

This type of sway control uses the hoist to vary the cable length in order to minimise the sway. In other words, this system tries not to control the payload sway with the force applied to the trolley and bridge, and the cable length is considered as the control input rather than the control output. The vast majority of the studies and papers published with this type of sway control comprise platform cranes, with a highly compact payload, and not overhead cranes. Hydro's overhead cranes also have a limited hoist drive, and a cable manipulation system would be time-consuming.

7.5.2 Sliding-mode Control

The Sliding-mode Control (SMC) is a widely used approach for sway control. It is especially suited for systems with uncertain and varying parameters. This method measures payload position, velocity and accelerations to control the payload to the desired position, and is considered as one of the more complex solutions. More specifically, the SMC works by creating a mathematical construct, called a sliding surface that represents the desired behaviour of the system. The SMC was not used in this thesis because of its complexity.

7.5.3 Lyapunov-based Control Design

The lyapunov-based control design is commonly used in nonlinear control systems to ensure performance and stability. The control system is based on a Lyapunov function, and the paper "*Enhanced damping-based anti-swing control method for underactuated overhead cranes*" [51] has proposed two Lyapunov functions for sway control for overhead cranes. The first function only includes the sway angles β and α, and by calculating the time derivative, obtaining the desired velocity trajectory. The second function includes both the sway angles and the trolley position and calculates the control law for force by calculating the time derivative. This is also regarded as a complex method and will require a nonlinear model

7.6 Results of the Complete Control System

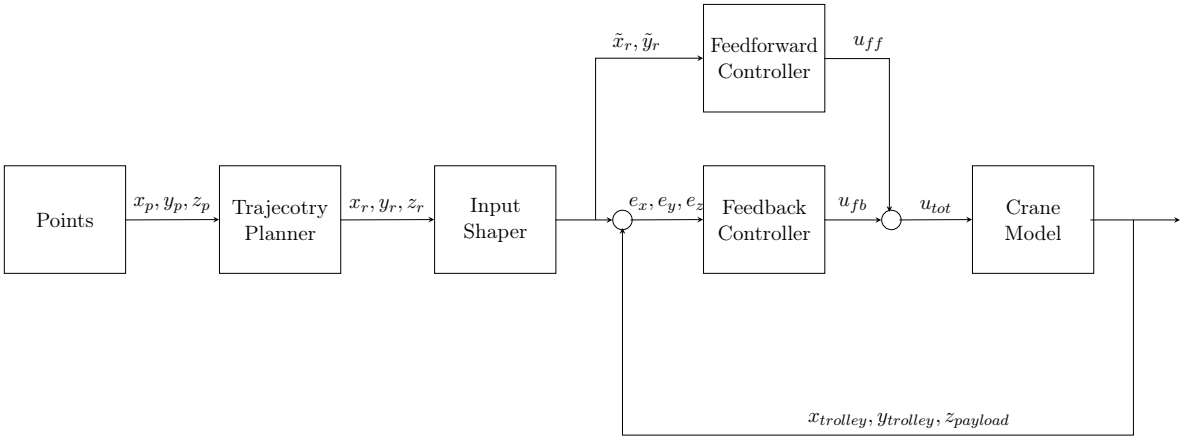

Figure 7.27: Complete control system block scheme.

The complete control system comes with feedback and feedforward control, as well as the ZVD input shaper. Through a comprehensive tuning process, the control parameters were optimised to achieve optimal control performance, while also exhibiting robustness across a diverse range of operating conditions. The focus of the control parameters was fast path following, as well as minimal sway.

A comprehensive simulation of the entire process of extracting a row of ingots was conducted. For generating a path for the lifting yoke and the trolley, a sequence of points was made that represent how the process moves, based on measurements done at the casthouse. The path shown in figure 7.28a is this path in the x direction. The simulation showed that with reasonable time for pickup and placements for the ingots, a row could be completed in under 5 minutes.

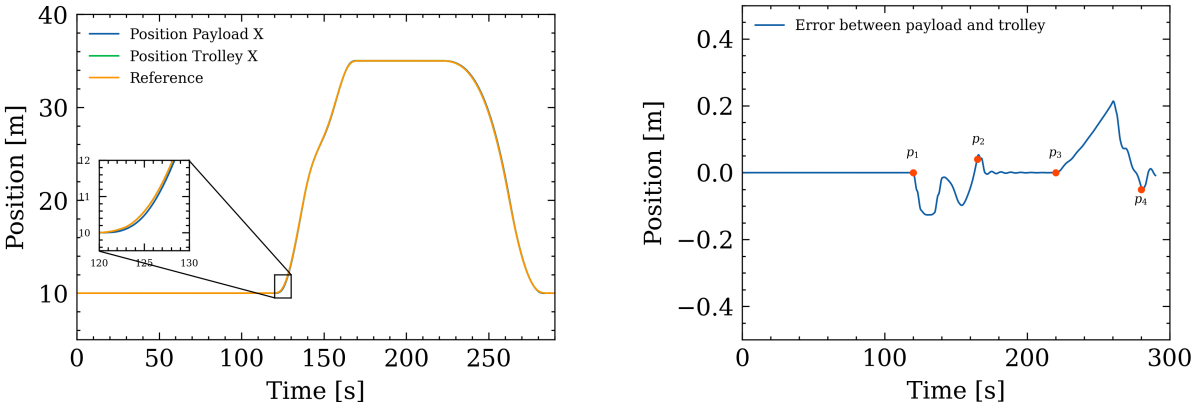

(a) Path-following with the complete control system.

(b) Error plot of trolley-payload displacement over time, with emphasis on critical time points.

Figure 7.28: Results of simulations for complete control system.

The parameters for best control, which were used in the figure above are as follows:

PID controller	P	1000
	I	0.05
	D	0
Feedforward	T_n	100
	T_d	0.1
Input shaper	ζ	0.03
	ω_n	0.99

Table 7.1: Control parameters for x direction

As can be seen in 7.28a, the trolley and load follow the desired reference path with great accuracy and minimal sway. The yellow graph is the position of the trolley, payload, and reference, where the error is so small that they appear on top of each other. Within the context of figure 7.28b, the trolley moves in the positive direction along the x-axis between points p_1 and p_2. Subsequently, between p_2 and p_3, it remains stationary along the same axis. Finally, between points p_3 and p_4, the payload retracts back to the casting pit. Although the input shaper delays the reference signal somewhat, the benefit is a precise path following with a sway of no more than $200mm$ in

its moving state, and less than $20mm$ when it comes to rest. It is important to note that the error is approximately zero when the payload reaches its desired position.

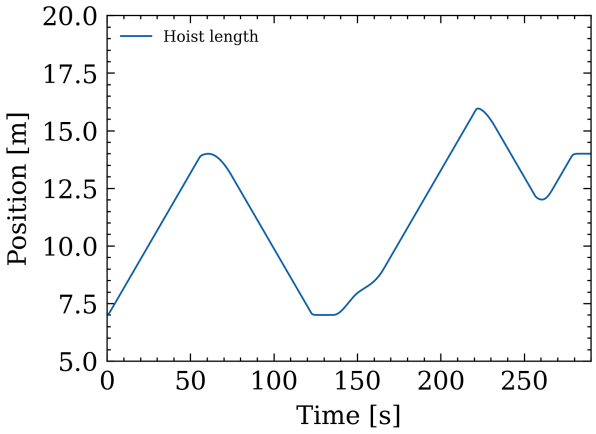

Figure 7.29: Path of the cable length during simulation.

In figure 7.29 the length of the hoist is shown during the simulation. Because of the slow speeds at which the hoist operates and the large gain of the PID controller, the control system effectively works as an on/off controller. During the hoisting and lowering of the lifting yoke, the hoist almost always operates at full speed, which can be seen by the straight lines on the path.

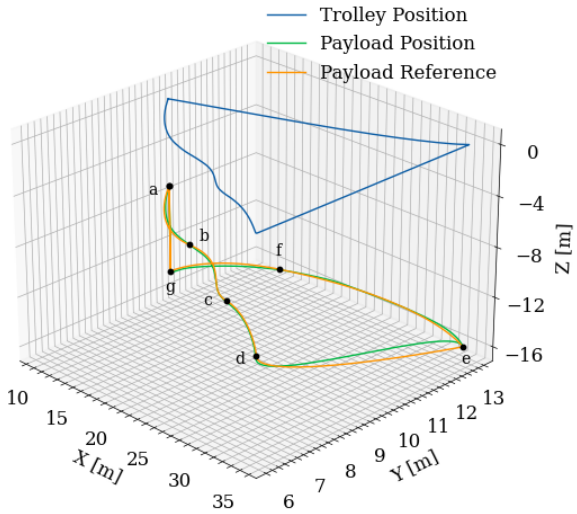

Figure 7.30: Blue line represents the position of the trolley in three-dimensional space, green line is the payload position and yellow line is the payload reference. (a) represent the position over the casting pit. (b) and (c) represent via points in space. (d) represent the position over the lay-down station. (e) represent the position of the lifting yoke when the billets are removed. (g) represent the position when attaching billets in the casting pit.

In figure 7.30 the simulation is presented in three-dimensional space. The points were chosen somewhat arbitrarily, the distances are however representative of the distances the crane moves in its operation at Casthouse Sunndal.

Chapter 8

Conclusion

Automatic pit stripping has been a focus area of Hydro for some time. Although several good and robust solutions have been proposed in the past, a common drawback is the extent of the modifications that are required to achieve automatic operation. The scope of this thesis has therefore been to evaluate the potential for automatic pit stripping, with only limited alterations to the existing installations in Hydro's extrusion ingot cast houses, using casting centre number 9 in Hydro Sunndal as a reference.

From an automation perspective, the most challenging part of the pit stripping sequence is attaching the ingots to the lifting yoke. This is done while the ingots are resting in the casting pit on the starter blocks, standing upright. Using the current lifting yokes, where billet rings are attached to the yoke girder through a chain link, would not be a viable solution for further automation. This is due to the unpredictable behaviour of the chain links and the risk of causing a "domino effect" if one ingot falls over. Even with a hydraulic billet tong, the lifting equipment would need to be controlled without oscillations and without contacting other ingots. This would demand a control system performing beyond what is reasonably implementable, given the size of the system.

Although sophisticated control systems, precise instrumentation and accurate actuators will increase the positioning accuracy until a certain point, the performance achieved is still not assumed adequate for reliable and robust ingot attachment. This points towards the need for a revision of the mechanical parts of the system, to increase the positioning margins and ensure the robustness and reliability necessary. The redesign of the billet rings (A1) would likely enhance the reliability of the ingot attachment process. By implementing a retractable cradle system, that guides a lifting yoke into position, the requirements for the positioning system are furthermore substantially reduced.

The mechanical solutions presented in this thesis are detailed but still flawed. The goal of these design proposals is however not to provide an "out-of-the-box" solution to the ingot attachment problem. On the contrary, the goal is to emphasise the mechanical aspects that need to be revised.

One challenge in automating the crane is ensuring its ability to control the load with high precision and minimal oscillations, while also maintaining operations within a reasonable time frame. The control system proposal provides accurate control of the payload at high velocities and with minimal sway, as shown in figure 7.28a. The modelled crane dynamics are however simplified and may deviate from the real system, causing more oscillations than simulated. However, it is anticipated that the implemented mechanical solutions presented in section 4.8, will effectively counterbalance any potential oscillations that may arise during the extraction process.

From this thesis' research and development, it appears that automatic pit stripping is achievable

through modest modifications to the existing installations. Accurate hoist trolley positioning can be achieved through classical control strategies, such as PID- and feed-forward controllers. Precise and oscillation-free payload positioning is however more intricate. The simulations carried out, where a simple input shaper was implemented to alleviate oscillatory behaviour in payload positioning, show promising results even with a simple controls architecture. These simulations are however carried out on a simplified crane model, and this approach to alleviating oscillatory behaviour would require further verification before being implemented in a full-scale system.

8.1 Further Work

The first step towards realising automatic pit stripping would be finalising and validating the required mechanical solutions. The initial approach would be finalising the billet ring design, iterating on the 3rd billet ring version (displayed in figure 4.3c). The final version would need to facilitate a full locking of the revolute joint when being threaded onto the extrusion ingots. Calculations of the biting force exerted on the ingots during lifting would furthermore need to be carried out. A prototype ring would then have to be made, validating lifting safety and reliability.

If the billet ring prototype test proves successful, the next step would be making a prototype of a new lifting yoke. As mentioned in chapter 4.2.1, it is recommended to base the revised lifting yoke design on the lifting yokes currently used in Casthouse Husnes, displayed in figure 3.3. As discussed in chapter 4.2.3, this is due to the simpler implementation of linearly actuated push-bars on each side of the yoke, pushing down on each side of the billet ring stem, fully locking the revolute billet ring joint.

After the lifting yoke design is finalised and tested, the guide cradles presented in figure 4.9 would need to be modified to fit the final lifting yoke design. The concept of mounting guide cradles to the safety platform is assumed a viable solution in order to accurately and reliably position the lifting yoke directly above the extrusion ingots.

In terms of control engineering, the simulations of the control system proposed in section 7, show promising results for the automatic pit stripping concept's viability. Before full-scale implementation, there are however aspects in need of validation, either in a test bench or through more accurate system models. The PID and feed-forward part of the control system, controlling the hoist trolley's position, is considered robust due to the simple dynamics of the trolley. The input shaper is, however, an open-loop control system, aiming to control the motion of a body with more complex dynamics. As such, it inherently represents a risk of unpredictable behaviour in case of modelling errors. Its aim is to generate destructive interference in the payload's oscillatory behaviour, but might, in case of modelling errors, instead generate constructive interference. This could result in greater oscillations.

If the performance of the proposed control system is considered adequate during validation, further development would be unnecessary. On the other hand, if its performance does not suffice, further development would be required. Basing the input shaper on a more accurate model of the crane hook's dynamics could be an initial step forward. The main features that will need to

be considered in a more complicated crane model are linked to its pendulum dynamics. Multiple hoist wires need to be taken into account as well as a more thorough model of the lifting yoke and the changing centre of gravity once the ingots are attached to the lifting yoke. If this does not result in sufficiently increased performance, more complex control strategies would be required. Chapters 7.5 and 7.3.5 mention different approaches, using more advanced control strategies.

Once the final control system is known, the necessary instrumentation package can be extracted from the proposal in section 4.6.2. This instrumentation package covers the required measurements for all the system's degrees of freedom and would suffice, even for a closed-loop anti-sway control system. If the system's oscillatory behaviour is sufficiently and robustly alleviated through an open loop control system, the need for accurately measuring the angles of the hoist wires could be reduced. It could however still be beneficial to monitor that the hoist wire angles do not surpass a certain threshold value, to detect if constructive interference causes oscillations with a large and increasing amplitude.

References

[1] AlCircle, "Top ten alumina companies in the world," Dec 2016. [Online]. Available: https://www.alcircle.com/news/top-ten-alumina-companies-in-the-world-26529

[2] Hydro ASA, "Wire rod for cable and wire solutions," [Accessed 25-April-2023]. [Online]. Available: https://www.hydro.com/en/aluminium/products/casthouse-products/wire-rod-for-cable-and-wire-solutions/

[3] Hydro ASA, "Primary aluminium for remelting," [Accessed 25-April-2023]. [Online]. Available: https://www.hydro.com/en/aluminium/products/casthouse-products/remelt-ingots/

[4] Hydro ASA, "Extrusion ingots – the raw material for extruded profiles," [Accessed 25-April-2023]. [Online]. Available: https://www.hydro.com/en/aluminium/products/casthouse-products/extrusion-ingots/

[5] Hycast AS, "Casting machine vertical," Feb 2022. [Online]. Available: https://www.hycast.no/products/cmv

[6] Hydro ASA, "Extrusion Ingots Data Sheet," [Accessed 26-April-2023]. [Online]. Available: https://www.hydro.com/Document/Doc/Hydro%20Extrusion%20Ingots%200918.pdf?docId=416541

[7] I. K. Steen and A. Håkonsen, *Hycast Gas Cushion (GC) Billet Casting System.* Cham: Springer International Publishing, 2016, pp. 793–796. [Online]. Available: https://doi.org/10.1007/978-3-319-48160-9_136

[8] U. Tundal, K. O. Tveito, S. S. Berg, L. Moen, M. Boge, A. Håkonsen, and R. Ledal, "Low-pressure casting technology represents step change in producing high quality forging stock," *Light Metal Age, reprinted for Hycast AS with permission*, 2020. [Online]. Available: https://www.hycast.no/assets/files/LMA_DEC_2020_reprints-Hycast-LR.pdf

[9] Hycast AS, "Hycast lpc technology," Mar 2020. [Online]. Available: https://vimeo.com/396768500?embedded=true&source=vimeo_logo&owner=109356794

[10] L&L Special Furnace Co., Inc., "Aluminum Heat Treatment: Homogenizing," Jun 2021, [Accessed 25-April-2023]. [Online]. Available: https://llfurnace.com/blog/aluminum-heat-treatment-homogenizing/

[11] TC Engineering AS, "Billet tong data sheet 001-2010," Jun 2016, [Accessed 25-April-2023]. [Online]. Available: https://tce.no/wp-content/uploads/2016/06/Data-Sheet-Billet-Tong.pdf

[12] B. E. Gihleengen, "Fully automated casthouse concept study - Pre-study," pp. 11–14, Feb. 2019.

[13] *Overhead Crane Machine*, Rockwell Automation, 2021.

[14] Munck Cranes USA Inc., "Overhead bridge crane components," [Accessed 01-May-2023]. [Online]. Available: https://www.munckcranesusa.com/crane-component-guide

[15] Nøsted & AS, "Løfteåk spesial," [Accessed 01-May-2023]. [Online]. Available: https://www.nosted.com/lofteak-spesial

[16] Wikipedia contributors, "KISS Principle — Wikipedia, the free encyclopedia," 2023, [Accessed 05-May-2023]. [Online]. Available: https://en.wikipedia.org/wiki/KISS_principle

[17] Wikipedia contributors, "Bellcrank — Wikipedia, the free encyclopedia," 2022, [Accessed 13-April-2023]. [Online]. Available: https://en.wikipedia.org/w/index.php?title=Bellcrank&oldid=1128193619

[18] Wikipedia contributors, "Rack and pinion — Wikipedia, the free encyclopedia," 2023, [Accessed 13-April-2023]. [Online]. Available: https://en.wikipedia.org/w/index.php?title=Rack_and_pinion&oldid=1149147933

[19] Danfoss A/S, "What is a variable frequency drive?" [Accessed 09-May-2023]. [Online]. Available: https://www.danfoss.com/en/about-danfoss/our-businesses/drives/what-is-a-variable-frequency-drive/#

[20] Motorman S.A., "Hook block with motorized rotation," [Accessed 09-May-2023]. [Online]. Available: http://www.motorman.es/en/divisions/material-handling/hook-blocks-with-rotation/hook-block-with-motorized-rotation/

[21] Sick AG, "Detection of the crane position," [Accessed 11-May-2023]. [Online]. Available: https://www.sick.com/au/en/industries/wood/sawmill-industry/storage-and-transport/detection-of-the-crane-position/c/p518948

[22] Schmitt Industries Inc., *AR1000 Laser Distance Sensor*, Acuity Laser Measurment, 2010, rev. 12/10. [Online]. Available: https://www.acuitylaser.com/wp-content/uploads/ar1000-data-sheet.pdf

[23] Gigasense AB, "Angle Measurement Unit for CSM," [Accessed 26-April-2023]. [Online]. Available: https://www.gigasense.se/product/angle-measurement-unit/

[24] A. Mashood, A. Dirir, M. Hussein, H. Noura, and F. Awwad, "Quadrotor object tracking using real-time motion sensing," in *2016 5th International Conference on Electronic Devices, Systems and Applications (ICEDSA)*, 2016, pp. 1–4.

[25] Bitcraze AB, "Motion capture positioning," [Accessed 19-April-2023]. [Online]. Available: https://www.bitcraze.io/documentation/system/positioning/mocap-positioning/

[26] NaturalPoint, Inc. DBA OptiTrack, "$Prime^x$41," [Accessed 11-May-2023]. [Online]. Available: https://optitrack.com/cameras/primex-41/

[27] S. Wighton. (2023) I made a 100mph flying hoop. Youtube. Fetched: 18.04.2023. [Online]. Available: https://youtu.be/xHWXZyfhQas?t=628

[28] D. Nardella and G. Molenaar, "Python Snap7," 2013, [Online; accessed 14-May-2023]. [Online]. Available: https://python-snap7.readthedocs.io/en/latest/introduction.html

[29] Beckhoff Automation GmbH, "TwinCAT Automation Software," fetched: 02.03.2023. [Online]. Available: https://www.beckhoff.com/en-en/products/automation/twincat/?pk_campaign=AdWords-AdWordsSearch-TwinCAT_EN&pk_kwd=twincat

[30] TechTarget Contributor, "What is kinematics?: Definition from TechTarget," May 2018. [Online]. Available: https://www.techtarget.com/whatis/definition/kinematics

[31] M. W. Spong, S. Hutchinson, and M. Vidyasagar, *Robot Modeling and Control*. John Wiley & Sons, Inc., 2020, p. 177–184.

[32] N. G. R. Center. (n.d.) Newton's laws of motion. Accessed: 16.05.2023. [Online]. Available: https://www1.grc.nasa.gov/beginners-guide-to-aeronautics/newtons-laws-of-motion/

[33] L. A. Williams, "Modelling; Simulation and Control of Offshore Crane," Ph.D. dissertation, University of Agder, 2018.

[34] D. L. Goodstein, "Lagrange's and Hamilton's equations." [Online]. Available: https://www.britannica.com/science/mechanics/Lagranges-and-Hamiltons-equations

[35] Wikipedia contributors, "Nonlinear system — Wikipedia, the free encyclopedia," 2023, [Accessed 13-February-2023]. [Online]. Available: https://en.wikipedia.org/wiki/System_of_linear_equations

[36] M. R. Mojallizadeh, B. Brogliato, and C. Prieur, "Modeling and control of overhead cranes: a survey," *Univ. Grenoble Alpes, INRIA, CNRS, Grenoble INP, LJK, 38000 Grenoble, France 1Univ. Grenoble Alpes, GIPSA lab, 38000 Grenoble, France*, 2023.

[37] D. T. Ho, H. Nguyen, and Q. C. Nguyen, "Input shaping control of an overhead crane," *Ho Chi Minh City University of Technology*, 2020.

[38] D. Yuan and T. Chang, "Trajectory control of robot with model reference zero vibration shaper," 07 2006.

[39] J. Walters, *Collection of technical formulae*. Gieck-Verlag, 1982.

[40] J. Vaughan, A. Yano, and W. Singhose, "Comparison of robust input shapers," *Journal of Sound and Vibration*, vol. 315, pp. 797–815, 09 2008.

[41] A. Aksjonov, "3d kraana juhtimiss$\ddot{U}$steem," 2015.

[42] P. G. Syvertsen, "Modeling and control of crane on offshore vessel," Ph.D. dissertation, Norwegian University of Science and Technology, 2011. [Online]. Available: https://ntnuopen.ntnu.no/ntnu-xmlui/handle/11250/237968show=full

[43] Wikipedia contributors, "Spline interpolation — Wikipedia, the free encyclopedia," 2023, [Online; accessed 09-May-2023]. [Online]. Available: https://en.wikipedia.org/w/index.php?title=Spline_interpolation&oldid=1151719077

[44] K. Bjørvik and P. Hveem, *Reguleringsteknikk*. Kybernetes, 2014.

[45] F. Dessen, "Lecture on feedforward control," 2021, unpublished lecture notes for IELET2101, NTNU.

[46] do MPC, "Basic of model predictive control," 2021, [Accessed 04-May-2023]. [Online]. Available: https://www.do-mpc.com/en/latest/theory_mpc.html

[47] Wikipedia contributors, "Linear-quadratic regulator — Wikipedia, the free encyclopedia," 2023, [Accessed 11-May-2023]. [Online]. Available: https://en.wikipedia.org/wiki/Linear%E2%80%93quadratic_regulator

[48] MATLAB, "What is linaer quadratic regulator (lqr) optimal control," 2023, [Online; accessed 11-May-2023]. [Online]. Available:

https://www.youtube.com/watch?v=E_RDCFOlJx4&t=12s&ab_channel=MATLAB

[49] LearnChemE, "Introduction to process control: Pid controller design," https://www.youtube.com/watch?v=EPaQWBWp064&ab_channel=LearnChemE, 2017, accessed: May 4, 2023.

[50] R. Piedrafita, D. Comín, and J. R. Beltrán, "Simulink® implementation and industrial test of input shaping techniques," *Control Engineering Practice*, vol. 79, p. 1–21, 2018.

[51] X. Wu, "Enhanced damping-based anti-swing control method for underactuated overhead cranes," *IET Control Theory Applications*, vol. 9, pp. 1893–1900(7), August 2015. [Online]. Available: https://digital-library.theiet.org/content/journals/10.1049/iet-cta.2014.1353

Appendix

A1 Billet ring V3

Figure A1.1: Enlarged version of figure 4.3c, displaying billet ring V3

A2 Revised lifting yoke design (unactuated)

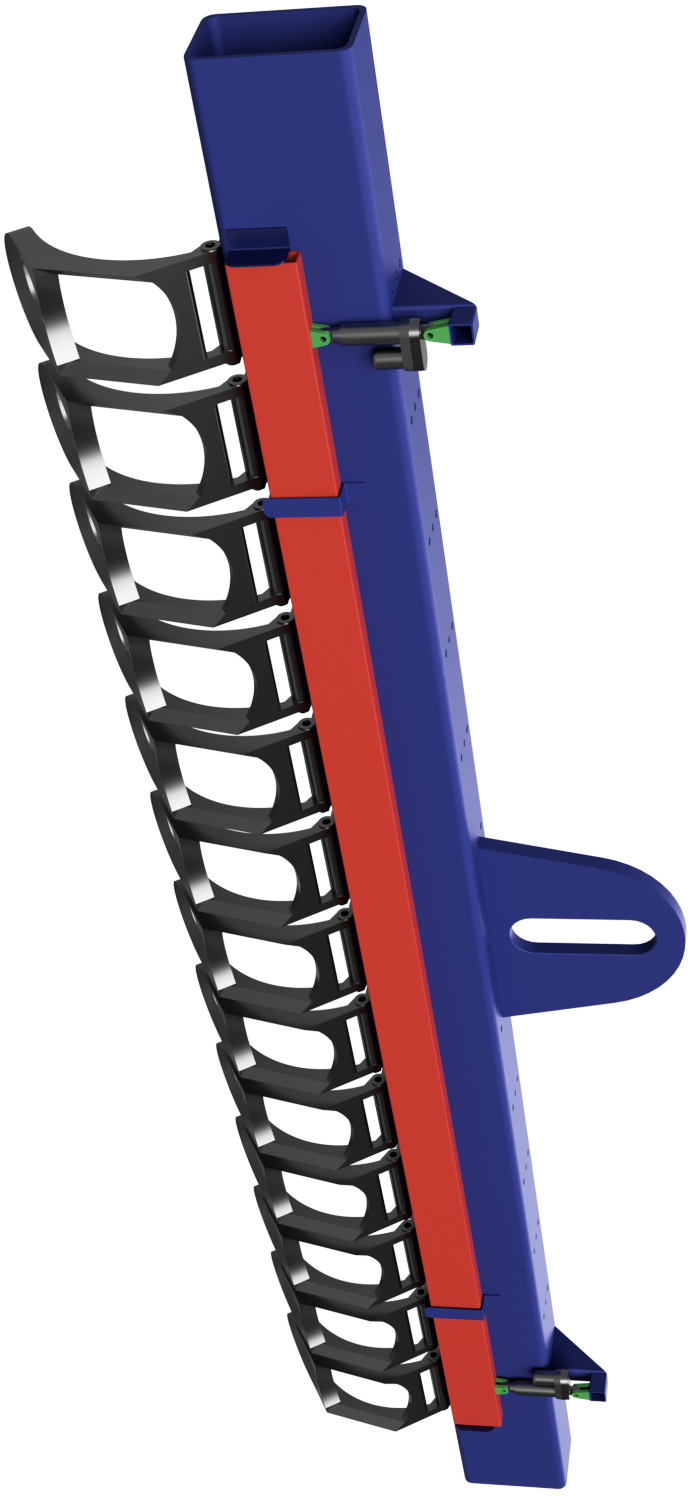

Figure A2.1: Enlarged version of figure 4.6, displaying the proposed lifting yoke, equipped with billet ring V3 (unactuated)

A3 Revised lifting yoke design (actuated)

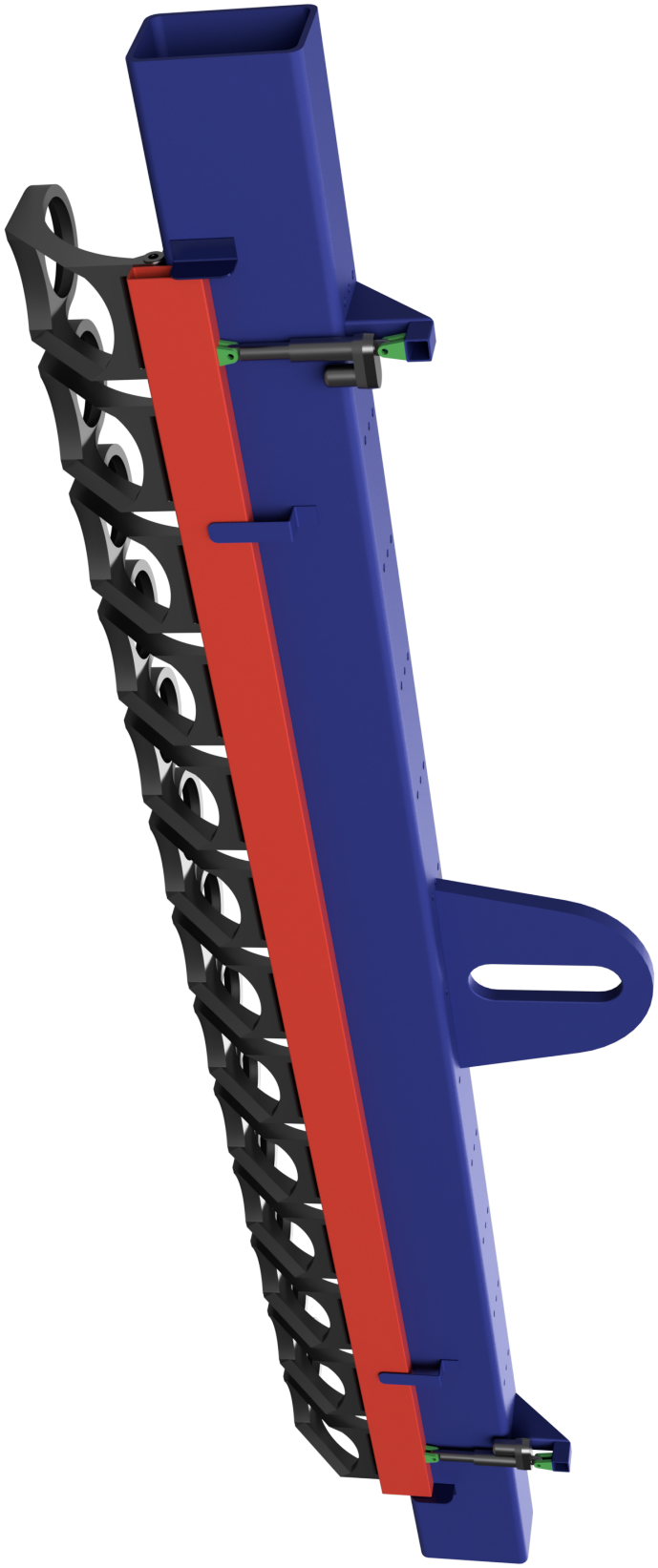

Figure A3.1: Enlarged version of figure 4.7, displaying the proposed lifting yoke, equipped with billet ring V3 (actuated)

A4 Revised lifting yoke design (profile)

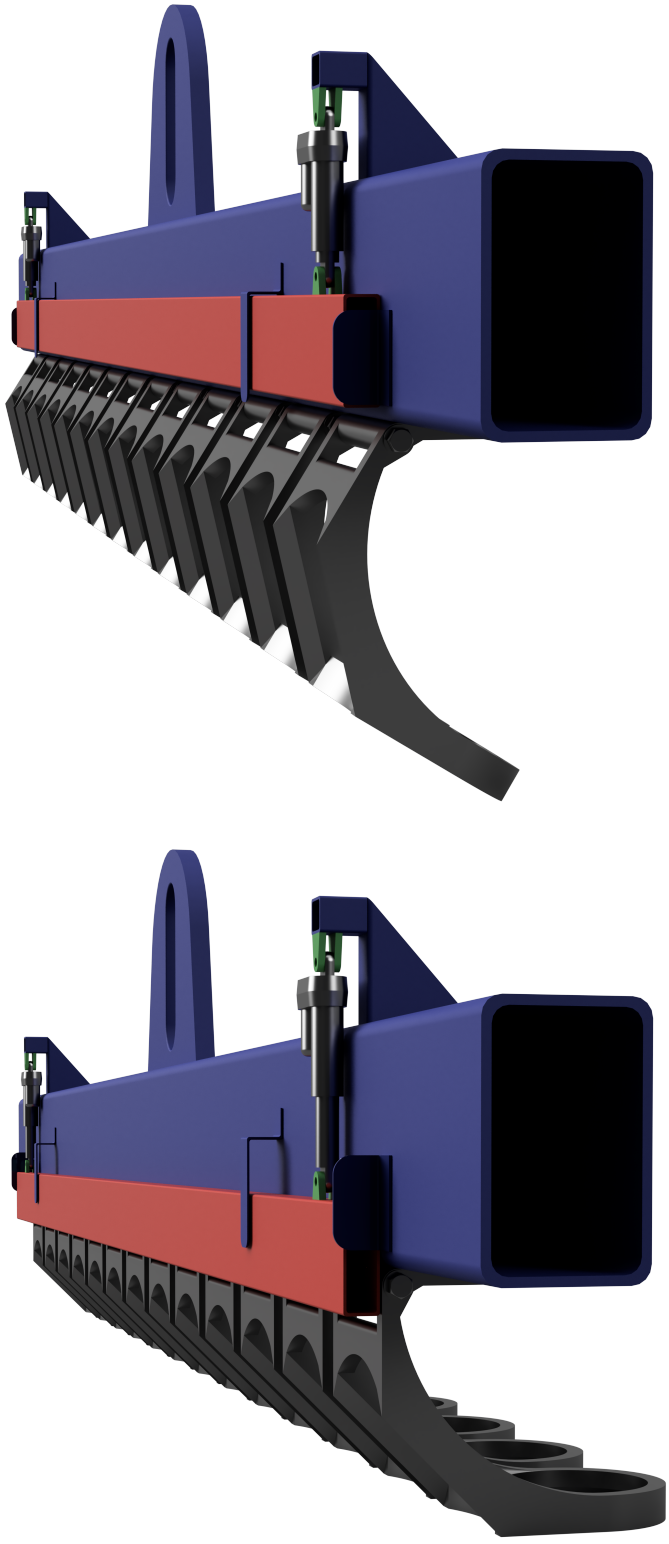

Figure A4.1: Enlarged version of figure 4.8

A5 Guide cradle assembly

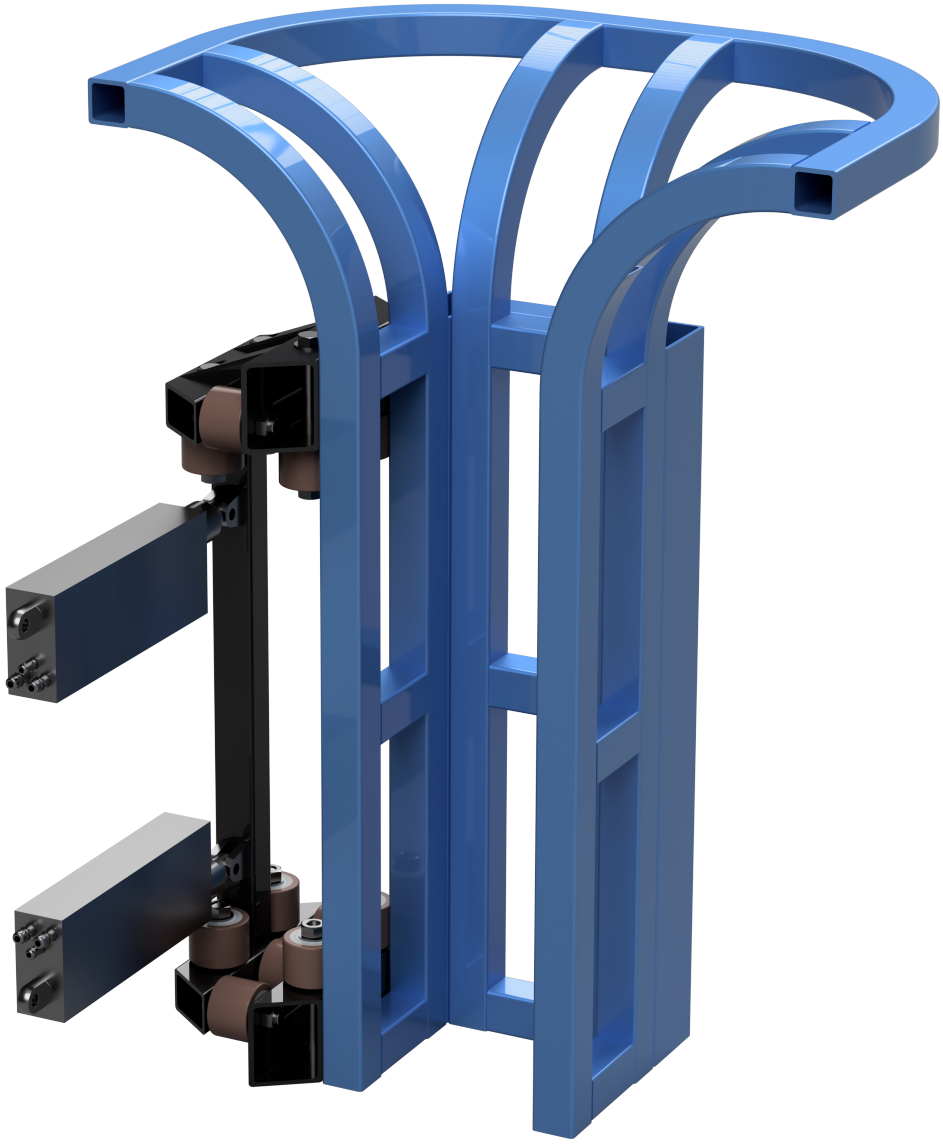

Figure A5.1: Enlarged version of figure 4.9, displaying a conceptual guide cradle design

A6 Matlab code Lagrangian

```
%Clearing the workspace
clear all;
clc;

%% Constants

% weight constants

m_trolley = 5600;           % Mass of the trolley [kg]
m_payload = 10000;          % Mass of the total payload [kg]
m_bridge = 7700;            % Mass of bridge [kg]


% Speed constants
g = 9.81;
max_speed_bridge = 1;       % Travelling speed bridge [m/s]
max_speed_trolley = 0.5;    % Travelling speed trolley [m/s]
max_speed_hoist = 0.125;    % Travalling speed hoist [m/s]
max_accelaratuion = 0.1;    % Max accelaratuion [m/s^s]

% Hoist constant
max_lengt_hoist = 22;       % Max lenght of hoist [m]
l = 22.5;                   % Lenght of hoist

% Gain constants
% Relationship between % and force

x_constant = ((m_trolley+m_bridge+m_payload)*max_accelaratuion)/100;
y_constant = ((m_trolley+m_payload)*max_accelaratuion)/100;
z_constant = (m_payload*max_accelaratuion)/100;

Gain = [x_constant y_constant z_constant];

%% State space of the crane with lagrain

eq1 = m_payload*g/(m_trolley*m_bridge*m_payload);
eq2 = m_payload*g/(m_trolley+m_payload);
eq3 = -g*(m_payload+m_trolley+m_bridge+m_payload)/(m_trolley+m_bridge
    +m_payload);
```

```
39 eq4 = -g*(m_payload+m_trolley+m_payload)/((m_trolley+m_payload)*l);
40 eq5 = 1/(m_trolley+m_bridge+m_payload);
41 eq6 = 1/(m_trolley+m_payload);
42 eq7 = -1/((m_trolley+m_bridge+m_payload)*l);
43 eq8 = -1/((m_trolley+m_payload)*l);
44 eq9 = 1/(m_payload+m_payload);
45
46
47 % Describes how the internal states are connected to each other,
48 % the uderlying dynamics of the system
49 A = [0  1  0  0  0  0  0  0  0  0;
50       0  0  0  0 eq1  0  0  0  0  0;
51       0  0  0  1  0  0  0  0  0  0;
52       0  0  0  0  0  0 eq2  0  0  0;
53       0  0  0  0  0  1  0  0  0  0;
54       0  0  0  0 eq3  0  0  0  0  0;
55       0  0  0  0  0  0  0  1  0  0;
56       0  0  0  0  0  0 eq4  0  0  0;
57       0  0  0  0  0  0  0  0  0  1;
58       0  0  0  0  0  0  0  0  0  0;];
59
60 % describes how the inputs enters into the system, and which states
       they
61 % are efficting
62 B = [0  0  0;
63      eq5  0  0;
64      0  0  0;
65      0 eq6  0;
66      0  0  0;
67      eq7  0  0;
68      0  0  0;
69      0 eq8  0;
70      0  0  0;
71      0  0 eq9;];
72
73 % Describes how the states are compined to get the outputs
74 C = [1  0  0  0  0  0  0  0  0  0;
75       0  0  1  0  0  0  0  0  0  0;
76       0  0  0  0  1  0  0  0  0  0;
77       0  0  0  0  0  0  1  0  0  0;
78       0  0  0  0  0  0  0  0  1  0;];
```

```
79
80 % D matrix is used to allow  the inputs to bypass the system all
       together,
81 % and feed-forward to the output
82 D = zeros(5,3);
```

A7 Matlab code Trajectory Planning

```
%ZV
```

```
function y = ZV(u, w0, zita)
    % Function to calculate coefficients based on input parameters
    % Inputs:
    %   - u: input parameter
    %   - w0: natural frequency in radians per second
    %   - zita: damping ratio
    % Outputs:
    %   - y: array of coefficients [A1, t1, A2, t2]

    % Convert w0 from radians per second to hertz
    % 1 Hz = 2*pi radians per second
    tau_d = 2 * pi / w0;

    % Calculate the value of K using the damping ratio
    K = exp((-zita * pi) / sqrt(1 - zita^2));

    % Calculate coefficient A1 and assign initial time t1
    A1 = 1 / (1 + K);
    t1 = 0;

    % Calculate coefficient A2 and assign t2 as half of tau_d
    A2 = K / (1 + K);
    t2 = tau_d / 2;

    % Multiply coefficients A1 and A2 by the input parameter u
    A1 = u * A1;
    A2 = u * A2;

    % Store the coefficients and times in the output array y
    y = [A1, t1, A2, t2];
end
%ZVD
```

```
function y = ZVD(u, w0, zita)
    % Function to calculate coefficients based on input parameters
```

```
36      % Inputs:
37      %   - u: input parameter
38      %   - w0: natural frequency in radians per second
39      %   - zita: damping ratio
40      % Outputs:
41      %   - y: array of coefficients [A1, t1, A2, t2, A3, t3]
42
43      % Convert w0 from radians per second to hertz
44      % 1 Hz = 2*pi radians per second
45      tau_d = 2 * pi / w0;
46
47      % Calculate the value of K using the damping ratio
48      K = exp((-zita * pi) / sqrt(1 - zita^2));
49
50      % Calculate coefficient A1 and assign initial time t1
51      A1 = 1 / (1 + 2 * K + K^2);
52      t1 = 0;
53
54      % Calculate coefficient A2 and assign t2 as half of tau_d
55      A2 = 2 * K / (1 + 2 * K + K^2);
56      t2 = tau_d / 2;
57
58      % Calculate coefficient A3 and assign t3 as tau_d
59      A3 = K^2 / (1 + 2 * K + K^2);
60      t3 = tau_d;
61
62      % Multiply coefficients A1, A2, and A3 by the input parameter u
63      A1 = u * A1;
64      A2 = u * A2;
65      A3 = u * A3;
66
67      % Store the coefficients and times in the output array y
68      y = [A1, t1, A2, t2, A3, t3];
69  end
70  %ZVDD
```

```
71  function y = ZVDD(u, w0, zita)
72      % Function to calculate coefficients based on input parameters
73      % Inputs:
74      %   - u: input parameter
```

```
75      %   - w0: natural frequency in radians per second
76      %   - zita: damping ratio
77      % Outputs:
78      %   - y: array of coefficients [A1, t1, A2, t2, A3, t3, A4, t4]
79
80      % Convert w0 from radians per second to hertz
81      % 1 Hz = 2*pi radians per second
82      tau_d = 2 * pi / w0;
83
84      % Calculate the value of K using the damping ratio
85      K = exp((-zita * pi) / sqrt(1 - zita^2));
86
87      % Calculate coefficient A1 and assign initial time t1
88      A1 = 1 / (1 + 3 * K + 3 * K^2 + K^3);
89      t1 = 0;
90
91      % Calculate coefficient A2 and assign t2 as half of tau_d
92      A2 = (3 * K) / (1 + 3 * K + 3 * K^2 + K^3);
93      t2 = tau_d / 2;
94
95      % Calculate coefficient A3 and assign t3 as tau_d
96      A3 = (3 * K^2) / (1 + 3 * K + 3 * K^2 + K^3);
97      t3 = tau_d;
98
99      % Calculate coefficient A4 and assign t4 as 3/2 times tau_d
100     A4 = K^3 / (1 + 3 * K + 3 * K^2 + K^3);
101     t4 = tau_d * 3 / 2;
102
103     % Multiply coefficients A1, A2, A3, and A4 by the input parameter
            u
104     A1 = u * A1;
105     A2 = u * A2;
106     A3 = u * A3;
107     A4 = u * A4;
108
109     % Store the coefficients and times in the output array y
110     y = [A1, t1, A2, t2, A3, t3, A4, t4];
111 end
```

A8 Matlab code Input Shapers

```
function y = fcn(t, path_points)
    % Function to interpolate and generate values based on
        path_points at time t
    % Inputs:
    %   - t: current time
    %   - path_points: matrix containing path points with format [x,
        y, t]
    % Outputs:
    %   - y: interpolated value at time t

    % Define persistent variables to store information across
        function calls
    persistent current_segment
    persistent y_temp

    % Check if the persistent variables are empty (first function
        call)
    if isempty(current_segment)
        % Initialize current_segment to the first segment
        current_segment = 1;
        % Initialize y_temp to the y-value of the first point
        y_temp = path_points(1, 1);
    end

    % Define an anonymous function to access viapoints easily
    viapoints = @(i) path_points(i + 1, :);

    % Calculate the number of path points and segments
    n_path_points = size(path_points);
    n_segments = n_path_points(1) - 1;

    % Check if the current segment is within the total number of
        segments
    if current_segment <= n_segments
        % Get the start and end times of the current segment
        t0 = path_points(current_segment, 3);
        tf = path_points(current_segment + 1, 3);

        % Check if the current time is within the current segment
```

```
35          if (t0 <= t) && (t <= tf)
36              % Get the previous and current path points for
                    interpolation
37              p1 = viapoints(current_segment - 1);
38              p2 = viapoints(current_segment);
39
40              % Calculate the interpolated value using a polynomial
                    function
41              y_temp = polynomial(p1, p2, t);
42
43          elseif t > tf
44              % Move to the next segment if the current time exceeds
                    the end time of the current segment
45              current_segment = current_segment + 1;
46          end
47      end
48
49      % Set the output value to the current interpolated value
50      y = y_temp;
51
52      % Nested function to calculate the polynomial interpolation
53      function r = polynomial(p0, p1, t)
54          % Calculate the coefficients of the polynomial interpolation
55          a0 = p0(1);
56          a1 = p0(2);
57          a2 = (3 * (p1(1) - p0(1)) - (2 * p0(2) + p1(2)) * (p1(3) - p0
                    (3))) / (p1(3) - p0(3))^2;
58          a3 = (2 * (p0(1) - p1(1)) + (p0(2) + p1(2)) * (p1(3) - p0(3))
                    ) / (p1(3) - p0(3))^3;
59
60          % Calculate the interpolated value using the polynomial
                    equation
61          r = a0 + a1 * (t - p0(3)) + a2 * (t - p0(3))^2 + a3 * (t - p0
                    (3))^3;
62  0(
```

A9 SU-M4-MUN-M60 layout

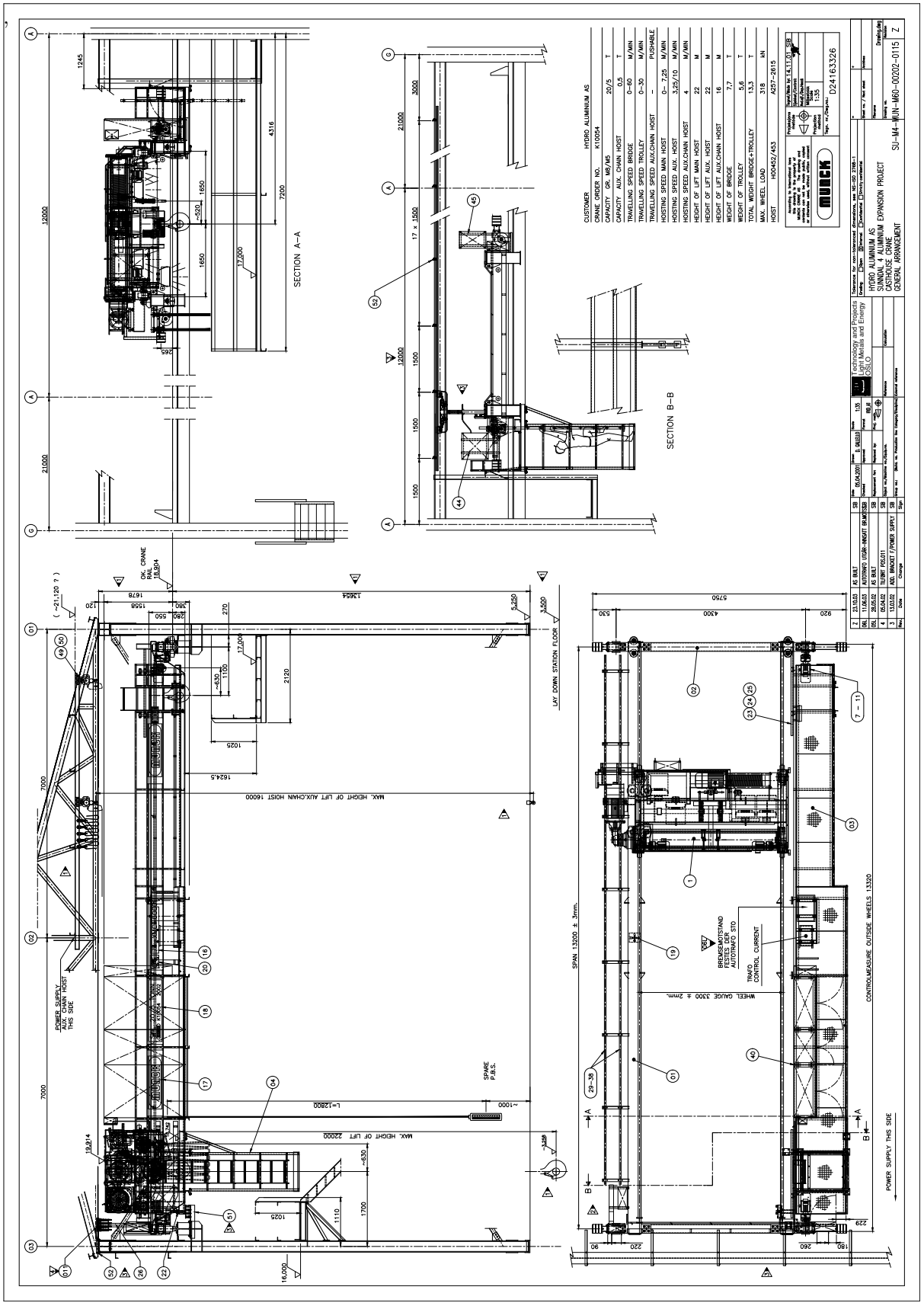

K10054\SIMATIC 300 Station\CPU315-2 DP(1)\S7 Program(1)\Blocks

Object name	Symbolic name	Creat	Last modified	Comment
OB1	Hovedprogram	FBD	19.08.2002 11:27:29	Hovedprogram
OB86	RACK_FLT	FBD	19.08.2002 11:29:01	"Loss Of Rack Fault"
FB50	DP_HzOmf	FBD	22.08.2002 15:45:39	Styring av frekvensomformer på ProfiBus DP Funksjonsblokk for styring av frekvensomformer på profibus DP.
FB51	SWP	FBD	19.08.2002 11:26:44	Funksjonsblokk for beregning av levetid.
FB53	Avg_Scan	FBD	19.08.2002 11:22:20	FB for å ta snitt av en verdi i et antall scan.
FC11	K10054_Kran	FBD	19.08.2002 11:22:38	Program for Styring av Traverskran Revisjoner Dato Nettverk Beskrivelse Sign. I de
FC12	1U1_BroStyring	FBD	06.02.2003 13:44:45	Bro Styring av frekvensomformer for bro
FC22	2U1_KattStyring	FBD	06.02.2003 13:04:14	Katt Styring av frekvensomformer for Katt 1 Rev. Dato Beskrivelse Sign A 17.12.
FC32	3U1_Heis1Styring	FBD	06.02.2003 11:19:24	Heis Styring av frekvensomformer for heis
FC42	4U1_Heis2Styring	FBD	20.08.2002 21:26:35	Heis Styring av frekvensomformer for heis
FC100	Skaler	FBD	23.08.2002 11:45:21	Funksjon for skalering av råverdi til ingeniørverdi. Funksjon for å skalere en råverdi til en ingeniørverdi mellom MIN
FC111	K10054_Alarmer	FBD	22.08.2002 14:58:40	Programblokk for håndtering av Alarmer, Lamper og Buzzer Denne programblokk brukes for Alarmhåndtering. Vec
FC112	K10054_Felles	FBD	19.08.2002 11:41:00	Programblokk for Felles signaler.
FC120	SystemFlagg	FBD	19.08.2002 10:07:26	Programblokk for generering av Systemflagg.
FC130	SWP_Heiser	FBD	21.08.2002 19:48:38	Program for Levetid på Heis
DB12	SWP_Heis1_DB	DB	19.08.2002 10:47:19	Instans DB for SWP Kran A
DB13	SWP_Heis2_DB	DB	19.08.2002 10:47:08	Instans DB for SWP Kran B
DB51	3U1_Heis	DB	20.03.2002 10:34:39	Instans DB for vekselretter 3U1 Heis A
DB52	1U1_Bro	DB	20.03.2002 10:35:22	Instans DB for vekselretter 1U1 for Bro
DB53	2U1_Katt	DB	04.01.2002 11:12:50	
DB100	DB_AI5_Avg	DB	04.01.2002 18:15:28	
DB101	DB_AI6_AVG	DB	07.01.2002 12:30:15	

A10 SU-M4-MUN-M60 PLC program

SIMATIC Program structure for K10054\SIMATIC 30...\S7 Program(1)\Blocks 11/19/2003 15:20:25

Program structure (tree representation)

```
S7 program
├─ OB1 (Hovedprogram) <Maximum: 126>                          [22]
│  ├─ FC120 (SystemFlagg)  [24]                               FBD, NW    1 [2]
│  └─ FC11 (K10054_Kran)                                      FBD, NW    2 [2]
│     ├─ FC111 (K10054_Alarmer)  [26]                         FBD, NW    1 [2]
│     ├─ FC112 (K10054_Felles)  [26]                          FBD, NW    2 [2]
│     ├─ FC130 (SWP_Heiser)                                   FBD, NW    3 [10]
│     │  ├─ FB53 (Avg_Scan), DB100 (DB_AI5_Avg)  [58]        FBD, NW    1 [24]
│     │  ├─ FB51 (SWP), DB12 (SWP_Heis1_DB)                  FBD, NW    2 [38]
│     │  │  ├─ FC100 (Skaler)  [116]                         FBD, NW    3 [44]
│     │  │  └─ FC100 (Skaler)  [116]                         FBD, NW    9 [44]
│     │  ├─ FB53 (Avg_Scan), DB101 (DB_AI6_AVG)  [58]        FBD, NW    4 [24]
│     │  └─ FB51 (SWP), DB13 (SWP_Heis2_DB)                  FBD, NW    5 [38]
│     │     ├─ FC100 (Skaler)  [116]                         FBD, NW    3 [44]
│     │     └─ FC100 (Skaler)  [116]                         FBD, NW    9 [44]
│     ├─ FC32 (3U1_Heis1Styring)                              FBD, NW    4 [18]
│     │  ├─ FC100 (Skaler)  [86]                             FBD, NW    9 [44]
│     │  └─ FB50 (DP_HzOmf), DB51 (3U1_Heis)                 FBD, NW   14 [38]
│     │     ├─ FC100 (Skaler)  [124]                         FBD, NW   12 [44]
│     │     ├─ SFC15 (DPWR_DAT)  [80]                        FBD, NW   14 [0]
│     │     ├─ SFC14 (DPRD_DAT)  [80]                        FBD, NW   15 [0]
│     │     ├─ FC100 (Skaler)  [124]                         FBD, NW   18 [44]
│     │     └─ FC100 (Skaler)  [124]                         FBD, NW   18 [44]
│     ├─ FC42 (4U1_Heis2Styring)  [40]                        FBD, NW    5 [16]
│     ├─ FC12 (1U1_BroStyring)                                FBD, NW    6 [20]
│     │  ├─ FC100 (Skaler)  [88]                             FBD, NW    7 [44]
│     │  └─ FB50 (DP_HzOmf), DB52 (1U1_Bro)                  FBD, NW   13 [38]
│     │     ├─ FC100 (Skaler)  [126]                         FBD, NW   12 [44]
│     │     ├─ SFC15 (DPWR_DAT)  [82]                        FBD, NW   14 [0]
│     │     ├─ SFC14 (DPRD_DAT)  [82]                        FBD, NW   15 [0]
│     │     ├─ FC100 (Skaler)  [126]                         FBD, NW   18 [44]
│     │     └─ FC100 (Skaler)  [126]                         FBD, NW   18 [44]
│     └─ FC22 (2U1_KattStyring)                               FBD, NW    7 [20]
│        ├─ FC100 (Skaler)  [88]                              FBD, NW    7 [44]
│        └─ FB50 (DP_HzOmf), DB53 (2U1_Katt)                  FBD, NW   14 [38]
│           ├─ FC100 (Skaler)  [126]                         FBD, NW   12 [44]
│           ├─ SFC15 (DPWR_DAT)  [82]                        FBD, NW   14 [0]
│           ├─ SFC14 (DPRD_DAT)  [82]                        FBD, NW   15 [0]
│           ├─ FC100 (Skaler)  [126]                         FBD, NW   18 [44]
│           └─ FC100 (Skaler)  [126]                         FBD, NW   18 [44]
└─ OB86 (RACK_FLT) [26]                                       [26]
```

SIMATIC ... Station\CPU315-2 DP(1)\S7 Program(1)\K10054_Symboler 11/19/2003 15:18:08

Properties of symbol table

Name:	K10054_Symboler
Comment:	Støperi Kran Sunndal 4 Munck Cranes as Controlteam as, Anlegg 3180
Created on	17.11.2003 11:43:52
Last modified on:	17.12.2002 14:53:42
Last filter criterion:	Alle Symbole
Number of symbols:	229/ 229
Last Sorting:	Address Ascending

Symbol	Address	Data type	Comment
SWP_Heis1_DB	DB 12	FB 51	Instans DB for SWP System Heis A
SWP_Heis2_DB	DB 13	FB 51	Instans DB for SWP System Heis B
3U1_Heis	DB 51	FB 50	Instans DB for Vekselretter Heis
1U1_Bro	DB 52	FB 50	Instans DB for Vekselretter Kranbro
2U1_Katt	DB 53	FB 50	Instans DB for Vekselretter Katt
DB_AI5_Avg	DB 100	FB 53	Instans DB for snittverdi AI5
DB_AI6_AVG	DB 101	FB 53	Instans DB for snittverdi AI6
DP_HzOmf	FB 50	FB 50	Funksjonsblokk for kjøring av frekvensomformer på Profibus DP.
SWP	FB 51	FB 51	Funksjonsblokk for levetid kran
Avg_Scan	FB 53	FB 53	Funksjonsblokk for snittberegning av verdi
K10054_Kran	FC 11	FC 11	Program for Kranstyring
1U1_BroStyring	FC 12	FC 12	Styring av frekvensomformer 1U1 for bro.
2U1_KattStyring	FC 22	FC 22	Styring av frekvensomformer 2U1 for Katt 1
3U1_Heis1Styring	FC 32	FC 32	Styring av frekvensomformer 3U1 for heis A.
4U1_Heis2Styring	FC 42	FC 42	Styring av frekvensomformer 4U1 for heis B.
5U1_Katt2	FC 52	FC 52	Styring av Frekvensomformer 5U1 for Katt 2
Skaler	FC 100	FC 100	Funksjon for skalering av Råverdi til Eng verdi og motsatt
K10054_Alarmer	FC 111	FC 111	Programblokk for Alarm lamper. ekskl. Frekv. omf.
K10054_Felles	FC 112	FC 112	Programblokk for styring av alarmlamper. (Blink ved ny alarm)
SystemFlagg	FC 120	FC 120	Generering av System bit M0.0-M1.0
SWP_Heiser	FC 130	FC 130	Programblokk for Levetid og last for begge heiser.
K10054_Q2	I 0.0	BOOL	Sikring til Air Condition OK
K10054_Q5	I 0.1	BOOL	Sikring til lyskastere på Katt 1 OK
K10054_Q22	I 0.2	BOOL	Sikring 400V til jordfeilvarsel -F2
K10054_Q7	I 0.3	BOOL	Sikring for Nødlys OK
K10054_Q8	I 0.4	BOOL	Sikring tilf. Bremser OK
K10054_Q9	I 0.5	BOOL	Sikring vifter vekselrettere OK
K10054_Q10	I 0.6	BOOL	Sikring lys i tavle OK
K10054_Q11	I 0.7	BOOL	Sikring PC / stikk OK
K10054_Q12	I 1.0	BOOL	Sikring tilf. PLS OK
K10054_Q14	I 1.1	BOOL	Sikring 24V Likeretter -U3 OK
K10054_Q15	I 1.2	BOOL	Sikring 24V Vekselretter 3U1 OK
K10054_Q16	I 1.3	BOOL	Sikring 24V Vekselretter 1U1 OK
K10054_Q17	I 1.4	BOOL	Sikring 24V Vekselretter 2U1 OK
K10054_Q20	I 1.5	BOOL	Sikring 24V styrestrøm OK
K10054_4Q1	I 1.7	BOOL	Sikring tilf. 400V Heis B
K10054_S1 Lampetest	I 2.0	BOOL	+VA Lampetest
K10054_S2	I 2.1	BOOL	+VA Kvitter alarm
K10054_F2	I 2.2	BOOL	+VA Jordfeil 1
K10054_F3	I 2.3	BOOL	+VA Jordfeil 2
K10054_K05	I 2.4	BOOL	+VA Loddbryter Løft 1 OK
K10054_K06	I 2.5	BOOL	+VA Loddbryter Løft 2 OK
K10054_K028_Lokal	I 2.6	BOOL	Omformere i Lokal
K10054_K02 Service	I 2.7	BOOL	Kommando fra servicetablå
K10054_K020_U3_OK	I 3.0	BOOL	Likeretter U3 OK
K10054_T4_Trafo_OK	I 3.1	BOOL	Autotrafo OK

SIMATIC ... Station\CPU315-2 DP(1)\S7 Program(1)\K10054_Symboler 11/19/2003 15:18:08

Symbol	Address	Data type	Comment
K10054_JGR_Y6_Opp2	I 3.3	BOOL	Heis B Opp
K10054_JGR_Ned2	I 3.4	BOOL	Heis B Ned
K10054_K0_EMS	I 3.7	BOOL	Nødstopp aktivert
K10054_S3 HeisA	I 4.0	BOOL	Heis A Valgt
K10054_3S1 Heis Opp	I 4.1	BOOL	Kjør Heis Opp
K10054_3S2 Heis Ned	I 4.2	BOOL	Kjør Heis Ned
K10054_3Sx Heis Tr2_	I 4.3	BOOL	Kjør Heis Høy hastighet
K10054_S3 Heis B	I 4.4	BOOL	Heis B Valgt
K10054_1S1 Bro Frem	I 4.5	BOOL	Kranbro frem
K10054_1S2 Bro Tilbake	I 4.6	BOOL	Kranbro tilbake
K10054_1Sx Bro Tr2	I 4.7	BOOL	Kranbro trinn 2
K10054_2S1_Katt_H	I 5.0	BOOL	Løpekatt høyre fra tablå/radio
K10054_2S2 Katt_V	I 5.1	BOOL	Løpekatt venstre fra tablå/radio
K10054_2Sx Katt_Tr2	I 5.2	BOOL	Løpekatt trinn 2 fra tablå på gulv.
K10054_1F2 Th OK	I 6.0	BOOL	Thermistor Kranbro. OK
K10054_6001 SlwFrem	I 6.2	BOOL	Bro GS sakte frem
K10054_6002 StpFrem	I 6.3	BOOL	Bro GS stopp frem
K10054_6004 SlwTilb	I 6.4	BOOL	Bro GS sakte tilbake
K10054_6003 StpTilb	I 6.5	BOOL	Bro GS stopp tilbake
K10054_3F2 Th OK	I 7.1	BOOL	Termistor Løft 1 OK
K10054_6011 SlwOpp	I 7.2	BOOL	Løft A GS sakte Opp
K10054_6012 StpOpp	I 7.3	BOOL	Løft A GS stopp Opp
K10054_6013 StpNed	I 7.4	BOOL	Løft A GS Stopp Ned
K10054_4F2 Th OK	I 7.6	BOOL	Termistor Løft 2 OK
K10054_6022 StpOpp	I 7.7	BOOL	Løft B GS Stopp Opp
K10054_6023 StpNed	I 8.0	BOOL	Løft B GS Stopp Ned
K10054_2F2 Th OK	I 8.3	BOOL	Løpekatt Termistor OK
K10054_6015 Slw_H	I 8.4	BOOL	Løpekatt GS Sakte Høyre
K10054_6016 Stp_H	I 8.5	BOOL	Løpekatt GS Stopp Høyre
K10054_6025 Slw_V	I 8.6	BOOL	Løpekatt GS Sakte Venstre
K10054_6016 Stp_V	I 8.7	BOOL	Løpekatt GS Stopp Venstre
AI1_Heis	IW 20	INT	AI Fra Radio for pådrag løft
AI2_Kranbro	IW 22	INT	AI fra Radio for pådrag kranbro
AI3_Katt	IW 24	INT	AI fra Radio for pådrag Katt
AI4_reserve	IW 26	INT	AI Reserve
AI5_LastHeis1	IW 28	INT	AI veiecelle Løft 1
AI6_LastHeis2	IW 30	INT	AI veiecelle Løft 2
AlltidAv	M 0.0	BOOL	System flagg Alltid AV
AlltidPaa	M 0.1	BOOL	System Flagg Alltid PÅ
BLINK 05	M 0.2	BOOL	Blinker med 0,5 Hz 1 sek PÅ og 1. sek AV
BLINK 1	M 0.3	BOOL	Blinker med 1 Hz.
BLINK 25	M 0.4	BOOL	Blinker med 2,5 Hz.
SekPuls	M 1.0	BOOL	Puls i ett scan hvert sekund
InitPuls	M 1.1	BOOL	På første scan
P_SekPuls	M 1.7	BOOL	Hjelp flanke BLINK 1 (Puls hvert sek.)
OppstartOK	M 2.0	BOOL	Oppstart OK.
Clk_100ms	M 4.0	BOOL	100 ms Klokkepuls (10Hz)
Clk_200ms	M 4.1	BOOL	200 ms Klokkepuls (5 Hz)
Clk_400ms	M 4.2	BOOL	400 ms Klokkepuls (2,5Hz)
Clk_500ms	M 4.3	BOOL	10 ms Klokkepuls (2 Hz)
Clk_800ms	M 4.4	BOOL	10 ms Klokkepuls (1,25 Hz)
Clk_1s	M 4.5	BOOL	1s. Klokkepuls 1Hz
Clk_1,6s	M 4.6	BOOL	1,6 s. Klokkepuls (0,625 Hz)
Clk_2s	M 4.7	BOOL	2s Klokkepuls (0,5Hz)
Heis A Valgt	M 6.0	BOOL	Heis A valgt
Heis B_Valgt	M 6.1	BOOL	Heis B Valgt
Heis1_OVL	M 7.0	BOOL	Overlast på Heis 1
Heis2_OVL	M 7.1	BOOL	Overlast på Heis 2

SIMATIC ... Station\CPU315-2 DP(1)\S7 Program(1)\K10054_Symboler 11/19/2003 15:18:08

Symbol	Address	Data type	Comment
Heis1_SWP_EXP	M 7.2	BOOL	Levetid Utgått på Heis 1
Heis2_SWP_EXP	M 7.3	BOOL	Levetid Utgått på Heis 1
Heis1_RedLoad	M 7.4	BOOL	Redusert last Heis A
Heis2_RedLoad	M 7.5	BOOL	Redusert last Heis B
Heis1_Load_ER	M 7.6	BOOL	Feil på Lastcelle Heis A
Heis2_Load_ER	M 7.7	BOOL	Feil på Lastcelle Heis B
U3_LikeretterOK	M 8.0	BOOL	Likeretter OK
Bro_OVL	M 8.4	BOOL	Overlast for Bro (Sum av Last A og B)
ResetFaults	M 9.0	BOOL	Reset Alarmer på frekvensomformere.
K10054_3U1 Drift	M 10.0	BOOL	3U1 i Drift
K10054_3U1 Alarm	M 10.1	BOOL	3U1 Alarm
K10054_3U1 Warning	M 10.2	BOOL	3U1 Advarsel
K10054_3U1 Klar	M 10.3	BOOL	3U1 Klar
K10054_6011_ER	M 10.4	BOOL	Endebryterfeil Heis Opp
K10054_1U1 Drift	M 20.0	BOOL	1U1 i Drift
K10054_1U1 Alarm	M 20.1	BOOL	1U1 Alarm
K10054_1U1 Warning	M 20.2	BOOL	1U1 Advarsel
K10054_1U1 Klar	M 20.3	BOOL	1U1 Klar
K10054_6001_ER	M 20.4	BOOL	Endebryter feil Bro Frem
K10054_6004_ER	M 20.5	BOOL	Endbryterfeil Bro Tilbake
K10054_2U1 Drift	M 30.0	BOOL	2U1 i Drift
K10054_2U1 Alarm	M 30.1	BOOL	2U1 Alarm
K10054_2U1 Warning	M 30.2	BOOL	2U1 Advarsel
K10054_2U1 Klar	M 30.3	BOOL	2U1 Klar
K10054_6015_ER	M 30.4	BOOL	Endebryterfeil Katt Høyre
K10054_6025_ER	M 30.5	BOOL	Endebryterfeil Katt Venstre
P_AL_Profibus	M 99.0	BOOL	Flanke Alarm profibus
P_Jordfeil1	M 99.1	BOOL	Flanke Alarm Jordfeil 1
P_Jordfeil2	M 99.2	BOOL	Flanke Alarm Jordfeil 2
Alarm_Q2	M 100.0	BOOL	Alarm Sikring til Air Condition
Alarm_Q5	M 100.1	BOOL	Alarm Sikring til lyskastere på Katt 1
Alarm_Q6	M 100.2	BOOL	Alarm Sikring til lyskastere på Katt 2
Alarm_Q7	M 100.3	BOOL	Alarm Sikring for Nødlys
Alarm_Q8	M 100.4	BOOL	Alarm Sikring tilf. Bremser
Alarm_Q9	M 100.5	BOOL	Alarm Sikring vifter vekselrettere
Alarm_Q10	M 100.6	BOOL	Alarm Sikring lys i tavle
Alarm_Q11	M 100.7	BOOL	Alarm Sikring PC / stikk
Alarm_Q12	M 101.0	BOOL	Alarm Sikring tilf. PLS
Alarm_Q14	M 101.1	BOOL	Alarm Sikring 24V Likeretter -U3
Alarm_Q15	M 101.2	BOOL	Alarm Sikring 24V Vekselretter 3U1
Alarm_Q16	M 101.3	BOOL	Alarm Sikring 24V Vekselretter 4U1
Alarm_Q17	M 101.4	BOOL	Alarm Sikring 24V Vekselretter 1U1
Alarm_Q18	M 101.5	BOOL	Alarm Sikring 24V Vekselretter 2U1
Alarm_Q19	M 101.6	BOOL	Alarm Sikring 24V Vekselretter 5U1
Alarm_Q20	M 101.7	BOOL	Alarm Sikring 24V styrestrøm
AL_3F2_Th	M 102.0	BOOL	Alarm termistor Heis A
AL_Heis1_SWP	M 102.1	BOOL	Alarm SWP utløpt Heis A
AL_Heis1_Load_ER	M 102.2	BOOL	Alarm lastsignal utenfor 4-20mA
AL_4F2_Th	M 102.3	BOOL	Alarm termistor Heis B
AL_Heis2_SWP	M 102.4	BOOL	Alarm termistor Heis B
AL_Heis2_Load_ER	M 102.5	BOOL	Alarm SWP utløpt Heis B
AL_Heis1_OVL	M 102.6	BOOL	Alarm Overlast Heis A
AL_Heis2_OVL	M 102.7	BOOL	Alarm Overlast Heis B
AL_1F2_Th	M 103.0	BOOL	Alarm termistor 1 Bro
AL_1F3_Th	M 103.1	BOOL	Alarm termistor 2 Bro
Alarm_4Q1	M 103.2	BOOL	Alarm Sikring til Heis B
AL_2F2_Th	M 104.0	BOOL	Alarm termistor Katt 1
AL_5F2_Th	M 104.1	BOOL	Alarm termistor Katt 2

SIMATIC ... Station\CPU315-2 DP(1)\S7 Program(1)\K10054_Symboler 11/19/2003 15:18:08

Symbol	Address	Data type	Comment
AL_T4_AutoTrafo	M 104.6	BOOL	Alarm Autotrafo T4
AL_K028_Lokal	M 105.0	BOOL	Alarm ved omformere i Lokal.
Alarm_Q22	M 105.2	BOOL	Alarm sikring Q22
Heis1ByPassLoad	M 105.5	BOOL	Tillat kjøring uten lastcelle Heis A.
Heis2ByPassLoad	M 105.6	BOOL	Tillat kjøring uten lastcelle Heis B.
AL_ProfiBus	M 105.7	BOOL	Alarm dersom profibus er Ute.
AL_K05_Loddbr1	M 108.0	BOOL	Alarm Loddbryter Heis A
AL_K06_Loddbr2	M 108.1	BOOL	Alarm Loddbryter Heis B
AL_U3_Likeretter	M 108.2	BOOL	Alarm fra Likeretter U3
AL_1U1_Bro	M 108.3	BOOL	Alarm fra Vekselretter 1U1 Bro.
AL_2U1_Katt1	M 108.4	BOOL	Alarm fra Vekselretter 2U1 Katt A
AL_3U1_Heis1	M 108.5	BOOL	Alarm fra Vekselretter 3U1 Heis A
AL_4U1_Heis2	M 108.6	BOOL	Alarm fra Vekselretter 4U1 Heis B
AL_5U1_Katt2	M 108.7	BOOL	Alarm fra Vekselretter 5U1 Katt B
BLK_NyAlarm	M 110.0	BOOL	Ny Alarm
BLK_NyJordFeil	M 110.2	BOOL	Ny Jordfeil
BLK_AL_K05	M 110.3	BOOL	Blink ny Alarm Loddbr. Heis A
BLK_AL_K06	M 110.4	BOOL	Blink ny Alarm Loddbr. Heis A
BLK_AL_U3	M 110.5	BOOL	Blink ny Alarm likeretter U3
BLK_AL_1U1	M 111.0	BOOL	Blink ny Alarm 1U1
BLK_AL_2U1	M 111.1	BOOL	Blink ny Alarm 2U1
BLK_AL_3U1	M 111.2	BOOL	Blink ny Alarm 3U1
hlpInitPuls	M 199.0	BOOL	Hjelpe flag for å generere puls for første scan.
AlarmOrd1	MW 100	INT	Alarm aktiv dersom <> 0
AlarmOrd2	MW 102	INT	Alarm aktiv dersom <> 0
AlarmOrd3	MW 104	INT	Alarm aktiv dersom <> 0
Heis1_WL	MW 120	INT	Vekt i 1/10 ton for heis A
Heis2_WL	MW 130	INT	Vekt i 1/10 ton for heis B
PLS_ScanTid	MW 190	INT	Scantid i ms.
Hovedprogram	OB 1	OB 1	Kjører hele tiden.
RACK_FLT	OB 86	OB 86	Loss of Rack Fault
K10054_H2 Buzzer	Q 10.0	BOOL	Lydsignal ved alarm
K10054_H3 Alarm	Q 10.1	BOOL	Lampe Alarm
K10054_H4 Jordfeil	Q 10.2	BOOL	Lampe jordfeil
K10054_H5 EMS	Q 10.3	BOOL	Lampe Nødstopp Aktivert.
K10054_H6 Lodd1	Q 10.4	BOOL	Lampe Loddbryter løft 1 aktivert.
K10054_H12 Lodd2	Q 10.5	BOOL	Lampe Loddbryter løft 2 aktivert.
K10054_H7 AL_U3	Q 10.6	BOOL	Lampe Alarm Likeretter U3
K10054_H8 AL_3U1	Q 10.7	BOOL	Lampe Alarm Vekselretter Løft 1
K10054_H9 AL_1U1	Q 11.0	BOOL	Lampe Alarm Vekselretter Bro kjøring
K10054_H10 AL_2U1	Q 11.1	BOOL	Lampe Alarm Vekselretter Katt kjøring
K10054_H11 AL_LS	Q 11.2	BOOL	Lampe Alarm endebrytere
K10054_U3_Start	Q 11.3	BOOL	Start signal til Likeretter U3
K10054_U3_Reset	Q 11.4	BOOL	Reset signal til Likeretter U3
K10054_K117 Opp2	Q 12.0	BOOL	Heis B Opp Tr.2
K10054_K118 Ned2	Q 12.1	BOOL	Heis B Ned Tr.2
K10054_K119 Opp1	Q 12.2	BOOL	Heis B Opp Tr.1
K10054_K120 Ned1	Q 12.3	BOOL	Heis B Ned Tr.1
K10054_K121 Brems	Q 12.4	BOOL	Brems av
DPRD_DAT	SFC 14	SFC 14	Read Consistent Data of a Standard DP Slave
DPWR_DAT	SFC 15	SFC 15	Write Consistent Data to a Standard DP Slave
BLKMOV	SFC 20	SFC 20	Copy Variables
TidResetFaults1	T 10	TIMER	Forsinkelse før Reset signal
TidResetFaults2	T 11	TIMER	Varighet Reset signal
ForsStartU3	T 20	TIMER	Forsinket start likeretter
tmForsHiSpd	T 22	TIMER	Forsinkelse før en tillater Høy hastighet
tmSlowHoyre	T 30	TIMER	Fors. Slowdown Høyre
tmSlowVenstre	T 31	TIMER	Fors. Slowdown Venstre

SIMATIC ... Station\CPU315-2 DP(1)\S7 Program(1)\K10054_Symboler 11/19/2003 15:18:08

Symbol	Address	Data type	Comment
tm6015_ER	T 32	TIMER	Fors.endebryterfeil Høyre
tm6025_ER	T 33	TIMER	Fors.endebryterfeil Venstre
VAT_AnalogIn	VAT 1		Variabel tabell for Analoge inng. signal.
VAT_Alarmer	VAT 2		Variabel tabell for Alarmer
VAT_DIG_IN	VAT 3		Variabeltabell for Digitale Innganger
VAT_SWP_Heis1	VAT 4		Variabel tabell for levetid Heis A
VAT_Vekselrettere	VAT 5		Variabel tabell for Vekselrettere.
VAT_SWP_Heis2	VAT 6		Variabel tabell for levetid Heis B

Modelling and assessment of overhead crane for automatic control

Halvor Tøfte Johnsen, Jørgen Andreas Mo, Eivind Stellef Rønningen and Sigurd Belland Hovet
Department of Engineering Cybernetics, Norwegian University of Science and Technology

Abstract

This poster provides a concise summary of a bachelor thesis focused towards automating the extrusion ingot pit stripping process at Hydro's casting centres, mainly using the existing infrastructure. In essence, this involves using the overhead cranes and laydown stations installed in the casthouses. Casthouse Sunndal was used as a reference for the analysis. The crane's behaviour has been modelled using Newton's Laws of Motion and has been implemented in MATLAB's Simulink. Furthermore, a control system has been proposed and implemented in Simulink, demonstrating the crane's controllability. The evaluations conducted on the overhead crane have resulted in various mechanical enhancements being proposed. This poster is based on the bachelor thesis by the same name and authors [1].

Assesment Of Existing Installations

Fig. 1: Current billet ring at Casthouse Sunndal.

The most challenging part of automating the pit stripping process is attaching the ingots to the lifting yoke. This operation occurs when the ingots are resting upright on their starter blocks inside the casting pit. The use of existing lifting yokes, where the billet rings are suspended by a chain link, proves to be impractical for further automation. This is because the chain link mechanism is unpredictable, and may cause the ingots to fall over. The existing overhead crane has limited instrumentation, providing only limited state feedback to the control system. Consequently, the current solution lacks the necessary capabilities to achieve the desired level of controllability for automating this process. Implementing a control system that is capable of delivering the required precision would surpass reasonable feasibility.

Mechanical Solutions

The difficulties in achieving adequate positioning accuracy from the crane control system have led to the development of mechanical solutions. These mechanical solutions are concept ideas developed to reduce the level of accuracy required from the control system. In order to attain the necessary precise positioning of the billet ring, a redesign with a rigid stem and a single revolute joint has been proposed. Additionally, a guide cradle system is developed to enhance the accuracy of the billet ring further, ensuring that the lifting yoke is guided to its designated position. By incorporating such a solution, the system can tolerate oscillations of 20cm in the lifting yoke position, thereby reducing the precision requirements placed on the control system and enhancing positioning reliability. Furthermore, the overhead crane must be equipped with a sufficient instrumentation package for further development of its control system.

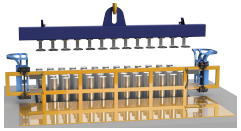

Fig. 2: Lifting yoke over extrusion ingots and guide craddle.

Mathematical Model

Since the actual crane was unavailable for testing, a simulation environment was required in order to test the control system's performance. A mathematical model of the crane was derived using Newton's Laws of Motion, and these dynamics were implemented in MATLAB's Simulink. Some dynamics had to be simplified somewhat, such as the dampening and wire dynamics. To ensure the accuracy and validity of the model, it was compared with recorded footage of the crane installed in Casthouse Sunndal.

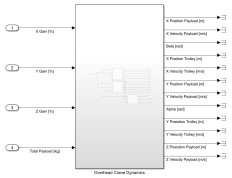

Fig. 3: Simulation environment in Simulink.

Control System Proposal

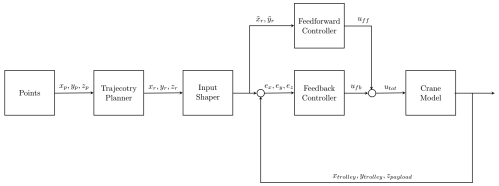

Fig. 4: Proposed control system block scheme.

The proposed and simulated control system is composed of a feedforward and feedback controller, as well as an input shaper. The trolley positioning is controlled by the feedforward and PID feedback controller and achieves precise control in the xy plane. In the z plane, a PID feedback controller is proposed. For sway control, a ZVD input shaper manipulates the calculated trajectory to ease the payload's oscillation. Through a comprehensive simulation and testing phase the ZVD input shaper gave an acceptable time delay, as well as not sacrificing the robustness of the system. This enables the control system to control the payload with less than five centimetres of sway. This is displayed in Figure 5.

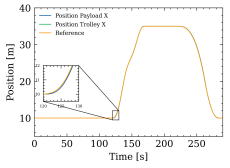

Fig. 5: Pathfollowing in x direction.

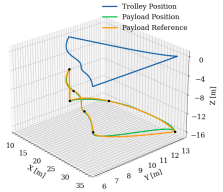

Fig. 6: Trajectory of trolley, and path-following of payload position.

Conclusion And Further Work

Based on the results from the simulations, it seems that automatic pit stripping is a viable option without excessive interventions. Accurate trolley positioning and path following can be achieved through PID and feedforward controllers, and using an input shaper shows promising results for sway control. The simulations have however been conducted using a simplified crane model, which raises the necessity of testing the input shaper on a more accurate model before implementing it on a full-scale system. Simultaneously, the mechanical solutions also alleviate the need for more sophisticated control strategies because the cradle allows for some minor oscillations.

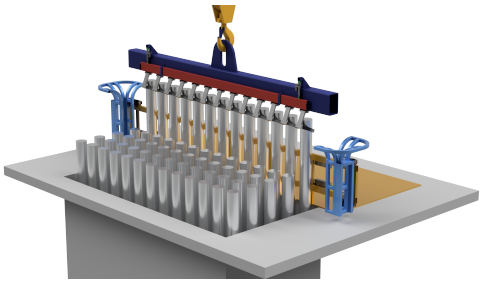

Fig. 7: Proposed living yoke with revised billet rings.

The first step for further work would be to validate the mechanical solutions, such as the design of the billet rings and lifting yoke. After validating the billet ring and lifting yoke, the guiding cradle should be designed to fit the lifting yoke and mounted to the pit's safety platform. The first step regarding the control system would be to develop a more accurate model of the crane's dynamics. This involves making a model that accounts for multiple hoist wires, as well as pendulum motion and torsion between the hook and the lifting yoke, and considering the pendulum motion of each suspended ingot. After making an accurate model, it is suggested to use the proposed control system and validate if an enhanced model results in increased precision. If it is deemed adequate, further development could be unnecessary. If the performance still doesn't suffice, more sophisticated methods for sway control are recommended.

References

[1] Eivind Rønningen. Sigurd Hovet. Jørgen Mo. Halvor Johnsen. "Modelling and Assessment of Overhead Crane for Automatic Control". Bachelor's thesis. NTNU, 2023.

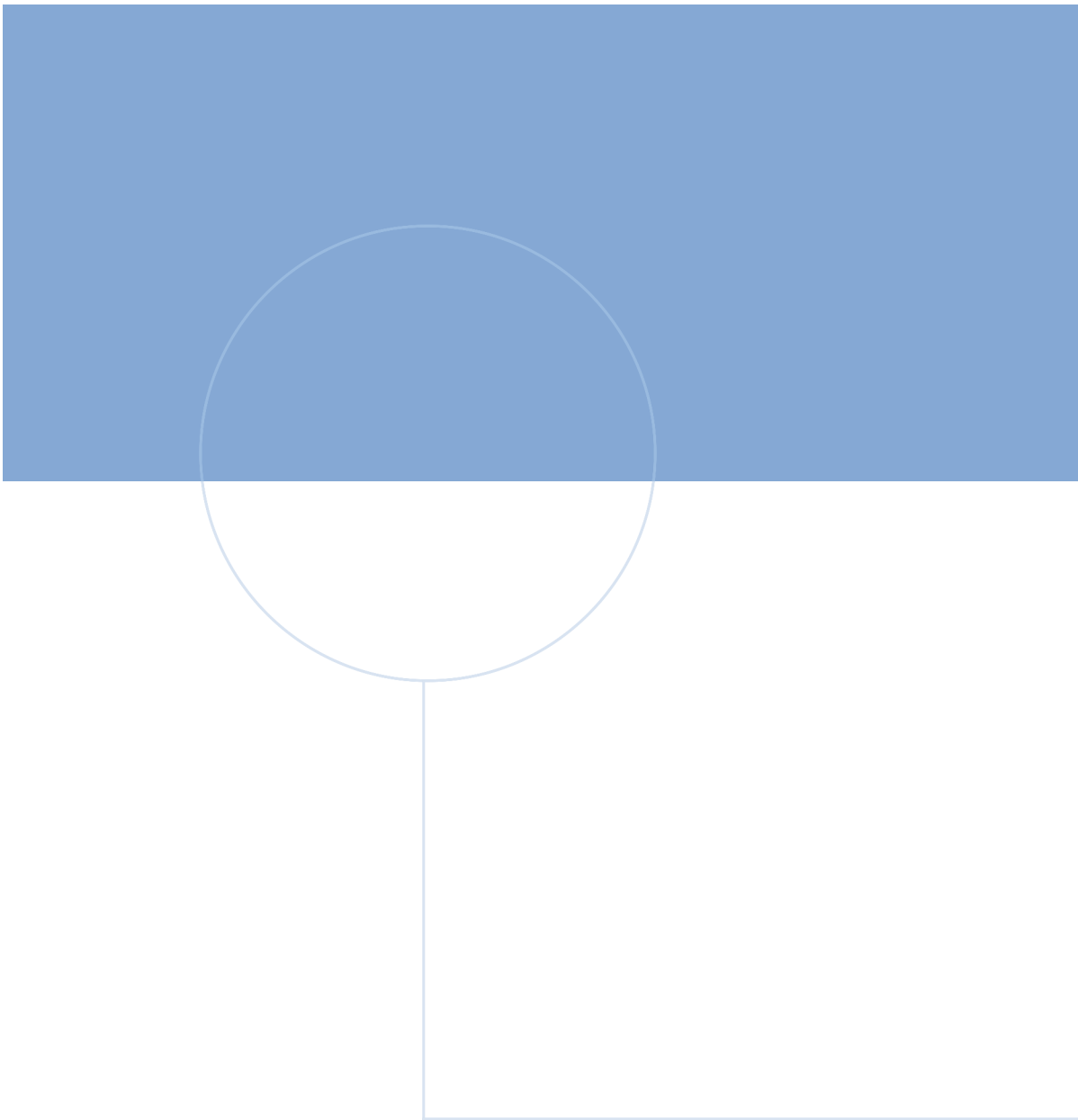

NTNU
Norwegian University of
Science and Technology

Hydro